THE GEOLOGY OF THE OCEANOGRAPHER TRANSFORM FAULT

by

Richard H. Moody Jr.

Abstract of a Thesis

Submitted to the State University of New York at Albany

in Partial Fulfillment of

the Requirements for the Degree of

Master of Science

College of Science and Mathematics

Department of Geological Sciences

1982

ABSTRACT

A detailed survey of the Oceanographer transform fault and environs at 35°N, 35°W has yielded detailed information with respect to the generation and evolution of seafloor at a slowly accreting plate margin. From this data detailed bathymetric maps and maps of depth to basement have been constructed for a swath of seafloor 1800 km long and 100-200 km wide centered about the offset region. This data was used to subdivide major phases of seafloor spreading during the Tertiary. The ridge crest and all major topographic features near the transform appear to be affected by their proximity to the transform. The ridge crest widens and deepens towards the transform, and the rift valley walls are higher when they lie on the transform side of the valley than when they lie on the fracure zone side of the rift. Based upon the observed topographic effects the physical properties of the crust and upper mantle must vary markedly near the transform.

Constraints provided by a combined ALVIN/ANGUS field program in the summer of 1980 indicate that the present zone of decoupling between the North American and African plates is located in the center of the transform valley; the zone of decoupling is less than 2 km wide, and is defined most often by discontinuous, variable degraded elongate fault or slump-degraded fualt scarps in sediment. Vertical tectonism and mass-wasting processes dominate near the axial deep whereas deposition and erosion dominate in the terraces and the upper wall province. The petrologic data and the rock distribution data confirm that the crust near the Oceanographer transform is thin and even, perhaps discontinuous

and indicates that the mode of crustal formation is likely to change significantly near transforms. Spectacular bedforms including abyssal furrows, dunes, longitudinal and transverse current ripples, and wave ripples are abundant. Except for the furrows these bedforms are concentrated in the very rugged, upper wall province of the transform.

Chapter 3 presents a model for the formation of transform topography. This model hinges upon the assumption of a curved zone of decoupling between the plates near each ridge-transform intersection. This curvature gives rise to a geometric peculiarity which requires a gap to open between the plates. This gap conceivably should alter significantly many of the physical properties of the transform such as its depth, the height of the crestal mountains, the presence and width of any transverse ridges, and gradients of the seafloor into the intersection deep. Many of these properties vary in a fashion consistent with the model.

PREFACE

Marine geology by nature tends to be a joint effort. In an attempt to clarify my role in the creation of this thesis, I take full responsibility for the text of chapter one. I readily acknowledge the assistance of the OTTER Field Team* in the collection and initial processing of the data which serves as the basis for chapter two. I am solely responsible for the figures and text of chapter three.

The format for this thesis will be apresentation of the large-scale features of the Oceanographer transform and the inactive fracture zone limbs in chapter 1. Chapter 2 will then narrow the discussion to a small work area in the center of the transform where more detailed near-bottom studies were conducted. Chapter 3 will be a synthesis of the data sets of chapters 1 and 2 and will concentrate on the origin of transform topography.

*OTTER Field Team: P.J. Fox, E. Bonatti, K. Crane, J. Casey, D. Elthon, D. Fornari, D. Gallo, P. Hamlyn, J. Karson, W.S.F. Kidd, R. Moody, E. Sartori, and J. Stroup

ACKNOWLEDGEMENTS

Many individuals have provided me with invaluable assistance prior to and during the writing of this thesis. I wish to thank Fred Schroeder for his counsel while I was working at Lamont-Doherty Geological Observatory. At Albany the challenging ambiance created by the students and faculty was largely responsible for whatever creativity resides within this thesis. Individuals I would single out for special thanks are Jeff Fox, my mentor and good friend for many years. Win Means kept me on the track when my exuberance carried me into uncharted waters. Bill Kidd was responsible for quality control while my thesis was in progress. Dan Fornari provided the necessary dynamism to get the job done.

Two individuals have been especially supportive throughout my graduate career--Dave Gallo and Heather Sloan. They have both friends and cohorts in the melee that constitutes modern science. Debbie Schwartz provided enthusiasm and good cheer at all times. Len Berdan, a lifelong friend, has been especially helpful in the latter stages of the thesis. I thank my parents, Richard and Suzanne, for their unswerving dedication and support on my behalf.

TABLE OF CONTENTS

LIST OF FIGURES

CHAPTER I

MORPHOLOGY AND TECTONICS OF THE OCEANOGRAPHER FRACTURE ZONE

INTRODUCTION

The Oceanographer transform fault, located on the Mid-Atlantic Ridge near 35°N, 35°W was first surveyed in 1967 during a USCGS OCEANGRAPHER cruise (Fox et al., 1969). During subsequent cruises of the R/V VEMA in 1973 and 1974 (V30-06, V30-07, V32-03) detailed investigations within and proximal to the transform were carried out (Fox et al. 1976; Schreiber and Fox, 1976; Schroeder, 1977; Kent et al., 1979). The purpose of these cruises was to attemp to trace the aseismic limbs of the Oceanographer fracture zone for a distance of 900 km to either side of the ridge axis (Figure 1-1). The integrated result of these four expeditions yielded 22,000 km of underway geophysical data. In this chapter the primary focus is upon the the seismic data (12 kHz narrow beam echo-soundings from the OCEANOGRAPHER survey; 3.5 and 12 kHz wide beam echo soundings and single channel reflection profiles from the VEMA surveys). These data are used to accurately map the morphotectonic character of the oceanic crust that is created within and proximal to a slowly-slipping ridge-transform-ridge boundary. Ancther focal point of this chapter is how this distinctive topographic expression changes with increasing distance from the ridge-transform intersection. This provides the necessary constraints in order to define the evolution of this important but poorly understood element of the evolving plate mosaic.

BATHYMETRY, STRUCTURE, AND MORPHOLOGY

There are three morphotectonic provinces proximal to the Oceanographer transform: the ridge crests, the transform proper, and

the inactive fracture limbs (Figures 1-2,3). The data are presented within the framework of these three provinces.

Ridge Crests: The mid-ocean ridge south of the Azores triple junction in the central North Atlantic is characterized by short (~ 60km) ridge segments which are offset a few tens of kilometers to many hundreds of kilometers by transform faults (Phillips and Fleming, 1978). In the 35°N area this plate boundary geometry is clearly exhibited (Figure 1-2). The Oceanographer transform dominates the morphologic fabric offsetting the ridge crest 128km in a right-lateral sense. The 65km to 85km long ridge crest segments to the north and south of the Oceanographer transform are in turn offset by two small-offset transforms.

The ridge crest lying directly to the north of the Oceanographer fracture zone is characterized by a V-shaped, N15°E striking rift valley (Figure 1-4) than is clearly defined by the 2000m isobath (Figure 1-2). The rift valley is 85 km long and is truncated at its northern end by a small, 30km offset, right-lateral transform fault called Fracture Zone F (Fox et al., 1969; Phillips et al., 1975). The floor of the rift valley is bounded by high rugged inward facing walls that are comprised of a series of blocks of variable widths. The summits of the blocks are often characterized by gently dipping (a few degrees) outward facing slopes (Figure 1-4) and the blocks are linked together by several steep inward facing escarpments with relief of a few tens to several hundred meters creating the distinctive staircase like morphology of the rift valley (Needham and Francheteau, 1974). The crest of the east wall of the northern rift valley shoals to less than 1600m, has relief above the rift valley floor ranging from 800m to 1200m and an inward-facing regional slope of 5°. The west wall rises 600m to 2000m above the rift floor and is characterized by regional slopes of 8°.

Rugged crestal mountains flank the rift valley, generally lying above the 2000m isobath, and they develop peak to trough relief of 400m to 800m. The terrain elements vary in width from 5 km to 10 km, range in length from 10 km to 20 km and trend subparallel to the strike of the ridge axis.

The physiography of the terrain comprising the northern ridge crest segment varies markedly along strike but does so in a very systematic and symmetric way; at a point that is located approximately midway along the rift valley floor (Figures 1-2,9), the rift valley floor is shallowest (2206m), and the width of the valley floork as defined by the 2200 m isobath, is narrowest (5km). The rift valley slopes away from this depth minimum with average gradients of 3^{o} to the north and 4^{o} to the south, with local depth maximums of the rift valley occurring at the intersections with the two boundary fracture zones- 4800m near the the Oceanographer fracture zone and 3646m near Fracture Zone F. The width of the rift valley floor continuously increases with distance away from the midpoint and reaches maximum widths ($>$ 20km) at the ridge crest-transform fault intersections. The depth to the crest of rift walls also changes systmetically along strike. North of the apparent inflection point midway along the rift valley the crest of the rift valley walls continuously deepens towards the intersections with Transform F but the crest of the eastern rift wall always stands a few hundred meters higher than the western crest. South of the rift valley inflection point, the crest of the eastern wall continuously deepens towards the Oceanographer transform. The depth-distance relationship for the western wall is obscured by an isolated peak and south of the inflection point the

western wall shoals to minimum depths at this peak.

South of the Oceanographer fracture zone the ridge crest segment is also characterized by a narrow, V-shaped, rift valley that is clearly defined by the 2200m isobath. This rift valley is 65km long, strikes N15^{o}E, and is truncated at its southern end by a small (20km offset) right-lateral transform, called Fracture Zone I (Fox et al., 1969; Phillips et al., 1975). With the exception of a large (400m high) semi-conical feature (volcanic constructional edifice?) the ambient relief of the rift floor is less than 200m. The rift valley floor is bounded by several blocks which have steep, inward-facing escarpments and relatively flat tops resulting in the characteristic morphology of rift valleys. The eastern wall rises 800m to 2000m above the rift valley floor with a regional slope of approximately 13^{o}. The western wall has over 1000m of relief and is characterized by a regional slope of 11^{o}. The flanking crestal mountains consist of elongate secondary ridges and troughs subparallel to the rift valley.

Like its northern counterpart, the terrain elements comprising the southern rift valley, although very heterogenous, vary in a systematic, symmetric way along strike (Figure 1-9). The sill of this rift valley segment (2278m) is located midway between the two truncating transforms; the rift floor slopes continuously away from this inflection point with regional dips of 1^{o} to 2^{o} reaching maximum depths at the transform intersections (3957m at Oceanographer; 3031m at Fracture Zone I). As defined by the 2200m contour, the rift valley exhibits a minimum width (5km) at the inflection point and widens continuously towards the transform intersections reaching widths of 20km. Furthermore, the crests of the rift walls along the southern ridge deepen away from the inflection point with the crest standing higher nearer an active transform

(Figure 1-9).

Oceanographer Transform: The Oceanographer transform offsets the northern and southern rift valleys by 128km (Figure 1-2). Over thirty north-south crossings with an average track spacing of 5km clearly delineate a deep, narrow, axial trough that is outlined by the 3600m contour (Figure 1-2). The trough is bounded to the north and south by steep (regional gradients of 10^{o} to 24^{o}) inward facing walls which rise 1000m to 3000m above the trough floor (Figure 1-10). Following the definition of ARCYANA (1975), the terrain lying between the crests of the opposing walls represents the transform valley.

The axis of the Oceanographer transformvalley is a line connecting the maximum depth along the valley floor. This line of maximum depth has been constructed (Figure 1-3) revealing that the path of the axial line is sinuous making it difficult to define the strike of the axis in terms more specific than an approximate strike of $N76^{o}W \pm 6^{o}$. Short, 20km long segments have strikes ranging from 45^{o} to either side of an east-west line with WNW-ESE trends characterizing the central portion of the transform and ENE-WSW trends becoming more evident proximal to the rift valley intersections. The interval chosen for our bathymetric maps is 200m, and if the floor of the transform is taken to be defined by the deepest contour shown at any point along the the transform axis then the entire length of the valley floor is very narrow ($\leq$ 2km) and strikes parallel to the axis of the maximum depth (Figures 1-2,3). It becomes increasingly more difficult to generalize about the width and trend of the transform as the value for the deepest contour chosen to define the valley floor diminishes because the transform valley physiography becomes more variable along strike at shallower depths.

Using a relatively shallow contour of 3000m to define the transform valley; the width of the transform varies from 8km to 35km. Although the first-order E-W trending fabric of the transform is still preserved, individual segments of the 3000m contour strike at a wide range of angles to the overall transform trend (Figures 1-2,3).

A plot of maximum depth versus distance along the transform (Figure 1-11) shows the long axis of the valley floor is an undulating surface that is locally very steep developing relief ranging from 500m to 1200m. The sill depth for the transform is 3700m and is located several kilometers east of the midpoint of the transform. West of the sill two depressions with depths in excess of 4500m are defined: one at the intersection of the transform valley with the southern rift segment; the other within an elongate basin along the western portion of the transform (Figures 1-3,7). Along the transform valley segment east of the sill the transform valley floor reaches a maximum depth of 4800m where it intersects the northern rift valley.

The terrain bounding the transform axis is variable but several important morphotectonic relationships can be defined. South of the transform axis the topography can be described as an E-W trending ridge that, as defined by the 2000m contour, is approximately 20 km wide and can be traced along most of the transform axis (Figure 1-2). The northern flank of this ridge forms part of the transform valley wall, is characterized by steep regional slopes (10^{o} to 25^{o}) and creates a few thousand meters of relief. The southern flank of the ridge rises only a few hundred to several hundred meters above the oceanic basement. The east-west morphotectonic grain of this transform ridge is interrupted by embayments (e.g. $35^{o}20'W$) giving the ridge a ragged outline in plan view (Figures 1-2,3).

The terrain to the north of the transform axis is not characterized by a relatively continuous east-west trending ridge. Rather, there is a series of elongate north-south trending ridges and valleys which terminate against the east-west trending escarpments of the transform. The north-south grain is best expressed at elevations shallower than 3000m and the east-west fabric of the transform dominates the morphology at deeper levels. The result is that the seafloor slopes continuously with regional gradients of 10^{o}into the transform trough over distances of a few tens of kilometers (Figures 1-2,6). Although the first-order morphotectonic character character is markedly different on either side of the transform trough, the fine-scale topographic fabric of the inward-facing walls appears to be similar. Conventional surface-ship wide beam echo sounding records obtained at speeds typical of underway surveys (7-12 knts) average out the fine scale relief developed on steep slopes giving the appearance on most of our data that the walls of the transform valley are relatively steep, continuous and unbroken (Figure 1-10) Several of our bathymetric profiles were recorded at slow ship speeds ($<$ 4 knts) and these sounding profiles show that the transform valley walls are characterized by numerous overlapping point source reflection hyperbolae suggestive of near vertical escarpments with relief of only a few hundred meters. A SEABEAM survey of portions of the Oceanographer transform demonstrates that the valley walls are generally characterized by a series of very steep, east-west trending escarpemnts a few hundred meters high that are linked by narrow terraces creating staircase relief in profile (D. Needham, CNEXO, in prep.). A recent submersible (ALVIN) and deep-towed camera (ANGUS) investigation of a portion of the south central

and north central walls of the Oceanographer transform demonstrates that the morphology of the walls is a variable mix of two distinctive terrain elements: steep, near vertical rock escarpments with relief ranging from a few meters to several tens of meters and broad inwardly facing talus ramps with slopes ranging from 10^{o} to 30^{o}.

Fracture Zone Limbs: With a line spacing of approximately one crossing every 20 km, the first-order morphology of the fracture zone limbs was mapped for a distance of 900km to either side of the center of the Oceanographer transform (Figure 1-4,5,6,7). Although the basement relief and tectonic grain of the fracture zone domain is muted beneath a thickening blanket of sediment that reaches a maximum thickness of approximately 500m at the distal ends of our survey (Figures 1-4,5), terrain similar to the physiography of the transform valley can be traced continuously across the flanks of the Mid-Atlantic Ridge. Seismic reflection profiles (Figure 1-12) were used to construct a map of basement relief (Figure 1-6,7) and, even at distances of 900km from the transform center, distinctive east-west trending troughs and ridges can be clearly recognized. Irrespective of plate age, over 1000m of relief is maintained between the axis of maximum depth along a fracture valley and the bounding walls (Figure 1-12).

For a distance of 500km to either side of the center of the transform the physiography of the fracture zone is characterized by a single trough that is bounded by high terrain of variable character creating over 1 kilometer of relief along the valley. On either side of the ridge crest the axis of maximum depth along the fracture zone valley defines a WNW-ESE trend. Subtle changes in strike cannot be resolved along the transform axis with this line spacing; however, segments with three distinct trends are recognized (Figures 1-4,5,6,7). The maximum

fracture valley depth is quite variable along strike but there is a systematic increase in depth with distance away from the ridge-axis-transform intersections (Figure 1-6,7). From the deep basement lows that characterize the ridge crest-transform intersections, the axis of the fracture valleys shallow by more than 1000m over a distance of 20 to 30km. From local sill depths of less than 3000m the basement subsides relatively continuously achieving depths greater than 5000m (Figures 1-6,7). The walls of the fracture valley exhibit the same morphologic heterogenity as the transform valley walls. Along some portions of the fracture valley either one or both walls are composed of elongate ridges which rise several hundred to over a thousand meters above basement (Figure 1-12, e.g. profiles U-U', N-N'); at other locations along the fracture valley a well defined ridge is not recognized and the basement slopes continuously down towards the axis of the fracture zone for distances of 30km or more (Figure 1-12, e.g. profiles Q-Q', S-S'). Consequently, the crosssectional profiles of the fracture zone valley exhibit considerable heterogeniety along strike and the width of the valley, between opposing wall crests varies from 20km to 40km. In general the younger wall of the fracture valley stands higher than the older opposing wall but the older side, which has experienced transform tectonics, ofter exhibits steeper regional slopes and better defined topographic elements (Figure 1-12, e.g. profiles Q-Q', P-P', T-T').

At a distance of approximately 500km away from the transform midpoint, the morphotectonic signature of the fracture zone valley becomes obscured on each limb by massifs, the Atlantis massif on the east side and the Western massif on the west. The Atlantis massif

is clearly a seamount complex and consists of a number of major and minor peaks that rise from a common base enclosed by the 2800m contour and attain depths as shallow as 330m (Figures 9, 11). The Western massif is characterized by at least peaks (either horsts, thrust sheets, or seamounts) which rise from a base enclosed by the 4000m contour and reach depths as shallow as 2720m (Figures 1-8, 10).

Beyond these massifs the seafloor is characterized by a number of discontinuous parallel valleys and ridges for distances of at least 300km (the limit of the survey data; Figures 1-4,5,6,7). This distinctive fracture zone terrain exhibits a ENE-WSW striking fabric that is at least 100 km wide when measured along a north-south line. To the east of Atlantis massif the data define four valleys separated by ridges wnich have relief in some cases of over 1000m (Figure 1-12). Along the western fracture zone limb are three valleys separated by ridges with relief similar to their eastern counterpart (Figure 1-12). The fracture valleys, as defined by the locus of maximum depth, are mutually parallel and, although not well constrained by this data, the axes seem to be comprised of three distinct trend segments.

DISCUSSION

The morphology in and proximal to the Oceanographer transform provides an important perspective on the creation of crustal structures at a slowly accreting ridge-transform-ridge plate boundary. These data permit the recognition of several first-order

morphotectonic relationships that must be manisfestations of the tectonics of this type of plate boundary. In addition, these data place important constraints upon kinematic models of the relative motion history of North America-Africa and models of transform tectonics.

Present-Day Relative Motion Along the Oceangrapher Transform: The basement structre of the Oceanographer fracture zone represents the time-averaged product of transform tectonics. It is generally accepted that the strike of the elongate fabric comprising fracture zone terrain accurately reflects the relative motion history of the plate boundary at that location (e.g. Morgan, 1968; LePichon, 1968; LePichon et al., 1973). The veracity of this notion is dependent on the assumption that large scale topography represents, without significant distortion, the small-scale structures which form in response to instantaneous strike-slip tectonics. The general consistency between solutions derived from earthquake first motion studies and the trends of transform valley topography indicates that, to a first approximation, this assumption is valid. However, detailed interpretation of fracture zone trends in terms of relative motion history is unwarranted until we know how instantaneous deformation integrates in time and space to create the large-scale, morphotectonic fabric of the fracture zone domain. With this caveat in mind, the significance of the Oceanographer fracture zone trends are discussed in general terms.

The WNW-ESE trend of the Oceanographer transform has been an enigma in terms of kinematic models describing the present-day motion between North America-Africa since most, but not all, solutions (see Table 1) predict an E-W strike at this latitude. These models

have relied heavily upon on the trend of major transforms in the equatorial and central north Atlantic (e.g. Vema, Kane, and Atlantis) and the reconstruction of young (anomaly 5 or younger) magnetic anomalies that flank the ridge axis. First-motion studies by Sykes (1967) and Udias et al. (1976) of a 5.6 magnitude earthquake located along the Oceanographer transform also predict E-W slip along the Oceanographer transform instead of WNW-ESE slip. Moreover, the strike of the small-offset transforms located proximal to the Oceanographer (Figure 1-2) and those two degrees farther north in the FAMOUS area (Macdonald, 1977; Phillips and Fleming, 1978) is about E-W. Although it is intuitively reasonable to think that small-offset ridge-transform-ridge boundaries should more accurately reflect the relative motion between two plates, the trend of the features may deviate significantly from parallellism with inferred plate motion (Gallo et al., 1980).

Given the resolution limitations of the bathymetric data the fine-scale structures developed along the zone of principal displacement which reflect the structural manifestations of slip between North America-Africa cannot be elucidated. These results do, however, clearly demonstrate that the WNW-ESE trends dominate the large-scale fabric of the Oceanographer transform. The apparent incompatibility between the large-scale fabric of the Oceanographer transform and the kinematic models predicting E-W motion cannot be readily resolved but a few speculative interpretations can be offered. If E-W slip has been the dominant motion for a long time at the Oceanographer, then the transform, given its sense of offset and orientation, is under a component of compression; the second-order NE-SW lineaments observed disrupting the WNW-ESE fabric of the fracture walls (Figures 1-2,3)

might reflect structures formed in response to the compressive component.

Another possibility is that field mapping yields transform trends that are slightly but systematically different for right-lateral transforms than for left-lateral transforms. Thus the misfit of pole determinations could be an artifact of the manner that transform trends are determined. A third possibility is that the Vema transform may be part of an Africa/ North America/ South Africa triple junction rather than a North America/ Africa two plate system. Finally, the time-integrated first-order WNW-ESE morphotectonic expression of the transform domain could approximate the average slip over long periods of time (millions of years) but that at any given time or place within the principal transform displacement zone, the structures developed and the trends produced may be complex and at variance with the time-integrated terrain.

Evaluating these alternatives correctly is difficult because the data necessary to do so are incomplete. Alternative one requires that the major disruptions of the north wall are the adjustment fractures of Menard and Atwater (1968) that form whenever a transform is placed in compression. A different interpretation of these disruptions of the north wall is that the structures are oblique terrain elements formed at the eastern ridge-transform intersection and translated west. Ocean-bottom seismometer studies by Rowlett (1980) demonstrate that the easternmost break in the north wall is seismically active thereby lending some credence to alternative one. However, the observed seismicity is also consistent with the formation of oblique structures.

Alternative two hinges upon an inferred relationship between

the sense of offset of the transform and the resulting pole determination. A possibility exists that the average morphotectonic trends of the transforms may be systematically different from the actual slip direction. This result could ensue if the principal transform displacement zone goes from the younger side of one ridge-transform to the younger side of the other ridge-transform intersection. In the case of the misfit of the Oceanographer transform trend with that of the Vema and the Kane transforms, the misfit is exacerbated by the preceding scenario. If the scenario is reversed, and the principal transform displacement zone goes from the older side of one ridge-transform intersection to the older side of the other ridge-transform intersection, then the misfit of the transforms is lessened. The only data to test this alternative were recovered from the Vema transform where it was discovered that the principal transform displacement zone went from younger wall to younger wall, just the opposite of what was needed to improve the fit of the transforms (P.J. Fox, pers. comm.).

Little data exist to test alternative three although Minster and Jordan (1978) have indicated that relative motion may occur between North America and South America. Thus the Vema transform may be indicative of North America-South America plate motion whereas the Kane and Oceanographer transforms reflect pure North America-Africa plate motion. While this could explain the misfit of the Vema and the Oceanographer transforms, it does not improve the Kane-Oceanographer misfit, so this alternative may be ruled out.

The final alternative is the most difficult to assess because it requires knowledge about the long term characteristics of transforms

versus their short-term behavior. Data collected during the summer of 1980 by the OTTER Scientific Team showed no evidence for large-scale readjustments in the central portion of the Oceanographer transform but that study was not designed to map structures formed in response to the readjustments. The study was designed instead to map small-scale faulting; megashears would have been difficult to detect even if present. Thus alternative four cannot be assessed on the basis of the available data.

Clay model experiments and the study of continental shear zones by Tchalenko (1970) and Wilcox and others (1974) show that strike-slip zones are characterized by second order en echelon folds, thrust faults and faults with both strike-slip and dip-slip components of motion. Submersible investigations with transform A (FAMOUS area: ARCYANA, 1975; Choukroune et al., 1978) and Deep-Tow studies of the Quebrada transform (Lonsdale, 1978) indicate that evidence for recent tectonism is confined to a very narrow zone less than a kilometer wide and is defined by the axis of maximum depth along the transform (Choukroune et al., 1978). This principal transform displacement zone is not characterized by one single fault, rather it is comprised of a family of anastomozing strike-slip lineaments that are linked together by relay zones. These structures are not steady-state but evolve in different ways creating complexly arranged terrain elements. Until high resolution surveys at a regional scale of the transform domain are implemented, it remains to be determined what the actual slip direction is along the Oceanographer transform and how the tectonics of the strike-slip domain

integrates in time and space to create the first-order morphologic fabric of the seafloor.

Central North Atlantic Plate Motion: Using magnetic anomaly data and/or the azimuths of Central North Atlantic fracture zones, Pitman and Talwani (1972), Francheteau (1973), and Collette et al. (1974) have computed plate motions for the Cenozoic relative history of North America-Africa (Table 1). Limits in these two types of data only allow finite difference relative motion solutions for intervals on the order of 10 million years or more. Although these models all differ in detail, the models predict that from the Quaternary to the Paleocene the relative motions of North America with respect to Africa in the vicinity of the Oceanographer fracture zone was 0^{o} to 15^{o} north of west (Table 1). The bathymetric data for the limbs of the Oceanographer fracture zone are consistent with these predictions (Figure 1-14). In fact, the data define three distinct azimuth components for this time of northwest relative motion suggesting that this Tertiary phase of NW-SE motion for North America-Africa could be more accurately be described by a least three poles of relative motion.

The work of Pitman and Talwani (1972) indicates that there was a major change in the spreading direction along the North America-Africa plate boundary at approximately 63 m.y.B.P. (anomaly 25). Along the plate boundary proximal to the Oceanographer fracture zone, finite difference solutions prior to anomaly 25 indicate approximate east-west relative motion; after anomaly 25 motion changed to NW-SE. As predicted by Pitman and Talwani, the Oceanographer fracture zone bathymetric data documents a major change in the azimuth of the fracture zone with the structural lineaments

changing strike from N89E to N73W at a distance of approximately 500km from the center of the transform (40 m.y.B.P.). Important differences in the morphotectonic style of the fracture zone domain correlate with the pronounced clockwise change in the regional fracture zone trend. Prior to the change in relative motion, several east-west striking ridges and valleys characterize the seafloor and suggest that this portion of the North America-Africa plate boundary was dominated by transforms linked by short ridge segments, a plate boundary geometry analogous to the Equatorial Atlantic. The change in relative motion resulted in a new plate geometry defined by a single transform with a WNW-ESE trend and suggests a significant reorganization in the ridge/transform/ ridge geometry. Reorientation of the slip vector from E-W to WNW-ESE indicates a clockwise shift in the pole of relative motion and such a change subjects a transform with left-lateral motion to a component of extension during the period of plate boundary adjustment. Large topographic highs are positioned between the two differently trending segments along the limbs of the Oceanographer fracture zone and they could represent volcanic edifices created by the leaking of basalt magmas along this portion of the plate boundary in response to extension caused by the pole change. This situation is analogous to the leaky transform phenomenon predicted by Menard and Atwater (1968, 1969) during their consideration. of transform tectonics and changes in the pole of relative motion.

Although not well constrained, the magnetic anomaly sequence for the central North Atlantic (Pitman and Talwani, 1972; Cande and Schouten, pers. comm.) indicates that this major change in the

Tertiary relative motion history of North America-Africa, which initiated the alteration in the ridge-transform-ridge geometry in the Oceanographer area, occurred at approximately anomaly 21 time (53 m.y.B.P.; Figure 1-14). Purdy and Rabinowitz (1976) in an investigation of the Kane fracture zone document that at approximately the same time the structural grain of the fracture zone changes from SW-NE to NW-SE.

Morphotectonic Fabric of Ridge-Transform-Ridge Intersections: The along-strike morphology of the northern and southern rift valleys is quite similar. The rift valley floor of both ridge segments have depth and width maximums where they intersect the Oceanographer transform and secondary maximums at the minor transforms located approximately 85km to the north and 65km to the south of the Oceanographer (Figures 1-2,5). Each rift valley segment narrows and shoals over distances of 40 to 50km towards the midpoint between the transforms. Our bathymetric data also shows that at the point midway between truncating transforms the rift valley exhibits the least relief and the crestal mountains, in general, are at their shallowest levels. As the transform intersections are approached, the relief of the valley walls increases and the depth to the crest of the rift mountains becomes greater except right next to the ridge-transform intersection where the topography shoals. These systematic, along-strike and gradual changes in morphology indicate that the depth of basalt emplacement and the timing and magnitude of crustal uplift along the rift valley is, for some reason, related to distance from the transforms that bound each ridge segment. Furthermore, the magnitude of these morphologic changes increases as the length of the transform offset

becomes greater.

Other well-mapped, slowly-slipping ridge-transform-ridge intersections exhibit similar along-strike morphologic changes (FAMOUS Rift-Needham and Francheteau, 1974; Macdonald and Luyendyk, 1977; Ridge south of FAMOUS- Ramberg and van Andel, 1977; Phillips and Fleming, 1978; Kane transform- Fox, 1972; Purdy and Rabinowitz, 1981). These systematic variations in morphologic parameters must reflect fundamental changes in the processes that are responsible for the creation of sea floor topography but definitive explanations must await the acquisition of high-resolution bathymetric and geophysical data. However, the significance of this distinctive morphotectonic fabric can be interpreted in the context of models that are presently in the literature.

Sleep (1969) and Osmaston (1971) proposed that heat lost by ascending magma to the conduit walls defining the edges of a slowly accreting plate boundary results in increased viscous drag and a loss of hydraulic head which, in turn, prevents the upwelling asthenosphere from rising to a level of isostatic equilibrium. Sleep and Biehler (1970) reasoned that at a ridge-transform intersection the juxtaposition of a cold edge of old lithosphere against the axis of plate accretion introduces a third thermal boundary enhancing viscous drag and hydraulic head loss in the ascending welt of asthenosphere. This thermal edge-effect model nicely explains the deep, closed-contour depressions known to characterize slowly-slipping ridge-transform-ridge intersections. The along-strike relationship between depth of the rift valley floor and distance to a transform is compatible with the Sleep and Biehler (1970) model, but the data presented here suggest that the upwelling asthenosphere

thermally senses and is affected by the presence of a transform over distances of 40 to 50 kilometers.

It has been argued elsewhere (Fox, 1978; Gallo and Fox, 1981) that the systematic increase in depth of the rift valley proximal to a transform is not solely a product of viscous head loss but is a bathymetric manifestation of along-strike changes in the properties of the oceanic lithosphere. The cold side of a transform lowers the temperature in the wedge of asthenosphere rising beneath the axis of accretion reducing the volume of basaltic partial melt derived from the source region and deflects downwards the lithosphere-asthenosphere isotherm (the thermal age of the lithosphere is greater than its chronological age). At the ridge-transform intersection, where the heat-sink effect is greatest, a minimum of basaltic melt is generated, the crust is very thin and the lithosphere is thick; with increasing distance from the transform boundary the edge effect decays, the amount of partial melt increases, the crust thickens and the underlying lithosphere thins. A corollary to this model is that there are profound changes in the distribution of mass parallel to isochrons as the fracture zone boundary is approached. This notion is supported by the fact that the depth of the crust comprising the foundation of a transform valley and fracture zone limbs is well below the elevation of oceanic lithosphere of similar age suggesting a marked contrast in density structure of rock bodies within transform valleys (Cochran, 1973; Robb and Kane, 1975; Detrick and Purdy, 1980; Fox et al., 1980). For a very young lithosphere depth to the floor of the rift valley increases steadily towards the transform for considerable distances (Figure 1-9). Furthermore, the depth along the crest of the rift mountains and

the depths along topographic profiles oriented perpendicular to the Oceanographer generally increase as the fracture zone boundary is approached (Figures 1-9,12). Probably the great relief associated with fracture zones, the deep trough flanked by high terrain that is recognized irrespective of plate age, has little to do directly with the structural manifestations of strike-slip tectonics. Rather, the distinctive lineated morphotectonic grain reflects marked changes in the distribution of mass at shallow levels in the oceanic lithosphere. High resolution, regional scale maps must be made of large segments of the world encircling plate boundary to test for systematic changes in morphology and depth to the sea floor adjacent to a suite of transforms.

The rift valley is narrowest and the relief of the rift walls is least at a point approximately midway between the two transforms; away from this point the valley steadily widens and its relief steadily increases as the transform intersections are approached (Figure 1-2). Woodside (1972) has shown that the rift valley floor of the Mid-Atlantic Ridge at $48^{o}N$ is not in isostatic equilibrium but that the bounding crestal mountains are compensated. Isostatic recovery results in the incremental uplift of lithospheric packets as the seafloor moves up and away from the axial zone of plate accretion creating the step-like relief of the rift walls. The driving force for the uplift of a block at the outermost margin of the valley could reflect the effects of viscous forces produced by a rising asthenosphere diapir along the plate boundary (Sleep, 1969; Osmaston, 1971; Lachenbruch, 1973, 1976; Sleep and Rosendahl, 1979). The reason for the marked change in morphology of the rift valley

is not well constrained, but it seems clear that the timing of the onset of isostatic recovery of the lithosphere and the amount of uplift are influenced by the cold edge of the transform.

The magnitude of crustal uplift also appears to be related to rift valley-transform geometry. At each of the four rift valley-transform intersections, peaks on the side of the ridge that abuts the active transforms are higher than the opposing mountains on the opposite side of the rift that face a seismically inactive limb of the fracture zone (Figure 1-2,9).

Morphotectonic Fabric of the Oceanographer Transform: The morphology of the Oceanographer transform is variable along and across strike and is comprised of several important structural provinces that create the distinctive and complex morphotectonic fabric of the transform valley. The floor of the transform is exceedingly narrow ($<$ 2km wide as defined by the deepest 200m contour recognized at any point along the valley floor, Figure 1-2) and can be described best as a line of maximum depth sandwiched between the two transform valley walls. Recent tectonism within and along portions of the Oceanographer transform (OTTER, 1980; unpub. data). and Transform A (Choukroune et al., 1978), as documented by submersible and deep sea camera data, is confined within a narrow zone no wider than 2km that is centered about the axis of maximum depth. These field relationships indicate that the principal transform displacement zone slowly-slipping transform faults ($<$ 4 cm/yr slip rate) is narrow and located along the transform axis. This focusing of tectonism within a narrow swath (2km) is a consequence of the relatively thick lithosphere that characterizes the transform fault boundary making it difficult, except for large changes in plate geometry caused by excursions in the pole of relative

motion, for the location of transform tectonism to migrate.

Detailed investigations of portions of several oceanic transforms (Transform A - Detrick et al., 1973; ARCYANA, 1975; Choukroune et al., 1978; Siqueiros - Crane, 1976; Quebrada - Lonsdale, 1978; Tamayo - Macdonald et al., 1979; CYAMEX and Pastouret, 1981; Tamayo Scientific Team, 1980a, b, c and in preparation; Oceanographer - OTTER, 1980, unpub. data) demonstrate that the surficial expression of the PTDZ is comprised of a family of anastomosing faults with orientations both parallel to the morphology of the transform and oblique to this trend. Fault traces that parallel the transform are discontinuous along strike and are offset by basins or ridges interpreted to represent extensional or compressional relay zones, respectively. In plan view (Figure 1-12), the axis of maximum depth of the Oceanographer has an overall trend of WNW-ESE but this trend is offset by two 10-15km long segments striking NE-SW. Given left lateral strike-slip motion along this transform, these two NE-SW striking segments probably represent extensional relay zones.

Along the transform axis a profile of maximum depth (Figure 1-11) defines an undulating seafloor with changes of relief ranging from 300m to 1000m. The origin and geologic significance of relief elements observed along the length of the transform are not easy to resolve unambiguously. A continuous linear parcel of crust accreted at each truncated accreting plate margin will travel along the transform valley and experience the panoply of transform tectonic effects - multiple igneous and metamorphic events and complex styles of deformation (Fox and others, 1976; Bonatti and

Honnorez, 1976; Karson and Dewey, 1978).

In general terms, the processes that condition the evolution of crust within a ridge-transform-ridge boundary will begin with the emplacement of a packet of rock along the transform fault at the accreting boundary. The juxtaposition of a cold edge of lithosphere against the zone of accretion will decrease the amount of basaltic melt generated in the underlying asthenosphere resulting in anomalously thin crust. The newly accreted crust within the transform valley will create complex igneous and metamorphic relationships with the older pre-existing tectonized crust which has passed through the transform domain (for a full explanation of the geologic complexities, see Karson and Dewey, 1978). The thermal sink of the transform boundary also results in crustal emplacement at a level below isostatic equilibrium (Sleep and Biehler, 1970) creating the depth maxima observed at the ridge-transform boundaries (Figure 1-2,11). Deep depressions dominate the morphology of the ridge-transform intersections, but these features shallow by 500-1500m over distances of 10km to 20 km towards the inactive fracture zone indicating that after emplacement of incremental parcels of crust, the crust isostatically rebounds seeking an equilibrium elevation along the axis of the fracture zone. A portion of the newly accreted crust is destined to pass through the principal transform displacement zone and will be subjected to brittle fracturing at shallow levels and ductile deformation at depth. As already outlined a complex, spatially and temporally variable fault pattern will characterize the shear zone with faults bounding slivers of crust which will be free to move with respect to one another. Furthermore, these faults will

create a network of permeable interconnected pathways that will cut through the thin crust allowing water to penetrate to depth and react with ultramafic rock at elevated temperatures and pressures. Metamorphism and hydration of rock bodies at depth will alter the density of blocks thereby contributing to vertical tectonism within the transform. Finally as a packet of rock leaves the transform domain, the rock body, as mentioned above, will be affected by thermal, metamorphic and igneous processes associated with the truncated accreting plate boundary (Karson and Dewey, 1978).

The tectonics within and proximal to the transform will be even more complex if, as some evidence suggests, the PTDZ does not approximate an arc of a small circle about the instantaneous pole of relative motion. Geological relationships along the boundary will change through time as the transform complex continuously seeks a copolar relationship with the instantaneous pole of relative motion (Dewey, 1975). Extension and resulting fracturing within the transform domain leads to additional serpentinization of ultramafics and to the production of several distinct kinds of terrain elements such as horsts and grabens. Compression will result in the mobilization of serpentinite bodies already in place along the transform domain and/or thrusting and resultant uplift of some rock bodies. The complexity of deformation of any rock body formed proximal to a transform is apt to be enormous and difficult to unravel. Thus the time-averaged products of that deformation which are the subject of this paper are not easily interpreted in terms of specific sites or kinds of deformation.

SUMMARY AND CONCLUSIONS

This analysis of the morphotectonic elements of the Oceanographer transform and adjacent ridge crests has provided constraints on the evolution of seafloor on a large scale and on an intermediate scale. The rift valley floor slopes systematically towards the bounding transform faults over distances as much as 50km. The width of the rift valley above any arbitrary isobath increases in tandem with an increase in depth to the rift valley floor. Also the crestal mountains facing the inactive fracture zone limb stand somewhat higher at the ridge-transform intersection than the crestal mountains facing the transform.

The Oceanographer transform has up to 3000m relief, a sinuous axis of maximum depth, and is bounded along the south by an E-W trending ridge that is roughly 20km wide above the 2000m isobath. The ridge to the north of the axial deep is not as continuous as the southern ridge and is interrupted by several N-S embayments. The finer details of the two sides of the transforms are similar and are comprised of numerous steep escarpments several hundred meters high connected by terraces of varible width that integrate to create the great relief of the transform. Deep, broad depressions characterize both ridge-transform intersections although the eastern intersection depression is deeper and better defined than the western intersection depression.

The seafloor morphology and the basement morphology were mapped out to a distance of 900km on either side of the transform thereby serving to define more precisely the relative motion of North-Africa. Much of the up to 3000m relief of the transform diminishes

just beyond the ridge-transform intersection. The loss of relief is presumably accomplished by faulting although details of the nature of this faulting are unclear. As the crust ages little additional relief is lost and the ridges flanking the fracture zone trough stand above it several hundred to over a thousand meters. Large massifs disrupt the fabric of the seafloor on either limb of the fracture zone and these massifs seem to be related to a major change in the pole of relative motion for North-America-Africa. In addition to this major change in the pole of relative motion five other changes in the azimuth of the fracture zones suggest that the Tertiary phase of seafloor in the Central Atlantic can best be described by six discrete rotations about six different poles.

On either side of the seamount massifs the character of the seafloor is markedly different. The younger seafloor in the vicinity of the Oceanographer transform consists of a single, well-defined valley bordered by high-standing fracture zone ridges whereas the older terrain beyond the massifs consists of several individual troughs separated by ridges. Although there is considerable variation along each limb in terms of their depths, the walls and the valley(s) subside as they age.

A major finding of this survey is that the process of crustal generation seems to be affected by the presence of transforms up to distances of 50km from the faults. Since the spacing of transforms in the Atlantic is usually 100km or less, then the entire fabric of the seafloor in slow spreading centers may be to some degree influenced by transform faults. One probable consequence is that the crust is likely to thin near the transform due to the cold,

adjoining plate which will tend to reduce the amount of basaltic fluid which is segregated. Thus strips of seafloor will be created parallel to the transform of differing petrologic and possibly different seismic properties. As the seafloor ages the initial differences of these parcels of seafloor may lessen and the seismic properties between crust affected by transforms and that which is not may diminish.

Figure 1-1 Index map showing the location of the of the Oceanographer transform with respect to other major features

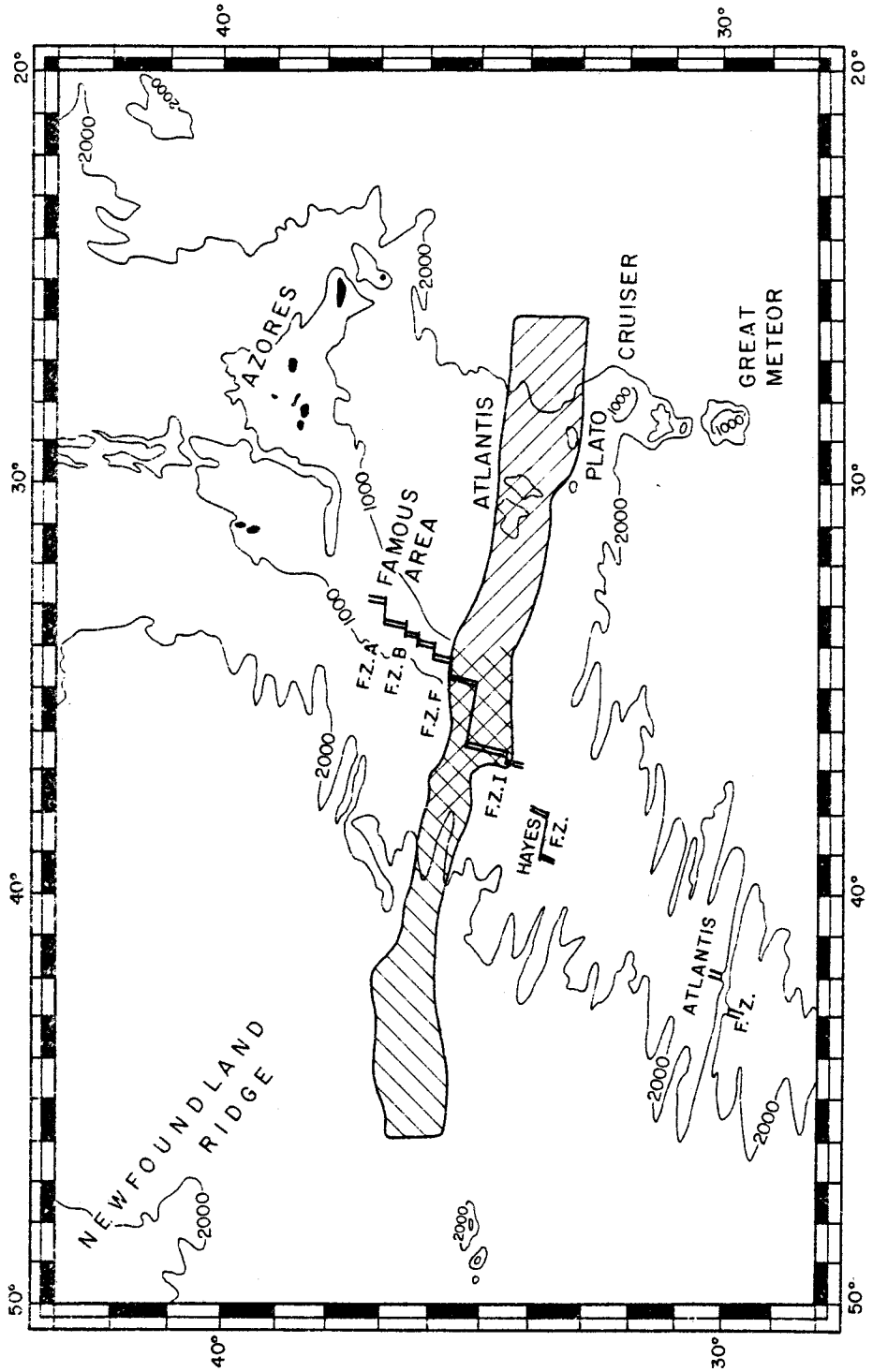
40°
30°
20°
50°
2000
1000
AZORES
FAMOUS AREA
ATLANTIS
PLATO
CRUISER
GREAT METEOR
F.Z.A
F.Z.B
F.Z.F
F.Z.I
HAYES F.Z.
ATLANTIS F.Z.
NEWFOUNDLAND RIDGE

Figure 1-2 Bathymetric map of the Oceanographer transform

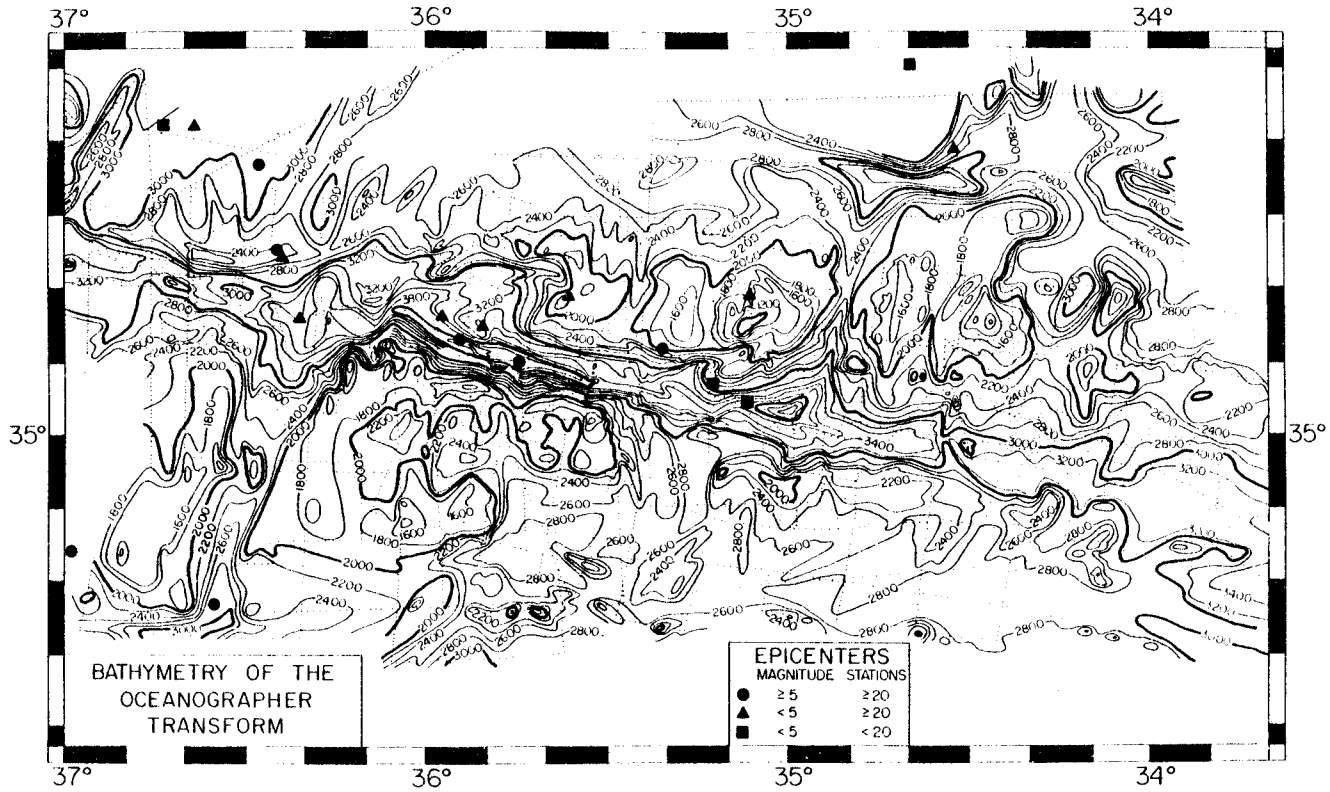
37°
36°
35°
34°
35°
BATHYMETRY OF THE
OCEANOGRAPHER
TRANSFORM
EPICENTERS
MAGNITUDE STATIONS
≥5 ≥20
<5 ≥20
<5 <20

Figure 1-3 Physiographic map of the Oceanographer transform

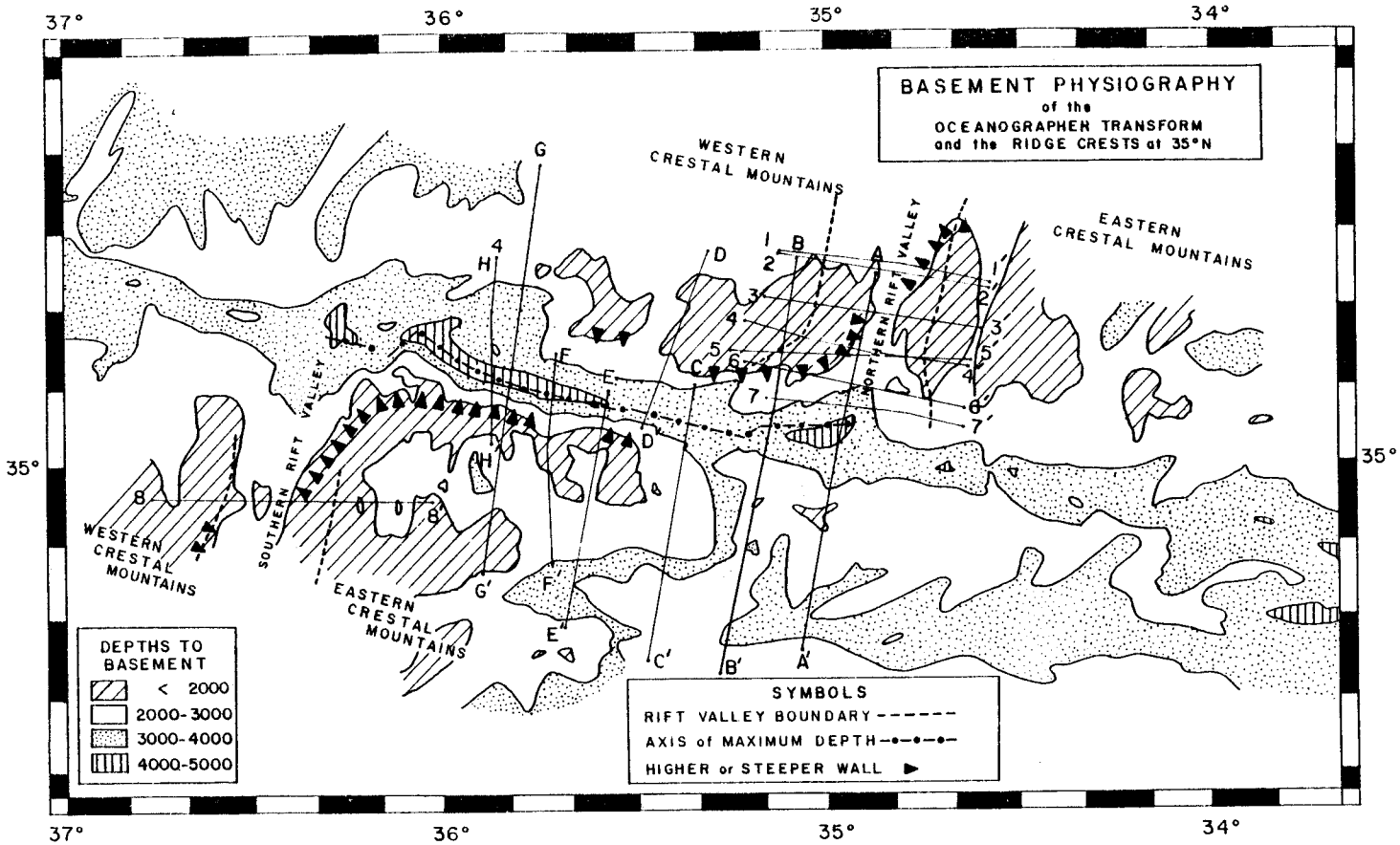
37°
36°
35°
34°
BASEMENT PHYSIOGRAPHY
of the
OCEANOGRAPHER TRANSFORM
and the RIDGE CRESTS at 35°N
WESTERN CRESTAL MOUNTAINS
EASTERN CRESTAL MOUNTAINS
SOUTHERN RIFT VALLEY
NORTHERN RIFT VALLEY
WESTERN CRESTAL MOUNTAINS
EASTERN CRESTAL MOUNTAINS
DEPTHS TO BASEMENT
< 2000
2000-3000
3000-4000
4000-5000
SYMBOLS
RIFT VALLEY BOUNDARY
AXIS of MAXIMUM DEPTH
HIGHER or STEEPER WALL

Figure 1-4 Bathymetry and physiography of the Oceanographer transform and the eastern fracture zone limb

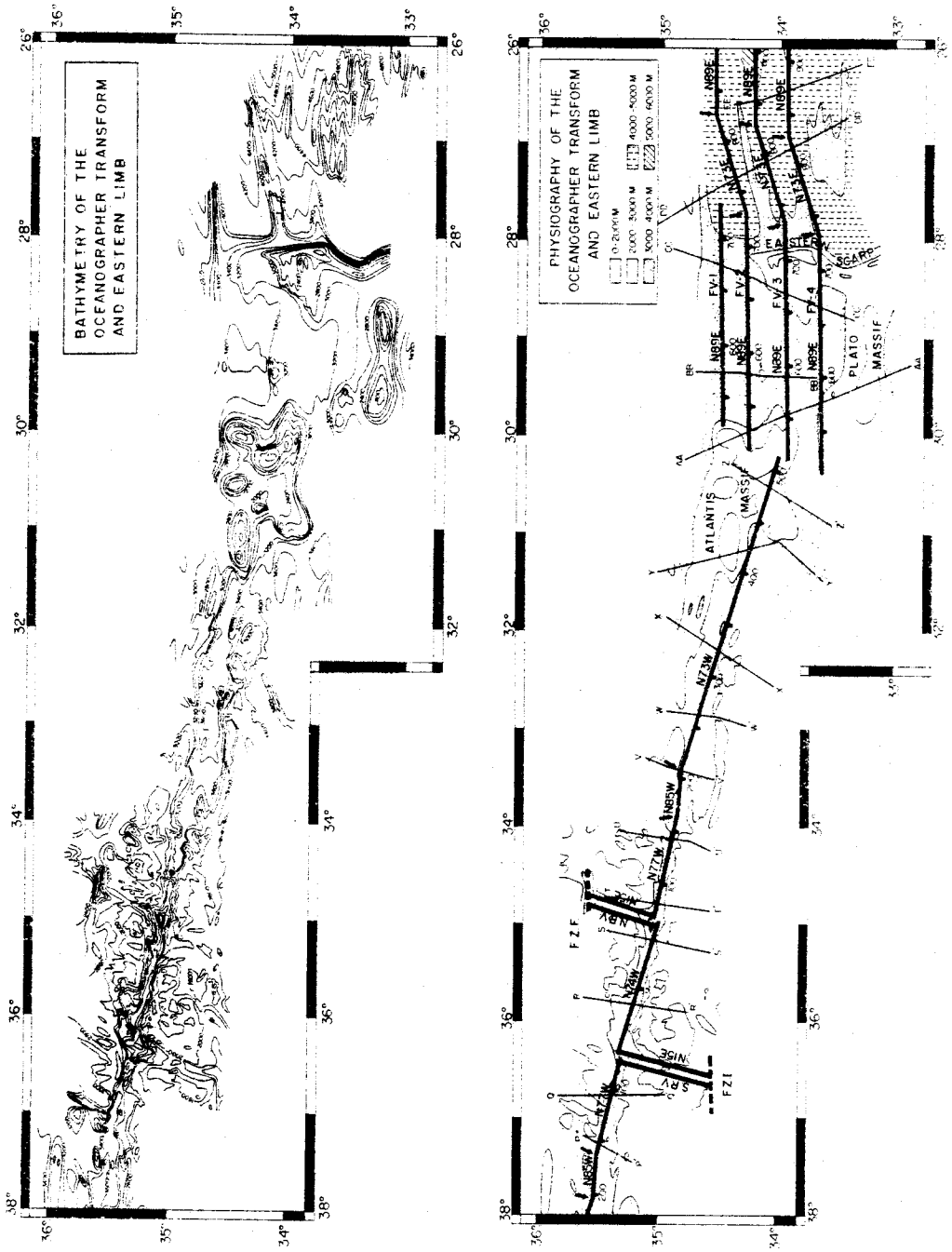
BATHYMETRY OF THE
OCEANOGRAPHER TRANSFORM
AND EASTERN LIMB
PHYSIOGRAPHY OF THE
OCEANOGRAPHER TRANSFORM
AND EASTERN LIMB
0-2000 M
2000-3000 M
3000-4000 M
4000-5000 M
5000-6000 M
ATLANTIS
(MASSIF)
PLATO
MASSIF
ESCARPMENT
FZF
FZI
FV1
FV2
FV3
FV4
N85E
N85W
N73W
N73E

Figure 1-5 Bathymetry and physiography of the Oceanographer transform and western fracture zone limb

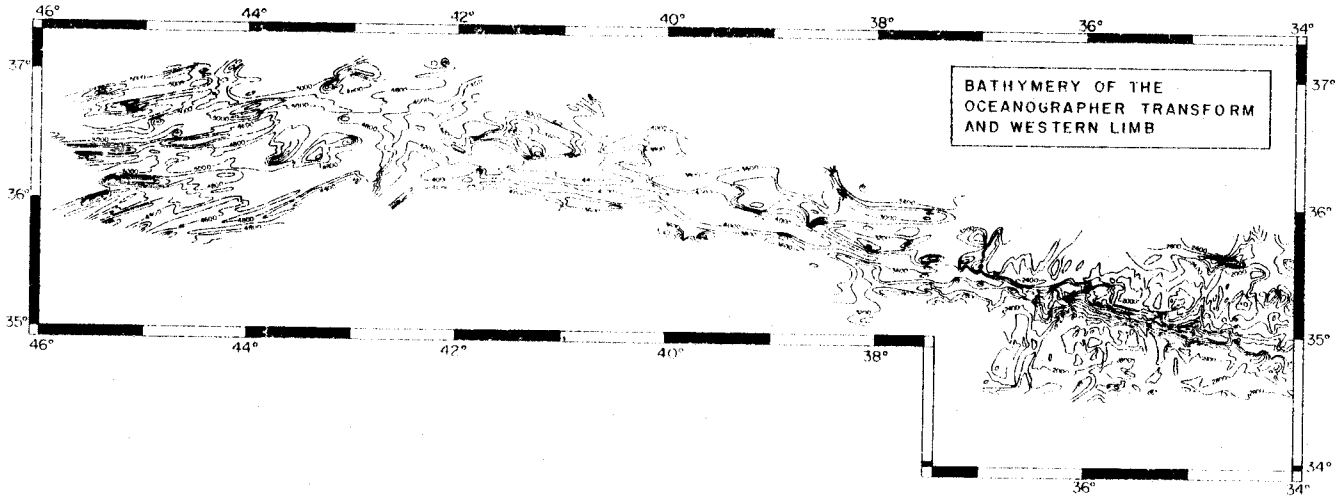
BATHYMERY OF THE
OCEANOGRAPHER TRANSFORM
AND WESTERN LIMB
46°
44°
42°
40°
38°
36°
34°
37°
36°
35°

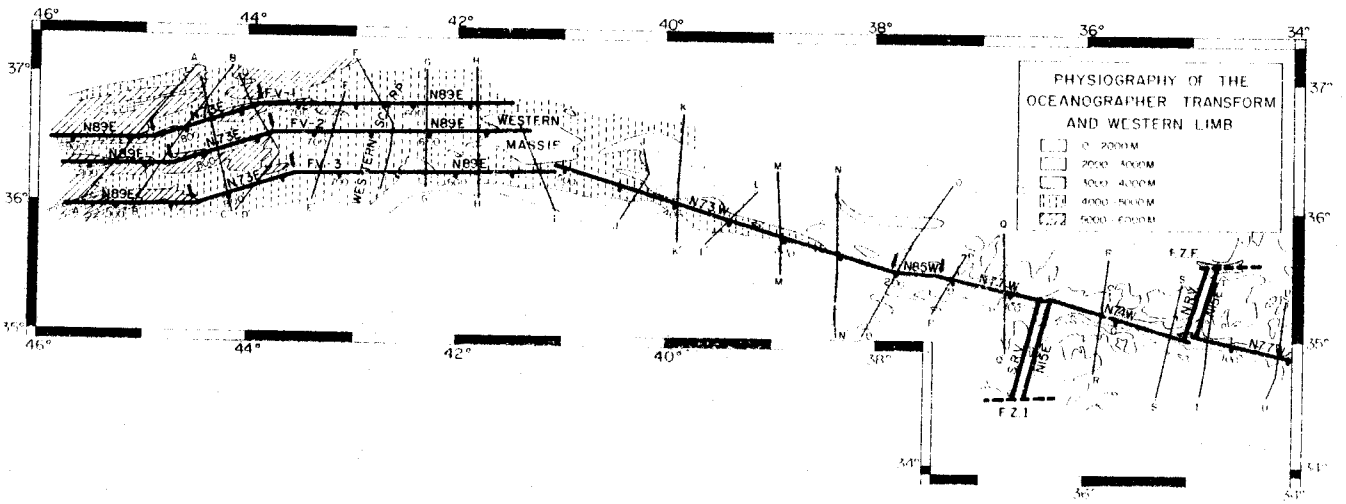
PHYSIOGRAPHY OF THE
OCEANOGRAPHER TRANSFORM
AND WESTERN LIMB
FV 1
FV 2
FV 3
N83E
N71E
N61E
WESTERN
MASSIF
N73W
N85W
N72W
FZ F
FZ E
FZ D
FZ C
FZ B
FZ A
FZ 1
46°
44°
42°
40°
38°
36°
34°
37°
36°
35°

Figure 1-6 Basement topography and physiography of the Oceanographer transform and western fracture zone limb

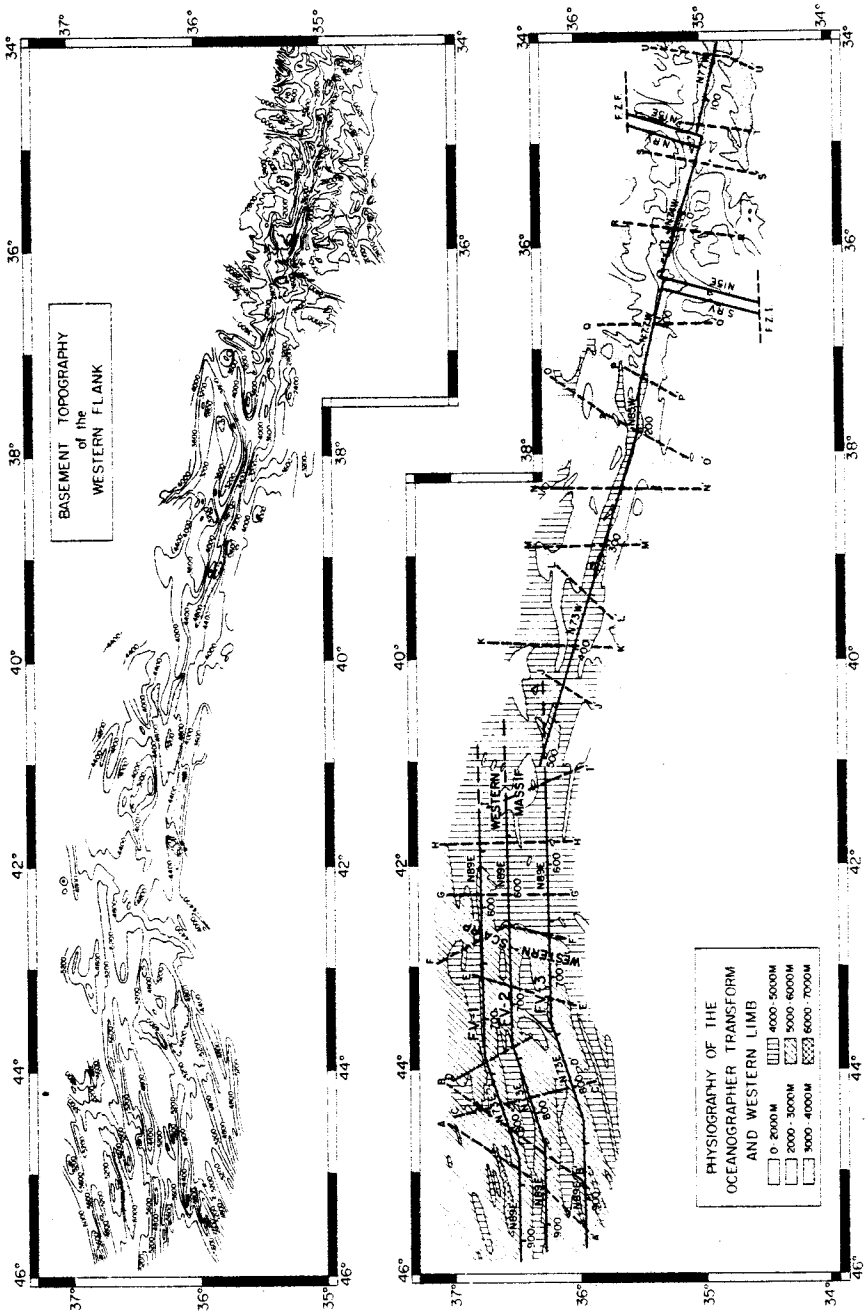
BASEMENT TOPOGRAPHY
of the
WESTERN FLANK
PHYSIOGRAPHY OF THE
OCEANOGRAPHER TRANSFORM
AND WESTERN LIMB
0-2000M
2000-3000M
3000-4000M
4000-5000M
5000-6000M
6000-7000M
WESTERN
MASSIF
FZ1
FZ2
FZ3
FZF

Figure 1-7 Basement topography and physiography of the Oceanographer transform and eastern fracture zone limb

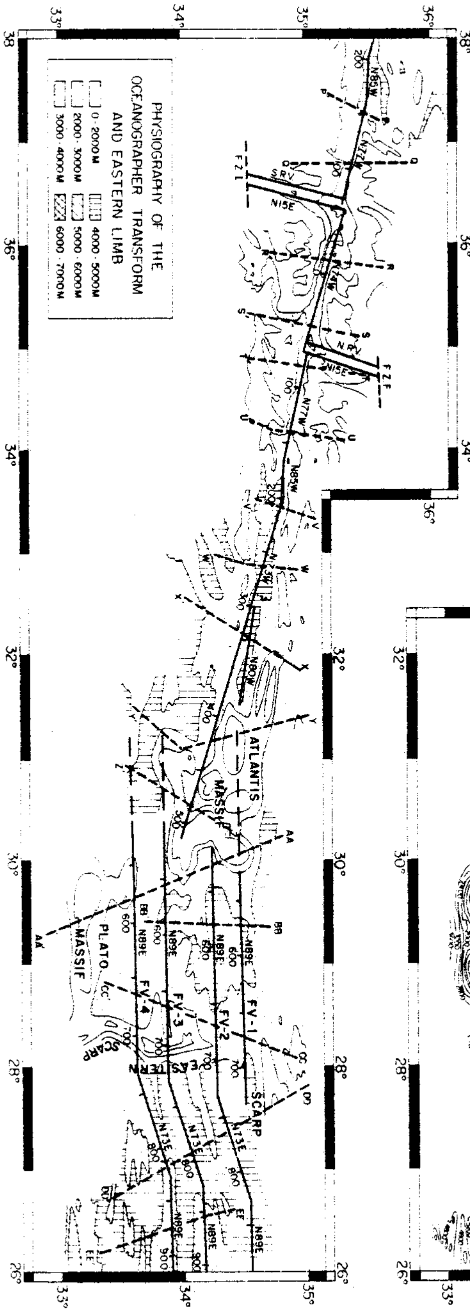
PHYSIOGRAPHY OF THE
OCEANOGRAPHER TRANSFORM
AND EASTERN LIMB
0-2000M
2000-3000M
3000-4000M
4000-5000M
5000-6000M
6000-7000M
ATLANTIS
MASSIF
PLATO
MASSIF
EASTERN
SCARP
SCARP
FV-1
FV-2
FV-3
FV-4

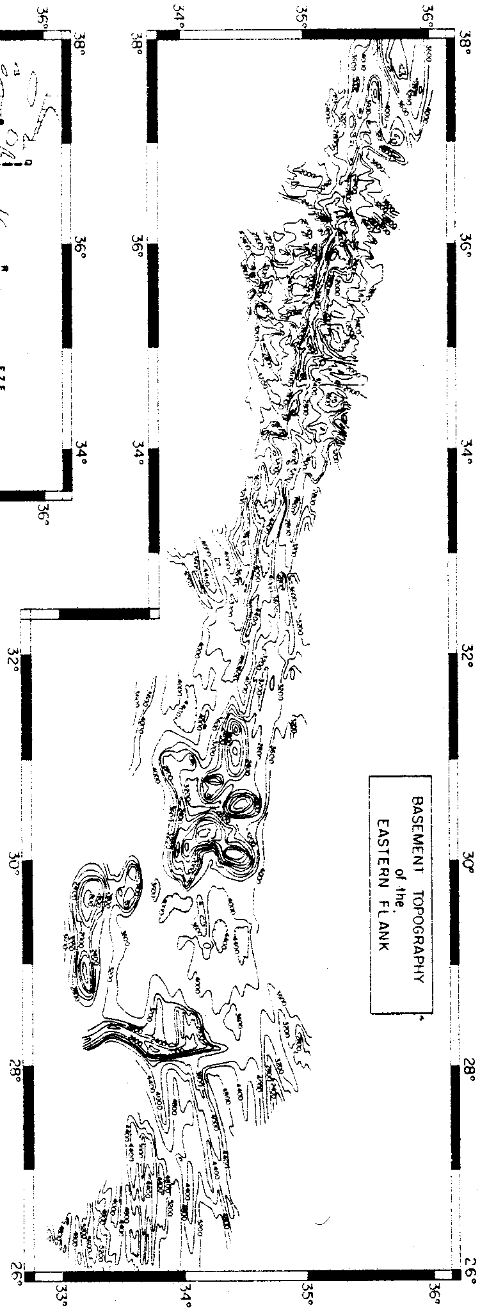
BASEMENT TOPOGRAPHY
of the
EASTERN FLANK

Figure 1-8 Bathymetric profiles of the northern and southern spreading ridge segments. Locations shown on Figure 1-3

NORTHERN RIDGE

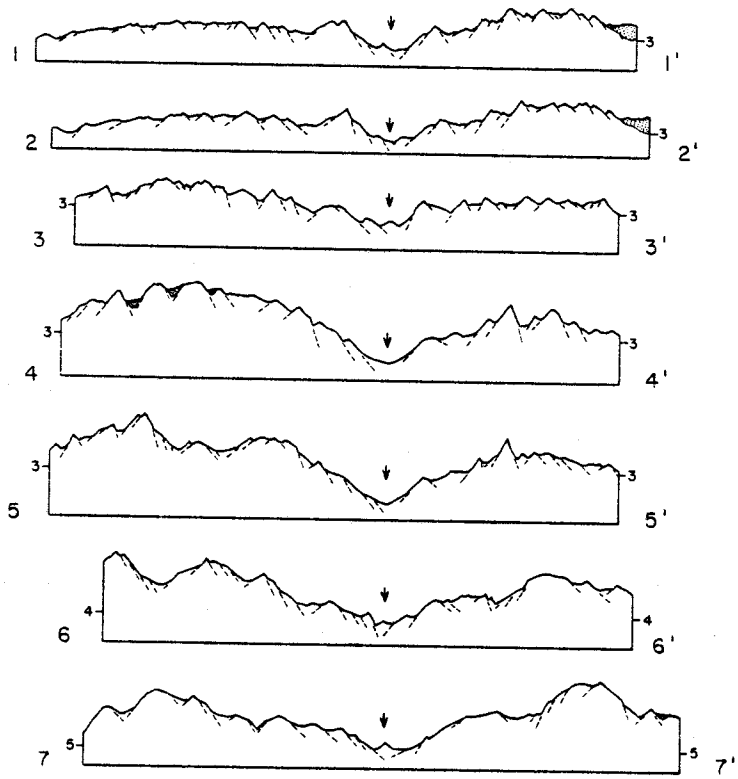

SOUTHERN RIDGE

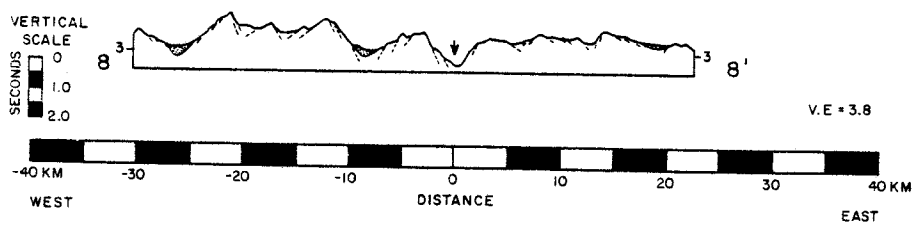

Figure 1-9 Depth versus distance and relative elevation plots for the Oceanographer transform and associated ridge crests

a.

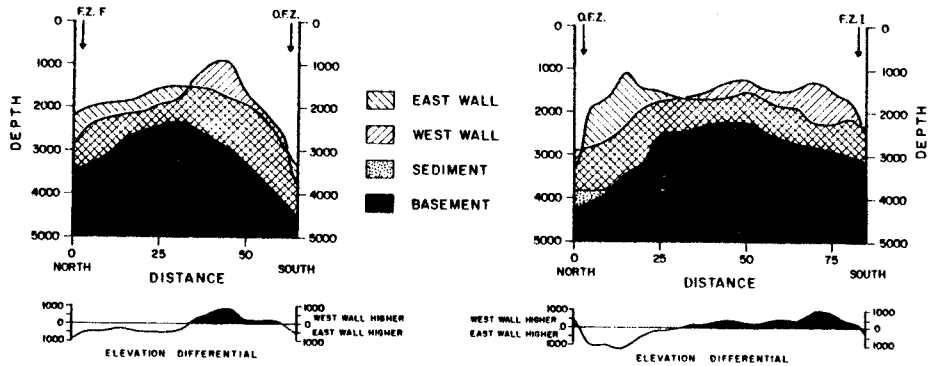

b.

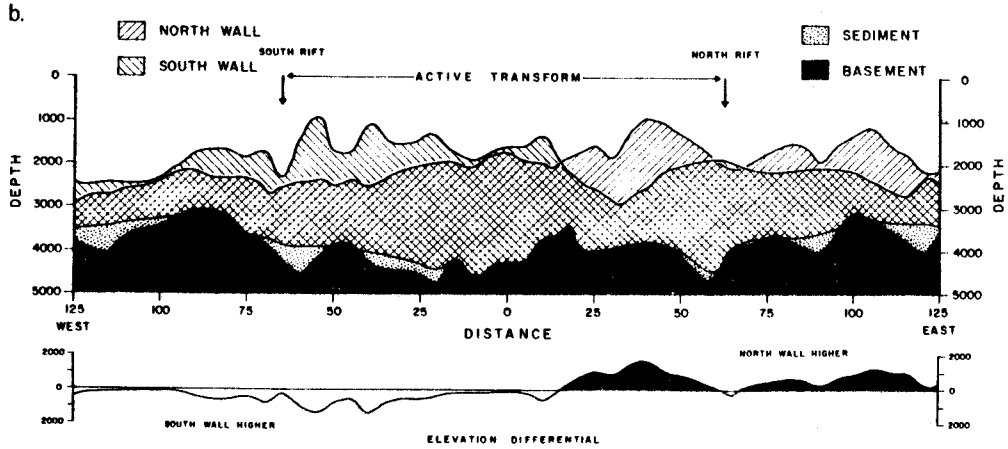

OCEANOGRAPHER TRANSFORM

Figure 1-10 Profiles across the Oceanographer transform
Locations shown in Figure 1-3

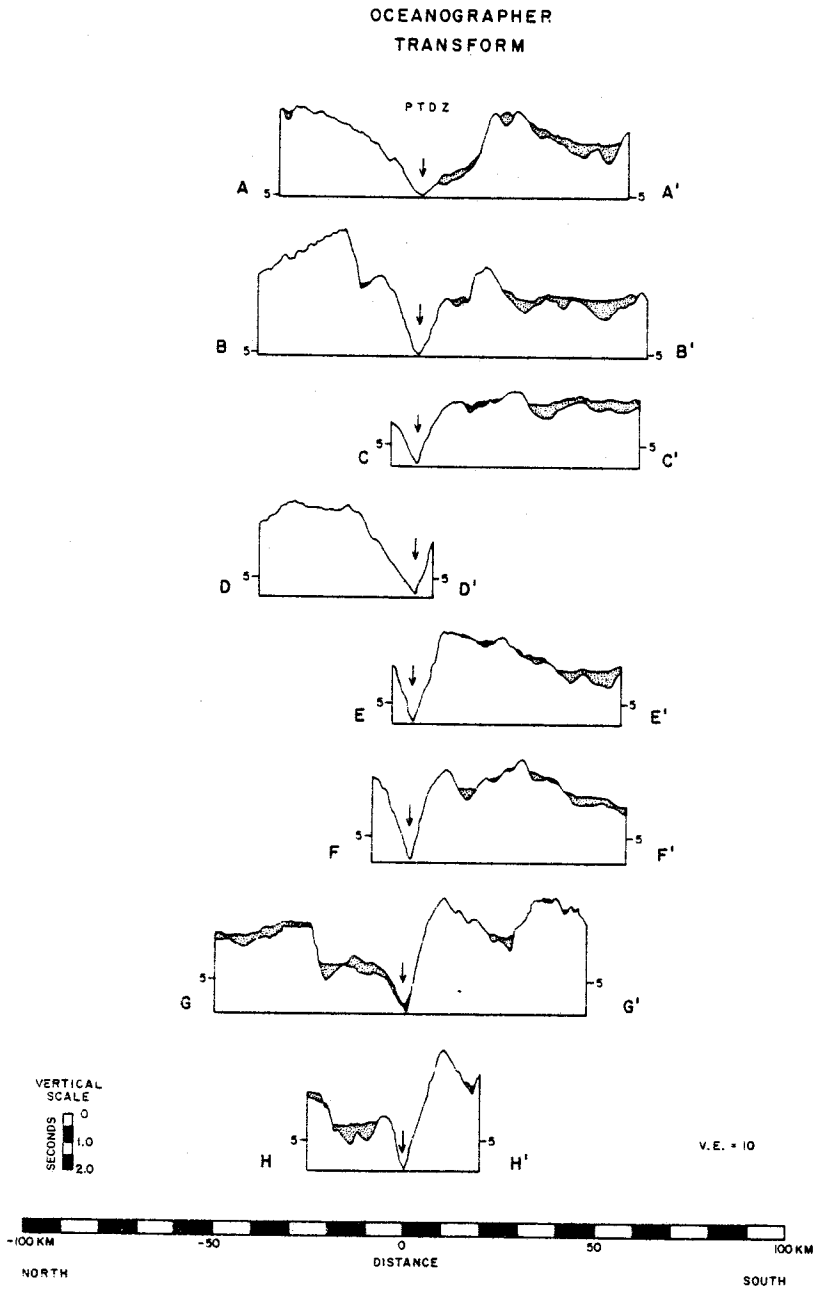
OCEANOGRAPHER
TRANSFORM
PTDZ
A
5
5
A'
B
5
5
B'
C
5
5
C'
D
5
5
D'
E
5
5
E'
F
5
5
F'
G
5
5
G'
H
5
5
H'
VERTICAL
SCALE
SECONDS
0
1.0
2.0
V.E. = 10
-100 KM
-50
0
50
100 KM
DISTANCE
NORTH
SOUTH

Figure 1-11 Down-axis profile of the Oceanographer transform and fracture zone extensions and elevation differentials

DOWN AXIS PROFILE OF THE OCEANOGRAPHER FRACTURE ZONE

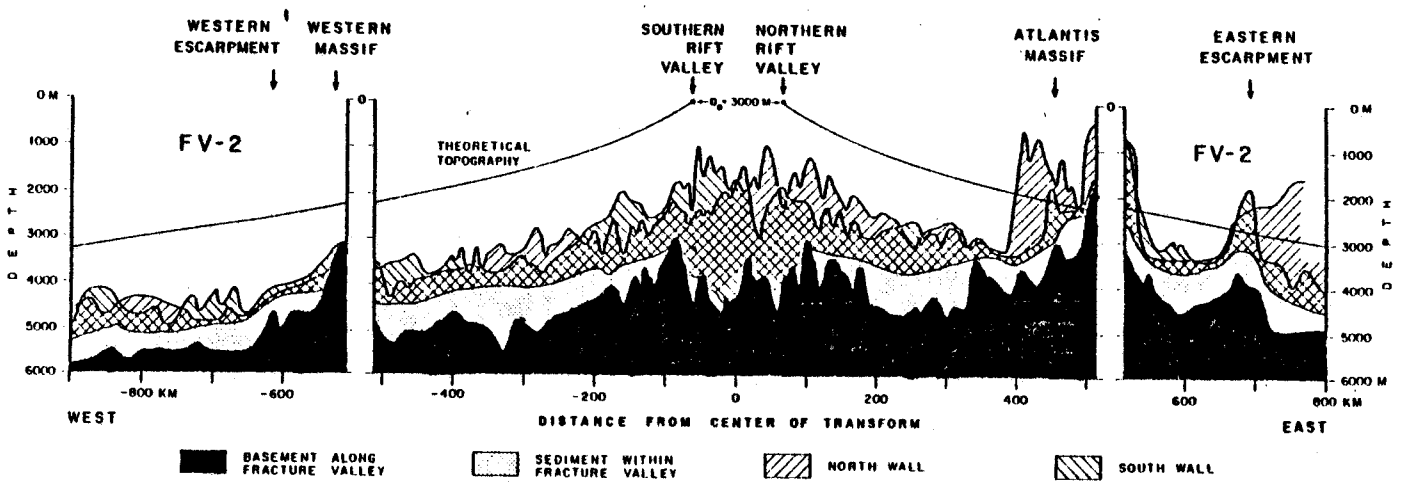

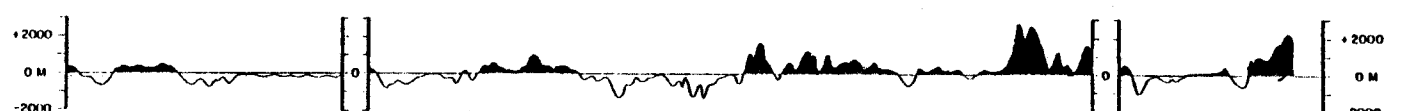

ELEVATION DIFFERENTIAL BETWEEN NORTH AND SOUTH WALLS
(POSITIVE = NORTH WALL HIGHER THAN SOUTH WALL)

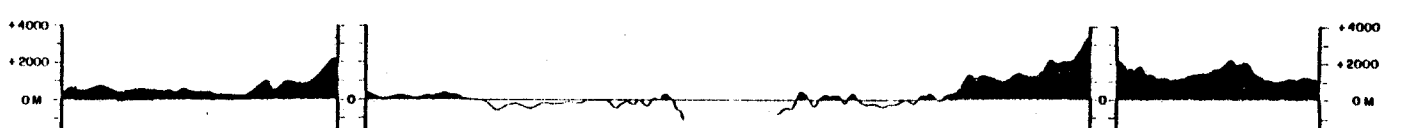

ELEVATION DIFFERENTIAL BETWEEN OBSERVED AND THEORETICAL TOPOGRAPHY
(POSITIVE = BASEMENT DEPTH OF FRACTURE VALLEY SHALLOWER THAN PREDICTED)

Figure 1-12 Line drawings of profiler records from the transform and both fracture zone limbs. Locations shown on Figures 1-4,5,6,7

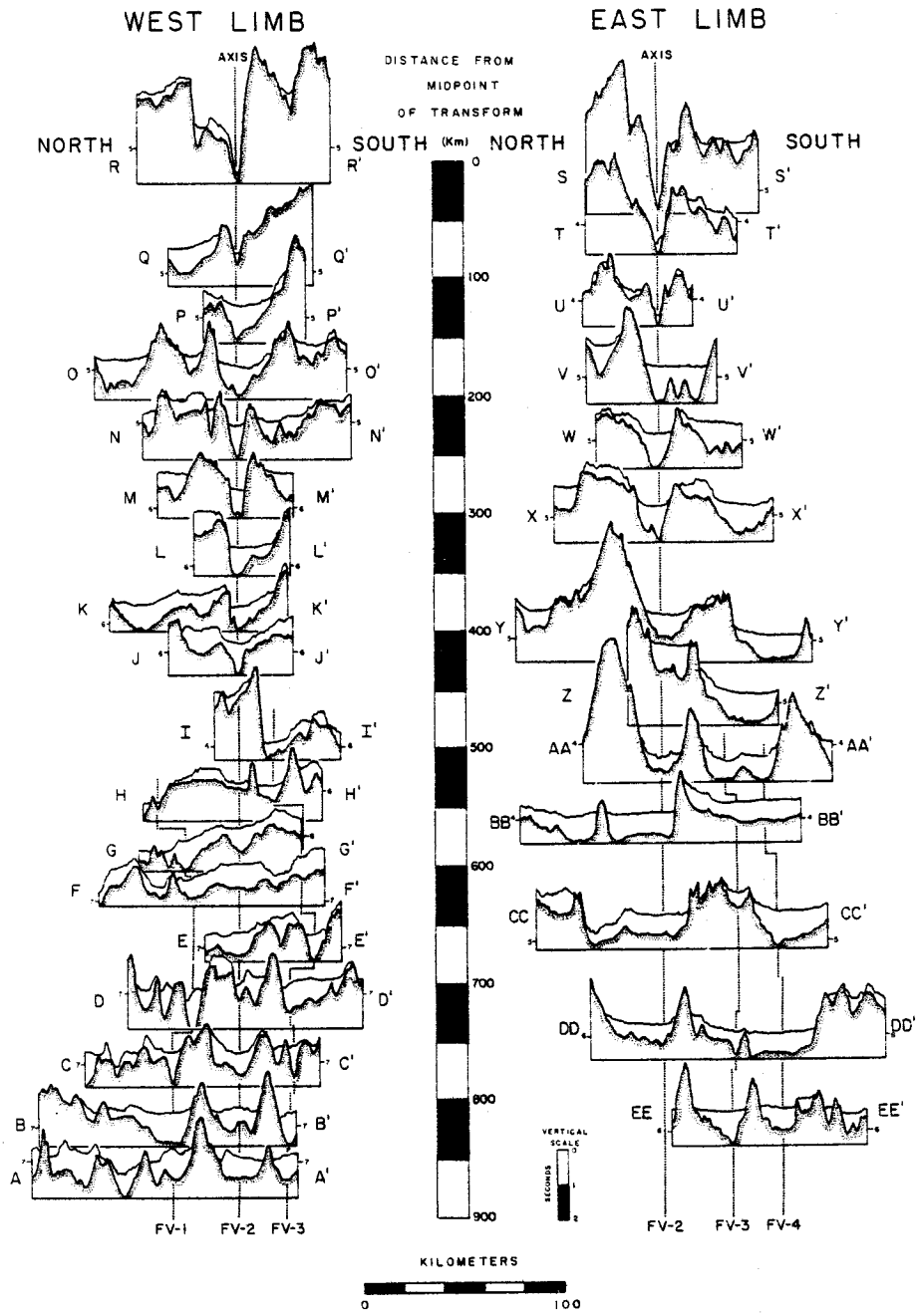
WEST LIMB
EAST LIMB
AXIS
AXIS
DISTANCE FROM MIDPOINT OF TRANSFORM
NORTH
SOUTH
NORTH
SOUTH
(Km)
0
100
200
300
400
500
600
700
800
900
R
R'
Q
Q'
P
P'
O
O'
N
N'
M
M'
L
L'
K
K'
J
J'
I
I'
H
H'
G
G'
F
F'
E
E'
D
D'
C
C'
B
B'
A
A'
S
S'
T
T'
U
U'
V
V'
W
W'
X
X'
Y
Y'
Z
Z'
AA
AA'
BB
BB'
CC
CC'
DD
DD'
EE
EE'
FV-1
FV-2
FV-3
FV-2
FV-3
FV-4
VERTICAL SCALE
SECONDS
KILOMETERS
0
100

Figure 1-13 Basement topography of the Oceanographer transform

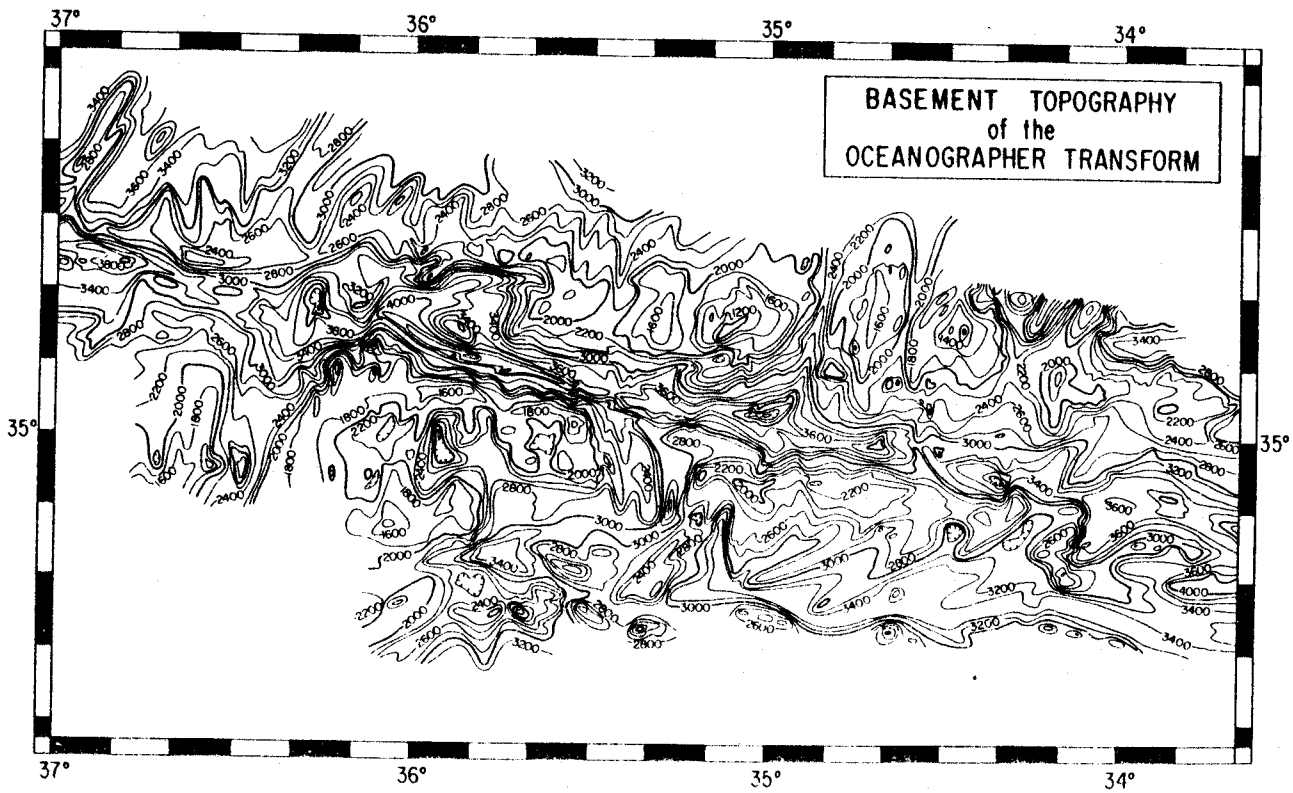
BASEMENT TOPOGRAPHY
of the
OCEANOGRAPHER TRANSFORM
37°
36°
35°
34°
35°

Figure 1-14 Predicted and actual trends of the Oceanographer transfrom and the fracture zone limbs

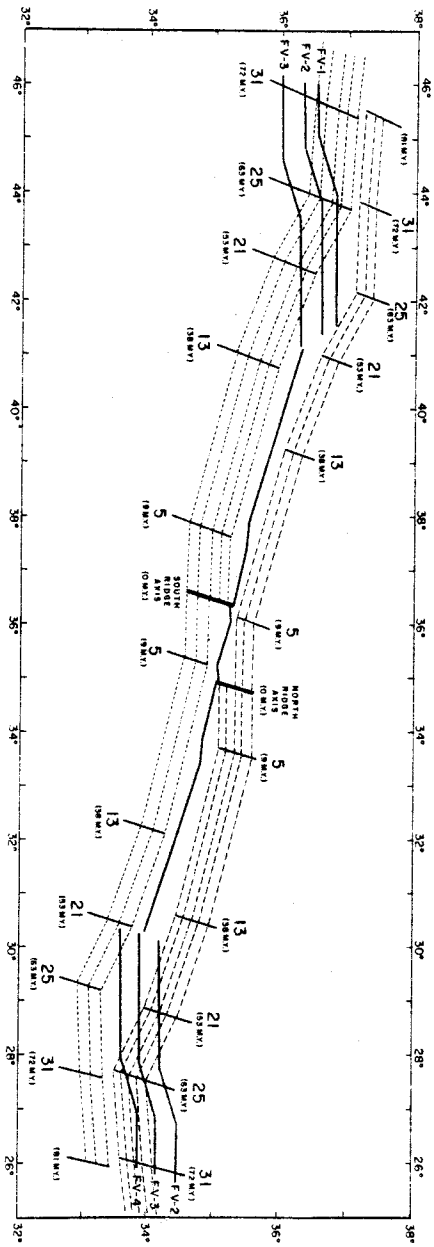
FV-1
FV-2
FV-3
31
(72 MY)
25
(65 MY)
21
(55 MY)
13
(38 MY)
5
(9 MY)
SOUTH RIDGE AXIS (0 MY)
NORTH RIDGE AXIS (0 MY)

CHAPTER II

THE GEOLOGY OF THE CENTRAL PORTION OF THE OCEANOGRAPHER FRACTURE ZONE

INTRODUCTION

In the summer of 1980 a DSRV ALVIN and deep-towed ANGUS camera field program was carried out in two field areas of the Oceanographer transform (Figure 2-1). The rationale for this program was to define the tectonic character of a slowly-slipping ridge-transform-ridge plate boundary and to test various models of the transform domain. The Oceanographer transform was chosen because of the numerous preceding field and laboratory programs (Fox et al., 1969; Fox et al., 1976; Schroeder, 1977; Shibata et al., 1979; Walker et al., 1979, Rowlett, 1981, Fox et al., in prep., Needham, unpub. data, Stroup unpub. data) which provided the necessary information to make this detailed investigation feasible.

In this paper results from the central area of the transform are discussed (Figures 2-1,2); results from the eastern intersection of the transform and the MAR (Figure 2-2) are presented in a companion paper (OTTER Scientific Team, in prep.). This paper covers the structural, sedimentary, and, to a lesser degree, the lithologic and petrologic findings from the center of the transform. More detailed follow-up papers are in preparation on several topics discussed here briefly.

MORPHOLOGY

The information from the mid-transform study area consists of three ALVIN dives and four ANGUS lowerings (Figures 2-3,4,5,6,7 8,9,10,11,12,13). The general morphotectonic setting of this area

consists of approximately 5 million year old crust on opposing sides of the transform with 2000m of relief created by the bounding walls as they rise out of the transform valley. The northern wall is not as rugged as the southern wall and the crest of the north wall is generally deeper (at 2200m) than the crest of the southern wall which rises locally to a depth of 1600m . The regional morphologic fabric of this transform terrain strikes WNW-ESE.

The major subdivisions of the transform proposed below should not necessarily be viewed as applicable to other transforms. At a minimum the classification "works" for a 20km long central region of the transform. The major elements of the central Oceanographer transform are: the transform valley floor, the lower walls, terraces, the upper walls, and the transverse ridges (Figures 2-3,15).

The transform valley floor is a sinuous feature that can best be described as consisting of several short E-W or WNW-ESE segments each less than 10km long that step to the south 2-3 km along NW-SE trending segments. At the eastern end of the work area (Figure 2-4) the transform valley floor is constricted by a small peak that does not appear on Figure 2-4. This peak shoals to less than 3800m and adjacent to it there is no indication of a flat, sediment-smoothed valley floor as there is to the west. The inner floor as defined by the major inflection in slope at the base of the inner walls is everywhere less than 2km wide. The inner floor topography appears flat-lying on the wide-beam echo-sounder records, but pinger located depths from ANGUS transects show that the valley floor sediments are gently undulating and slope inwards towards a narrow axis that in turn slopes downhill 500m from east to west (Figure 2-4).

The lower wall province is a narrow zone one-half to two km wide (Figures 2-3,15) with 200 to 500m relief that flanks the axial deep where the first major set of scarps appears. Inward facing scarps predominate but outward facing scarps, some of which are presently active were also mapped here (Figure 2-4). North of the axial deep, steep, fresh (45^{o}+) scarps in poorly consolidated sediment were crossed on ANGUS 122 and 124 (Figures 2-16,17).

Above the inner wall province the terraces are much wider on the northern side of the deep and the steep slopes separating terraces are farther apart (Figure 2-3). In addition to these observations slope reversals are somewhat better represented to the north of the axial deep than to the south of the deep. Although the slope reversals are usually very minor two of them have over 60m relief. Some of the smaller outward facing scarps are presently active fault/slump scarps (Figure 2-4).

North of the axial deep a prominent splaying of the contours is apparent at progressively shallower elevations from west to east (Figure 2-3). This splaying of the contours is due to the presence of terraces up to 2km wide that shoal eastwards and in places have outward facing slopes. Narrow terraces also occur along the comparable portion of the south wall, some as shallow as 2300m. One of these between 2300m-2700m depth is 400-600m wide, over two and one-half kilometers long, and tilts down to the NW obliquely across the contours (Figure 2-4). This terrace parallels the overall rise in the axial valley floor and the overall rise of the upper wall province.

The terraces are sediment sinks that may inhibit the downslope transport of sediment. Once formed a terrace could isolate scarps from being covered with talus from other scarps farther upslope.

Most samples collected by the ALVIN in the center of the transform are from talus ramps and they probably experienced little or no displacement from the sample site. While this observation cannot be established unequivocally, the rapid rate talus acquires strength and the probability that most terraces form in or near the rift valley renders the conclusion a reasonable inference.

All three ALVIN dives in the western work area crossed the upper wall province. This area contains the steepest sustained regional gradients (38^{o}) over a vertical drop of 500m (Figure 2-8). Scarps farther downslope may be as steep, but only over a lesser vertical drop. This province tends to have consistently inward facing scarps a few meters to a few tens of meters high composed of outcrop or scree deposits with narrow intervening terraces. Most scarps tend to be discontinuous along strike on a scale of a few tens of meters(visual observation) to a few hundreds of meters (weak and discontinuous CTFM sonar targets). On the upper slopes both the promontories and reentrants in the scarps are preserved with the latter serving as the conduit for the transport of debris spalled from the steep terrain above. Farther downslope the reentrants are buried and only more massive rock promontories poke through the sediment cover.

Dive 1019 crossed over the top of the outer scarp into a zone of low relief scattered rock outcrops and piles separated by large rolling expanses of muddy sediment. In this zone a small 10m high N-S trending scarp was crossed similar to the cross-cutting scarps observed in Transform A (Choukroune et al., 1978). While all provinces show some evidence of current scour the outer wall province is where evidence for current activity is concentrated.

One unknown in our efforts to map zones of recent tectonism is the rate talus is lithified and thereby can maintain slopes in excess of the angle of repose for unconsolidated material. Both manganese crusts and carbonate rapidly cement fragments, so much so, that the ALVIN mechanical arm was frequently unable to break fragments loose from apparently unlithified talus piles. On the ANGUS films huge boulders of lithified talus attest to downslope movement of coherent lithified blocks of talus.

At no location outside the ridge-transform intersection did we observe any fault or fissure related separation between talus ramps and rock faces, nor form that matter did we see any compelling evidence for any recent tectonism except along the 2km wide axial deep. Even bounce and roll marks in the sediment surface are missing from the upper wall province. While age determinations on these steep scarps are speculative, the matrix has been eroded and/or dissolved from steep walls leaving some scarps studded with protruding clasts.

Even though unconsolidated talus can maintain slopes in excess of 40^{o} (Young, 1972) and partially consolidated talus can presumably maintain an even higher angle of respose, few large scarps approach this value (Figure 5,7,9). Locally, however, near vertical walls of breccia were photographed on ANGUS lowering 126 (Figures 2-19,24). At the end of Dive 1017 very steep lithified talus slopes were also observed. Although little evidence for recent downslope movement of talus is apparent anywhere within the center of the transform, sediment overlying a talus pile near the end of ANGUS 124 appears to have torn loose exposing the talus below. The general absence of recent slide scars or even

old slide scars along the outer scarp province is probably the result of very active bottom currents which tend to strip the carbonate ooze and redeposits it at lower elevations. This not only prevents large areas of unstable sediment from building up, it also smooths over any slide scars very quickly.

The high resolution near bottom data from three ANGUS lowerings plus the three ALVIN dives in the western field area, and an additional ANGUS lowering between the two field areas, have permitted the delineation of a zone of presently active tectonism within the transform. This zone is usually less than 2km wide and is defined most often by elongate, irregular scarps of variable orientation in slightly indurated carbonate sediment (Figure 2-16, 17). These scarps are interpreted as fault-generated and subsequently degraded by burrowing, current activity, small debris flows, and other mass wasting phenomenon (see following section). Only a few scarps were observed that are not degraded; one of these is flanked by a debris flow at its base the surface of which is crisscrossed by tracks of bottom dwellers presumably feeding on exhumed organic debris accumulating in the lee of the scarp (Figure 2-16).

A rose diagram generated from scarps within the PTDZ does not show a significant clustering that is not readily matched to any systematic stress regime (Figure 2-20). The orientations of most of the old scarps high up the wall on Dive 1018, though, are roughly subparallel to a northwesterly facing promontory seen on the detailed bathymetric map of Needham (unpub. data). These scarps may be oblique structures inherited from the western ridge/transform intersection region. The origin of such oblique structures has been the topic of much recent debate (Whitmarsh and Laughton, 1976; Crane, 1976; Lonsdale, 1977; Searle, 1979;

Macdonald, 1981; Lonsdale and Shor, 1979; Gallo and Rowley, 1980; Gallo, Fox, and the Tamayo Scientific Team, in prep.) and they they clearly reflect the effects of the transform upon the accretion process and subsequent tectonism.

No second-order shear structures such as riedel shears or tension gashes were observed in any photographs of individual scarps hence it was not possible to infer the sense of motion along the faults. All the faults exhibit a component of dip-slip motion as shown by elevation differences across steep scarps. Where the faulting appears to be most recent (Figure 2-16), the scarp edges are very sharp with minimal evidence of scarp retreat by slumping or gullying. As scarp degredation proceeds, cuspate slide scars, rills, and intricate dendritic erosion patterns are etched into the scarp face. Eventual muting of the secondary "drainage" patterns imparts an undulating or hummucky character to the scarps. Along subaerial faults the rate of scarp degredation has been used successfully to date the timing of motion on the faults (Wallace, 1978). Very little data has been collected in the submarine environment that permits us to determine the numerical ages of the majority of the scarps or their rate of degredation. The occurrence of outward facing scarps and slopes, some of which may be active north of the axial deep (Figure 2-4), is an indication that recent deformation extends outside the axial deep but apparently not as far as the base of the upper walls.

ROCK DISTRIBUTION

Three highly successful dives in the center of the transform yielded a suite of samples whose spatial distribution (Figure 2-4) is indicative of sampling from different levels within the stratigraphy of the oceanic lithosphere. Earlier work along the Oceanographer transform (Shibata, 1976; Fox et al., 1976) demonstrated that basalt and gabbro or their metamorphosed equivalents are the most commonly recovered rock types along the south wall. The submersible program (Figure 2-4) confirmed this general distribution of rocks and also demonstrated that partly or wholly serpentinized ultramafics are abundant along portions of the north and south wall.

Because almost all submarine rock outcrops except very young volcanics are covered with a manganese oxide crust, one of the very useful field observations that was discovered during the Cayman Trough project (CAYTROUGH, 1979; Stroup and Fox, 1981) and applied to Dives 1017, 1018, and 1019 was that ultramafic rocks often have a bulbous outline with a gravelly surface texture which serves to distinguish them from extrusive basalts and gabbro. Some of the gabbros are lineated or foliated (Figure 2-26) and frequently are cut by orthogonal joint sets that permit outcrops to calve off large, rectangular blocks. These apparently diagnostic characteristics are particularly useful along areas of extensive outcrop exposure where it is impossible to sample every outcrop, and for interpretation of bottom photographs. One drawback to this scheme is that massive basalts are similar in appearance to the gabbros and thus photographic interpretation of

of blocky-jointed outcrops is suspect when not accompanied by bottom samples.

Dive 1017 traversed up the south wall and collected a suite of samples from the upper wall province of the transform. The first steep slope that looked promising on the echo-sounder records turned out to be covered with mud; only after a kilometer and a half did the ALVIN encounter the first major rock escarpment. While travelling parallel to the the scarp for a couple of hundred meters the submersible passed a small canyon cutting into the scarp face. Numerous outsized blocks 5m long were observed here as well as possible outcrops. Near the base of the major scarp two stations were completed; one of these, Station 1A yielded gabbro, tronhjemite, and ultramafics all from the same locality. The trondhjemites are of variable grain size and exhibit a sharp reduction in grain size towards their gradational contacts with the gabbros. The total scarp height was in excess of 150m and consisted of sediment sprinkled with rock chips and gravel, coalescing talus fans, chutes, and massive boulders. Several of the blocks were slabby with rhombohedral joints and they ofter rested precariously on the sediment cover. Since the ALVIN did not travel quite directly upslope the steepness of portions of the scarps may be greater than that depicted in some of the figures.

Once beyond the top of the first major scarp the ALVIN crossed over a broad terrace whose surface dipped gently towards the south. This terrace is traceable on the echo-sounder records

as well despite its relatively narrow width (< 500m). Between the next two stations the ALVIN passed by either an enormous boulder or a possible outcrop with rhombohedral joints. The next part of the traverse was over a completely sedimented but steeper bottom as the base of the major part of the upper wall province was crossed. The upper wall province here is very rugged with minor amounts of outcrop poking through the rubble. In general this part of the traverse, as depicted, lacked large expanses of sediment yet there were many scattered tracts of sediment particularly filling in and over talus. The top part of the upper wall province here as elsewhere provided the best exposures of talus with minor amounts of outcrop perhaps exposed in places. The last and steepest part of the wall consists of cemented peridotite breccia (cemented talus). The dive was terminated before the top of the scarp was reached, but the depth recorded at the end point is close to that from the echo-sounder bathymetry.

Dive 1018 was located farther upslope and to the east of Dive 1017 in an attempt to conduct a second traverse up the steep upper wall province. The first station was from a rock pile with two contrasting lithologies: one lithology was rounded and knobby and had fruitcake surface texture; the second was more massive and angular and turned out to be basalt; the first was ultra-mafic. The ALVIN then retrieved a sample of basalt which was from an exposure that was large and exhibited a weakly layered appearance. This part of the dive was characterized by an apparently equilibrium surface with no evidence of mass wasting and a predominantly carbonate ooze covered surface.

The next part of the dive was a climb up the very steep talus ramps and rock faces of a large promontory (Figure 2-3). The preponderance of the scarps faced northwest and appeared inactive; no evidence of recent faulting was encountered. Several of the outcrops and loose blocks exhibited a platy structure or foliation; the more spectacular vistas here included vertical rock faces, small overhangs, and otherwise rugged terrain. The major lithology recovered from this region is gabbro.

The final part of the Dive was subparallel to the contours probably along a large bench inasmuch as the top of the scarp was over 200 meters higher. This part of the dive was characterized by numerous ridges and swales of rubble with no exposure of outcrop. The local relief was much less here than earlier in the dive. Basalt was recovered from one of the rubble ridges.

Attempts to correlate these samples with those of Dive 1017 were not successful. No basalt was recovered on Dive 1017 whereas basalt was recovered at five stations on Dive 1018. The major scarp which forms the bulk of the upper wall province on either side of the transform axis appears to be a plutonic or ultramafic escarpment with subordinate amounts of basalt being recovered there. This conclusion is partly supported by the work of Shibata (1976) and Fox et al., (1976).

Based upon ANGUS lowering 124 which showed numerous blocks and possible outcrops, Dive 1019 was deployed just to the east of that lowering (Figure 2-4). From the ANGUS photographs it was believed that extensive outcrops or blocks of ultramafic rocks were present along the north wall. The dive started off over a gently dipping mud bottom which had a small depression (moat?) at

the base of the first scarp. After collecting one sample of serpentinite breccia in a carbonate matrix from a weakly layered exposure of talus, the ALVIN first crossed a narrow bench, collected a second sample of serpentinite, and then proceeded to the top of the scarp.

After going across sediment for a couple of hundred meters a third station of harzburgite was collected from an isolated rock pile. This was the last exposure of rock for almost a kilometer. Prior to the next outcrop the ALVIN crossed several spectacular pteropod dunes and weakly defined mud ripples. These dunes abutted the several meter high outcrop face where the next station was attempted. Above this outcrop were weakly defined mud ripples in pteropod shells.

A chalk sample was collected at Station 5 and the terrain there had a somewhat raised appearance probably due to current scour. The chalk outcrop is visibly burrowed and also appears to be foliated. Between Station 5 and Station 6 is a sediment surface speckled with gravel. This surface is periodically broken up by burrowers who excavate material from beneath the gravel and build miniature mud volcanoes on top of the gravelly surface. The main part of the upper wall province begins at the top of the gravelly surface (Figure 2-10). The terrain here and for the next several hundred meters is extremely rugged. In a few places rows of blocks mark the tops of scarps. What is lost at the scale of the Dive profiles here is the rather dramatic microtopography in the form of steep rock faces a few meters high, gullies, overhangs and boulder strewn terrain through which the ALVIN navigated. What is also lost on this dive is a precise

knowledge of the macrotopography because this part of the dive could not be acoustically navigated hence the slopes as depicted here (Figure 2-10,15) should be regarded as minimum estimates of their ruggedness.

Near the top of the composite escarpment where samples six through ten were collected the ALVIN again travelled into carbonate (chalk) terrain that was characterized by a distinctive foliation that was visible on a scale typically of several centimeters spacing. Besides being foliated the chalk tended to be worm-burrowed, pitted and slabby; in a few places log-shaped fragments were observed. Above this scarp the ALVIN traversed over a zone of scattered rock piles with broad expanses of carbonate sediment in between the piles (Figure 2-10).

When it became clear that few more outcrops were likely in this gently sloping terrain, the ALVIN headed back to the top to the scarp where it was believed more outcrops would be encountered. The next station was at or near the contact between the foliated chalks and the less obviously foliated ultramafics. It is likely the chalks are resting upon the ultramafics since that would be the predicted sequence in this setting.

The overall impression from this dive was that the lower part of the dive crossed terrain where at least several tens to perhaps hundreds of meters of pelagic carbonate debris or drift may cover the talus fans and fault scarps below (Figure 2-15). Above the first major scarp there is another large expanse of sediment suggesting that the main part of the upper wall province had not been reached. The isolated fault scarp

and the average slope of the terrain suggest that the terraces give way to the upper wall province by an increase in the throw of individual faults, by an increase in the number of faults per unit length of traverse, by a change in the polarity of the faults from both inward and outward facing faults in the terraces to consistently inward facing faults in the upper wall province, or by a combination of all three. None of these alternatives is particularly well constrained so Figure 2-15 should be regarded as a preliminary interpretation.

The recovery of harzburgite, peridotite, and serpentinite from low relief scarps suggest that the crust here is thin and that ultramafics at least locally are a significant part of the upper part of the oceanic lithosphere. While several samples were clearly from second generation talus others were collected from the vicinity of outcrops. The terrain from which these samples were collected is rugged and in plan view the scarps are very irregular with numerous promontories and reentrants. The ultramafics had surface textures variously described as "fruitcake", "popcorn", knobbly, or gravelly and an overall shape that was often bulbous.

The steeper terrain in the upper wall province can be described as similar to the topography above the snow line in an Alpine setting, that is, coalescing talus fans covered with large boulders characterize the lower slopes, the upper slopes of some scarps have steep rock faces that are flanked laterally by talus accumulations. Few of the scarps on this dive were laterally continuous for an appreciable distance. Judging by the lack of continuous targets on the side-looking sonar, the upper

part of the dive consisted of scattered rock piles less than 100m across.

ANGUS 124 was a wall to wall traverse that crossed all the major physiographic provinces (Figures 2-3,15). The purpose of this lowering was to define zones of recent tectonism in the axial deep as well as locating zones of extensive exposures of outcrop or talus for future sampling by ALVIN. Both objectives were successful (Figure 2-4).

The first part of this lowering was over mud interrupted by a single outward facing scarp. Above this single scarp the sled encountered little of interest until the base of the upper wall province (Figure 2-3). As the sled climbed uphill, it crossed scattered piles of boulders and patchy areas of lithified carbonate for over a kilometer. Near the top of the upper wall province the carbonate mud is heavily rippled and signs of lithification of the carbonate ooze are abundant. The first indication of lithification is that patches of sediment start to stick out of the ooze a few centimeters. These patches are white and usually possess indications of bedding. As lithification occurs synchronous with erosion the foliations become enhanced and the carbonate becomes encrusted with manganese and turns black. At this stage the carbonate (chalk) behaves as a rock and fragments break off to form talus. One of these talus fragments was so friable that it broke apart in the ALVIN's mechanical claw.

On its oblique crossing down the north wall (Figure 2-12) the ANGUS sled crossed several elongated talus ridges but not until halfway down the slope did it encounter a rubbly escarpment

a few meters high. Erosion appears to have left several gravel streamers leading into the head of the scarp and the rocks there were similar in appearance to the ultramafics observed on Dive 1019 suggesting a possible correlation between the two.

Once the ANGUS sled got to the base of the upper wall province it crossed several kilometers of mud. Only one possibly active scarp was observed on ANGUS 124's western crossing of the axial deep. South of there and at a much shallower elevation the ANGUS sled photographed what appeared to be a slide scar. Apparently the carbonate ooze cover of a talus ramp had torn free exposing the talus below. Beyong this,several minor scarps in talus were encountered, none very large. The lowering was then terminated midway up the upper wall province.

SEDIMENTARY PROCESSES

A bonus of the more than 20,000 deep-sea photographs collected during the Oceanographer cruise was the ability to delimit several zones of well-defined current-induced bedforms (Figure 2-4,14). These range from subtle indications of current scour such as degraded burrow exit heaps and mounds, and gouge marks filled with shells to more obvious features like triangular ripples of shelly debris up to several 10's of meters long, 1-2 meters wide, and 20-50 cm high. Most rocky exposures showed some evidence of current-scour, some in the form of moats in the adjoining sediment, others in the form of manganese encrustations, or differential dissolution in the carbonate terrane that serves to accentuate structures (bedding, joints, foliations, etc.;

(Figure 2-18). No systematic effort was made to measure current activity within the transform yet we can infer the relative strength and orientations of currents at several localities.

In the western work area along the northern wall of the transform the current appeared to be generally from the east towards the west and occasionally impeded sampling efforts. At other times we observed rattail fish "swimming in place" against a gentle current from the northeast. Sessile faunas, though, showed few signs of deflection in the current.

The best examples of rippled bedforms occur along the north wall, typically at depths of about 3000m which coincides with the first appearance of abundant talus and the start of the upper wall province (Figure 2-14). These bedforms include possible wave ripples; see Harms, 1969, Plate 4) and a variety of current or combined flow ripples. The current ripples vary from strongly asymmetric sharp crested ripples to spectacularly developed longitudinal triangular ripples (terminology from Flood, 1981). The latter bedform has been recognized in shallow marine environments (van Straaten, 1951) and in several abyssal localities i.e. (Mozambique Basin - Heezen and Hollister, 1964; Central Atlantic - Ewing and Mouzo, 1968; Nova Scotian continental rise - Zimmerman, 1971, Heezen and Hollister, 1971, Tucholke et al., 1979; Blake-Bahama Region - Bryan and Markl, 1966, Lonsdale and Spiess, 1977, Flood, 1981).

The longitudinal triangular ripples are positioned in a gully in a narrow zone about 200m wide in the northeast sector of ANGUS 126 (Figure 2-13,22) and although not far from talus accumulations on either side, the ripple field does not appear

to be related to the talus. The ripples are composed of shelly debris, probably pteropods, that are scattered over a tranquil carbonate substrate devoid of obvious current lineations. Thus I cannot claim unequivocally that they are longitudinal ripples and not transverse ripples. However, they do share characteristics common to other longitudinal triangular ripples such as sharp crests, a tendency for heads of individual ripples to start in the spaces between other ripples (Figure 2-22), their overall dimensions (one to more than ten meters X 1-2m X 20-30cm) and their spacing (one to more than ten meters). The abrupt change in orientation of the ripples over a distance of 200m is not surprising in view of their setting (i.e. a narrow gully between two talus deposits). Flood (1981) observed a silimar change in ripple orientationn over a distance of several kilometers within an embayment of the Blake-Bahama abyssal plain.

Several authors, Bagnold, 1941; Karcz, 1967; Hanna, 1969; Jackson, 1976; Folk, 1976; Lonsdale and Spiess, 1977) attribute formation of regularly spaced longitudinal bedforms to a secondary helical flow that is transverse to the main flow. Flood (1981) further suggest that longitudinal triangular ripples may be due to "short periods of strong current flow" that may be at variance to the steady-state flow regime.

There are both longitudinal and very large transverse triangular ripples within the Oceanographer transform. On Dive 1019 we followed a transverse ripple or dune for over 30m to the base of a 3-4m high escarpment. This dune was sharp crested, although not continuously so, and consisted of fairly long, high ($>$ 50cm) segments with widely-spaced saddles. The slight to moderate

asymmetry of the feature caused by its northwesterly facing slip-face and the presence of weakly developed mud ripples parallel to the long dimension comprising the dune are indicative of a current flow from ESE-WNW. The material comprising the dune is a shelly debris of very low specific gravity. Passage of the submarine within a foot of the bottom was sufficient to entrain shells which stayed in suspension in the turbulence for several seconds. The dynamic equivalence of these pebble-sized particles is probably less than that of fine sand, a suggestion favored by Laughton (1963) for the formation of transverse ridges of similar appearance. At other locations we observed collections of shells on the lee side of larger blocks and these shells in a few instances extended downcurrent for several meters in a manner analogous to that of sand distribution around obstacles or downwind from cliffs (c.f. Bagnold, 1941).

ABYSSAL FURROWS

One of the more problematical features that we observed on several ANGUS lowerings are long, straight, parallel grooves, either as regularly spaced bedforms spaced from 5 to less than 2m apart, or as isolated troughs. The largest concentration of these grooves occurs in the axis of maximum depth where they were crossed by ANGUS 126 (Figure 2-23). Over 40 grooves were observed there within a span of 400m. Most grooves within sets are uniformly spaced but the sets appear to be concentrated on the floors of small troughs. Intervening highs lack grooves, are extensively burrowed, and usually do not show even subtle indica-

tions of bottom current:current activity such as smoothing of animal tracks and mounds.

The residual uncertainty in the orientation and depth of the camera sled and the fact that this lowering was not acoustically navigated prohibits a detailed analysis of the microtopography. The reconstruction of the bottom terrane, however, shows that the larger troughs are probably more that 30m across and less than 10m deep whereas the grooves within the troughs are probably about .5-2m deep. These furrows and grooves bear some resemblance to erosional/depositional bedforms in the Samoan Passage (Lonsdale, 1973) and the Blake-Bahama Rise (Hollister and others, 1974; Lonsdale and Spiess, 1977; Tucholke, 1979) with one major difference: most furrows and grooves within the Oceanographer transform show little independent evidence for formation from bottom bottom currents such as current lineations or heavily rippled banks. Of the 50+ grooves only two exhibited the characteristic tuning fork juncture opening upcurrent (Hollister and others, 1974). Most grooves are confined to the inner valley of the transform where current lineations and bedforms are scarce, and few occur in the region above 3000m where rippled bedforms are abundant (Figure 2-3).

The proximity of the grooves to the presumed location of the principal transform displacement zone could indicate an origin by deformation, yet this interpretation suffers from the same inconsistencies that an erosional origin does. There is no sign of horizontal displacement across any of the grooves although a few may have a small vertical offset across them. No secondary features like tension gashes or riedel and antiriedel shears are apparent. Elevation differences across some grooves on a

on a slope are consistent with an origin by faulting or erosion, but it is conceivable that these furrows are slightly degraded fault strands. In a study of the Quebrada transform Lonsdale (1978) traced for over 50m an anastomozing sediment furrow that he believed was a minor fault strand. While this explanation is attractive for isolated grooves, it is less appealing for regions where the grooves are regularly and densely spaced. I favor an erosional origin for the furrows for three reasons:

1) Bottom photographs of some furrows of clearly erosional origin from the Blake-Bahama region show little independent evidence for their formation by bottom currents (Tucholke and others, 1979), thus the absence of clearly defined bedforms along most of the Oceanographer furrows does not disprove an erosional origin for them. Also, if some or all of the furrows are relict, sediment burial and surface burrowers would perhaps tend to obscure the current lineations and ripples before the furrows become unrecognizeable.

2) The most densely furrowed area is downslope from a region of gravel pavement that floors part of a large gap in the south wall whose minimum depth exceeds 2600m (Schroeder, 1977; Fox and others, in prep.). The manganese and gravel pavement and dense communities of sessile faunas flourishing along one of the steep talus slopes (Figure 2-24) demonstrate that this gap is a conduit for bottom currents.

3) The boulder strewn and highly irregular bottom terrain within the transform severly limits the utility of 3.5 kHz records for echo-character analysis. However, my preliminary analysis of records just to the east of the ridge-transform

intersection does confirm the presence of isolated regions of current induced bedforms along the floor of the fracture zone valley.

DOWNSLOPE PROCESSES

Soon after a fault scarp or a slide scar in partially consolidated sediments is created it undergoes rapid degradation. What we interpret as very recent scarps are only slightly incised by channels and have locally steep, near vertical sections with possible throws of several meters or more. Burrowers disgorge and dislodge material onto the bottom and and it dribbles downslope eroding small channels and leaving behind streamers of lighter colored sediments (Figure 2-17).

Localized high velocity bottom currents are a significant factor in the entrainment and transport of sediment to the heads of most scarps there the sediment may become incorporated in small scale turbidity currents or grain flows. Rippled bedforms are relatively sparse within the confines of the inner valley of the transform; their largest population is adjacent to the heads of several scarps. The slip-face of the ripples is clearly towards the scarp in at least one instance, thus proving the scarp face is subjected to a steady-state bombardment of particles as well as receiving small pulses of sediment when the slip-face fails.

A few scarps appear to have undergone a complicated history of scarp degradation and burial followed by rejuvenation. Heavily sedimented dendritic patterns are recognizeable in

a few places upslope from more recently active channels. Many of these partially buried channels appear as isolated troughs farther upslope thereby establishing an erosional origin for at least some of the furrows discussed in the previous section. What is also significant is that one of the few demonstrably active furrows was formed as part of a larger drainage network (Figure 2-24). Thus furrows may form on fairly steep gradients perpendicular to slope when conditions are favorable.

Another unusual "drainage" pattern that develops on fairly steep slopes are long parallel rills that are possibly analogous to subaerial shoestring rills (Horton, 1945). These rills evolve over a span of 50m from minor depressions with only a few centimeters relief to gullies over 30cm deep. The main channels (no master gully was observed, Horton, 1945) and the subsidiary feathering are disrupted somewhat where ledges of semiconsolidated sediment outcrop, but the channels soon recombine downslope (Figure 2-25). Where the rills are particularly well-developed, slope parallel ripples are present immediately upslope.

This observation again supports the notion that deep-sea currents moving over and around obstacles are a major contributing factor to the degradation of fault/slump scarps in sediment. These currents are probably not turbidity currents in sensu strictu although small-scale turbidity currents and grain flows undoubtedly initiated by the downslope flux of material. Geostrophic currents are also accelerated and deflected over and around obstacles thereby inducing obvious signs of current

activity at only a few locations. Horton (1945) suggests that rills develop wherever there is an "accidental concentration of sheet flow". Whether an analogous agent like the nepheloid layer is responsible for their formation in the deep-sea or whether rill formation is due to a secondary helical flow transverse to the main flow is unclear.

SUMMARY AND CONCLUSIONS

One major theme that emerged from this cruise is that mass wasting in various guises easily keeps apace with tectonism. Since the axis of most large-offset transforms in the Atlantic will be floored with substantial amouts of sediment, most recent faulting will create highly unstable sediment scarps that are susceptible to immediate and severe degradation. Despite being relatively sheltered from major steady-state flows of bottom water masses such as the Antarctic Bottom Water or the North Atlantic Deep Water, the Oceanographer transform displayed a rich variety of current induced bedforms ranging from fairly common low and high energy current ripples to abyssal furrows and longitudinal triangular ripples.

Evidence for recent faulting within the transform is usually sparse and equivocal. What faulting there is appears to be confined to a narrow zone consisting of the transform valley floor and the lower walls; this zone is confined to within two kilometers of the axial deep and in most places we observed not precisely centered over the axial deep but is slightly towards the north wall (Figure 2-4). Recent faulting does not appear to bear any simple relationship to the inferred spreading

direction whereas some of the older fault scarps along the south wall may be oblique structures formed at the western ridge-transform intersection that were translated east to their present location by seafloor spreading.

The lower walls flanking the transform valley floor are sites of recent faulting, slumping, and intricate "drainage" systems. Above the inner walls are broad, irregular terraces that rise gradually away from the axis. The terraces and a few outward facing slopes inhibit downslope motion of talus and may isolate segments of the transform walls from being covered with blocks from uphill sources. The steepest (38^{o}) sustained gradients (500m drop) are beyond the terraces in the upper wall province where most of the ALVIN dive samples were collected. Steep talus ramps cemented in places by manganese and carbonate are punctuated by discontinuous, generally small outcrops of mafic, plutonic, and ultramafic rocks.

The abundant recovery of ultramafic rocks interspersed with ferrogabbros and basalt from the south wall and the almost exclusive recovery of ultramafic rocks along the north wall is confirmation that the crust is exceedingly thin and discontinuous along this transform. The terrain from which these samples were collected, the upper wall province, is very rugged with locally precipitious scarps that are never more than a few tens of meters high and discontinuous along strike. Most samples were collected from slightly lithified talus of a highly variable appearance. The plutonic rocks and the massive basalts were often cut by rectilinear joint sets that permit outcrops to calve off large rectangular blocks. The ultramafics, on the other hand, have more curvilinear joints and the individual blocks are often bulbous with a "gravelly", "popcorn", or

"fruitcake" surface texture.

While the igneous, structural, and tectonic history of transform faults is predictably complex, the sedimentary history is less obviously, but equally complex. The transform valley floor and the lower walls are apt to be floored by an admixture of multi-generational fault breccias, disaggregated turbidites, debris flows, slump deposits, and minor drift deposits. The terraces are probably underlain by a series of coalescing talus fans and wedges and blanketed with carbonate and drift deposits that are comparatively stable. Near major scarps within the terraces and adjacent to the upper wall province, talus fans forming clast-supported breccias will grade laterally and upwards into matrix-supported breccias that eventually are covered with drift deposits or pelagic debris. Current activity within the upper wall province is thought to leave behind locally thick lag deposits of sand, gravel, and resistant shelly fragments. The carbonate is inferred to have been lithified to chalk near the sediment/water interface. These chalks have a variety of expressions: some are foliated, others are worm-burrowed and coated with a thick manganese crust; they tend to break apart easily, sometimes into fragments of unusual shape. One unknown is the origin of the foliation which is being studied further.

Figure 2-1: Index map showing the location of the Oceanographer transform with respect to other major features.

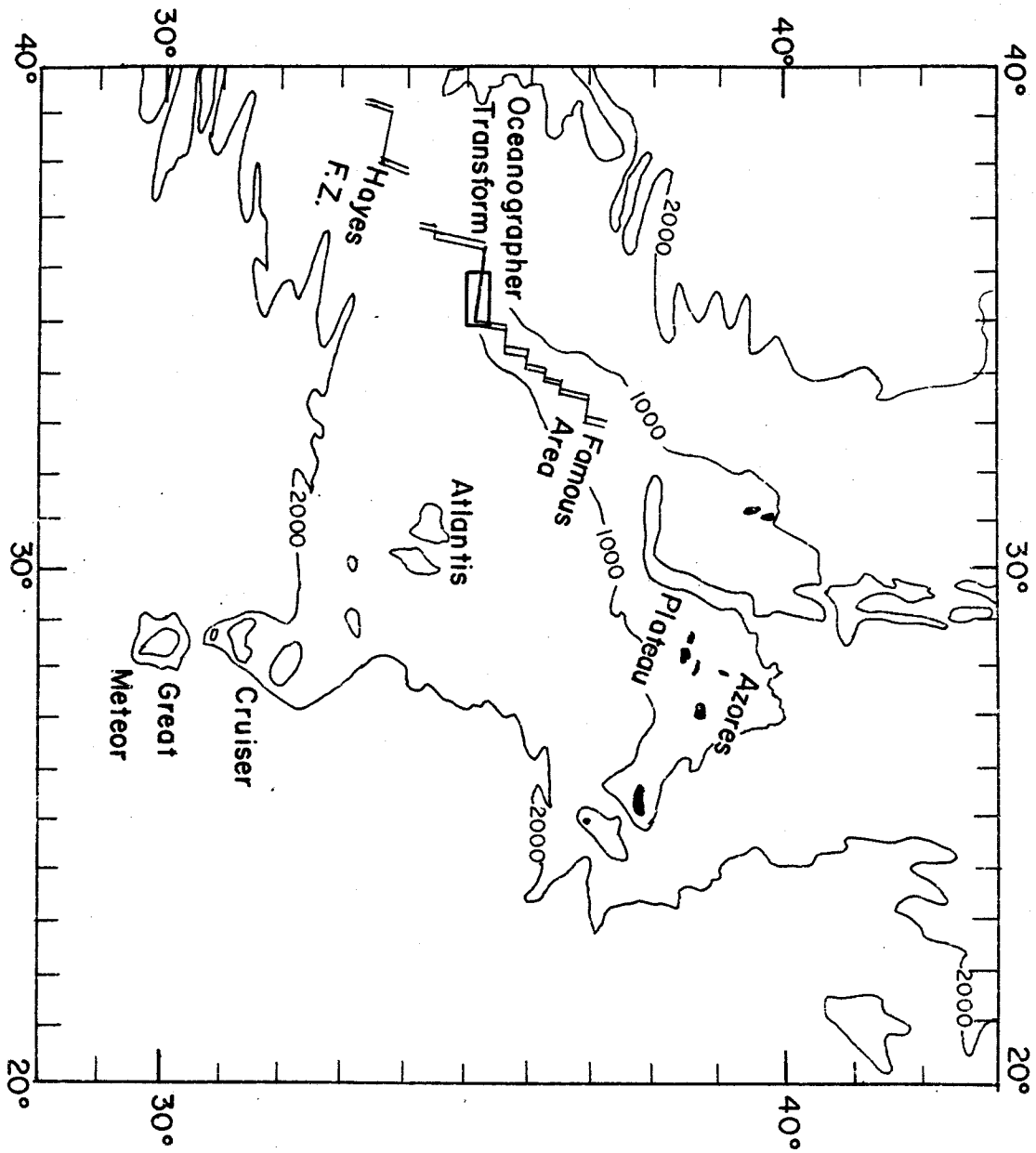
40°
30°
20°
40°
30°
20°
Oceanographer Transform
Famous Area
Hayes F.Z.
Atlantis
Great Meteor
Cruiser
Plateau
Azores
2000
1000
1000
2000
2000
2000

Figure 2-2: Generalized bathymetry of the Oceanographer transform from Schroeder (1977) and D. Needham (CNEXO) compiled by J. Stroup (1980). ANGUS and ALVIN coverage also shown.

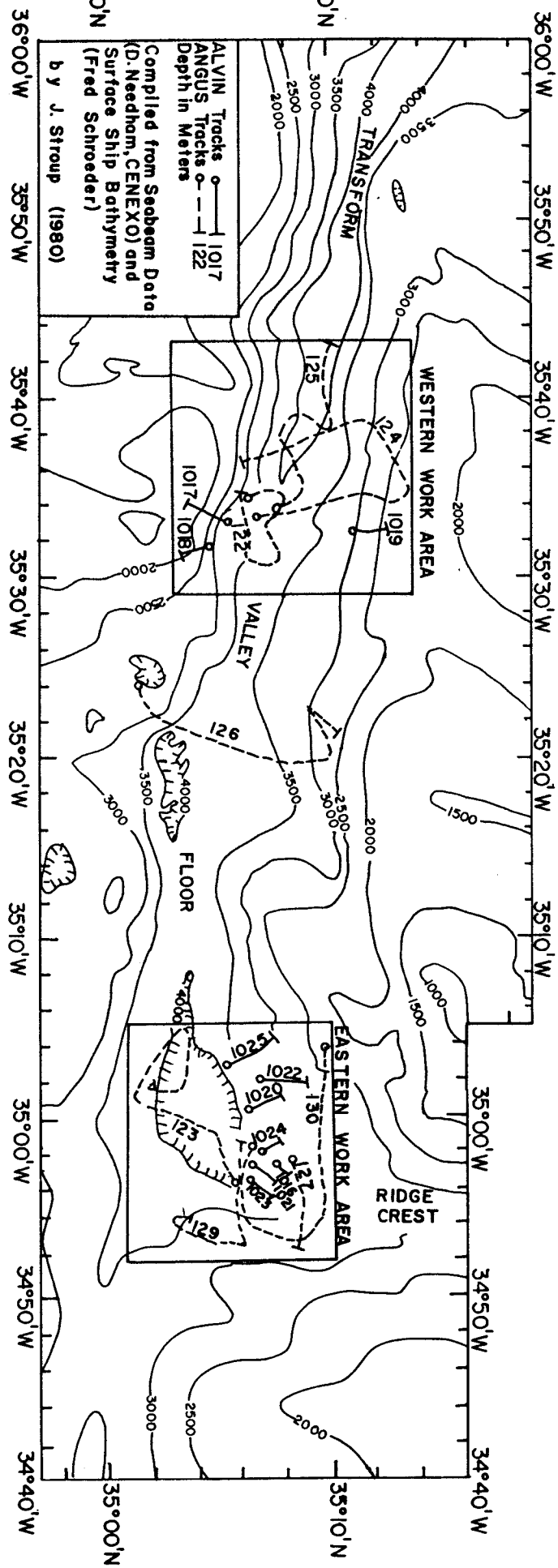
ALVIN Tracks
ANGUS Tracks
1017
122
Depth in Meters
Compiled from Seabeam Data
(D. Needham, CENEXO) and
Surface Ship Bathymetry
(Fred Schroeder)
by J. Stroup (1980)
TRANSFORM
WESTERN WORK AREA
VALLEY
FLOOR
EASTERN WORK AREA
RIDGE
CREST
36°00'W
35°50'W
35°40'W
35°30'W
35°20'W
35°10'W
35°00'W
34°50'W
34°40'W
35°10'N
35°00'N

Figure 2-3: Physiographic diagram of the central portion of the Oceanographer transform. Figure is based upon bathymetric, ALVIN, and ANGUS data. ALVIN and ANGUS coverage also shown.

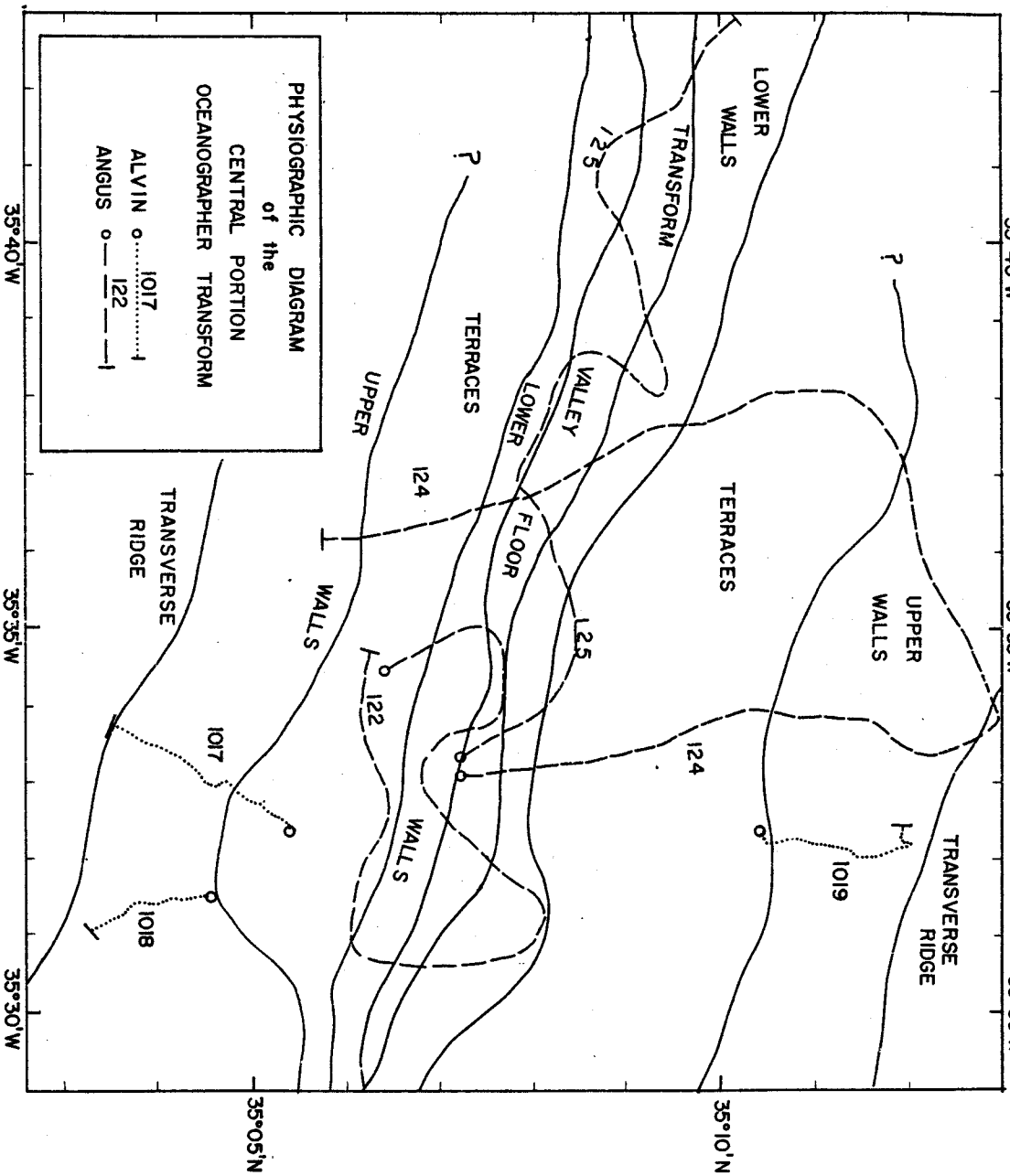
35°40'W
35°35'W
35°30'W
35°10' N
35°05' N
LOWER WALLS
TRANSFORM
UPPER WALLS
TRANSVERSE RIDGE
TERRACES
VALLEY
LOWER FLOOR
UPPER WALLS
TERRACES
TRANSVERSE RIDGE
123
124
125
122
1017
1018
1019
PHYSIOGRAPHIC DIAGRAM
of the
CENTRAL PORTION
OCEANOGRAPHER TRANSFORM
ALVIN 1017
ANGUS 122

Figure 2-4: Bathymetry of the central portion (western work area) of the Oceanographer transform showing geology along ANGUS camera lowerings 122, 124, and 125 and ALVIN dives 1017, 1018, and 1019. ALVIN sample locations also shown.

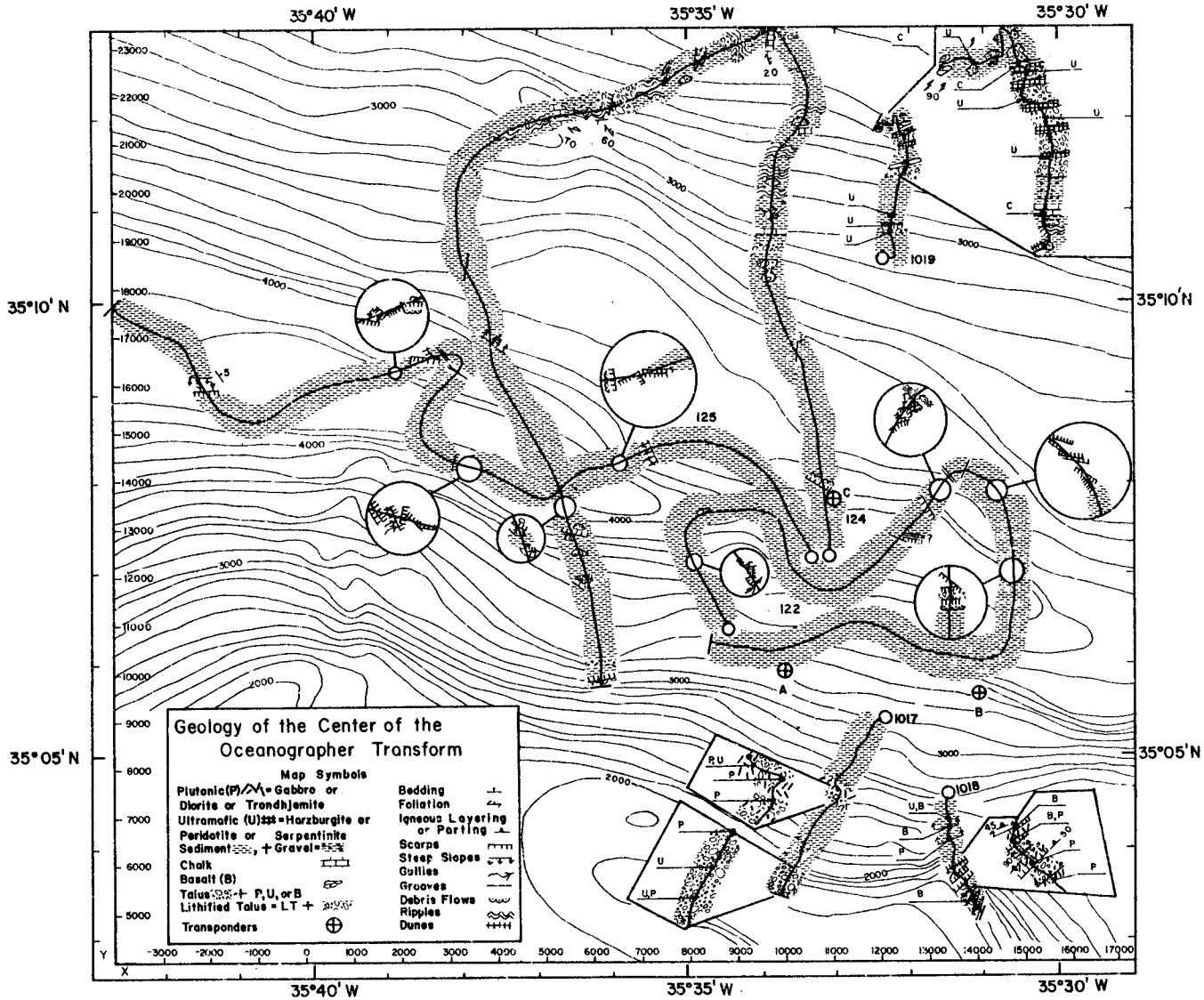
35°40' W
35°35' W
35°30' W
35°10' N
35°05' N
Geology of the Center of the
Oceanographer Transform
Map Symbols
Plutonic(P) = Gabbro or
Diorite or Trondhjemite
Ultramafic (U) = Harzburgite or
Peridotite or Serpentinite
Sediment, + Gravel =
Chalk
Basalt (B)
Talus + P, U, or B
Lithified Talus = LT +
Transponders
Bedding
Foliation
Igneous Layering
or Parting
Scarps
Steep Slopes
Gullies
Grooves
Debris Flows
Ripples
Dunes
125
124
122
1019
1017
1018
A
B
C

Figure 2-5: Geology along track, X-Y, ALVIN 1017. Symbology and track location are shown in Figure 2-4.

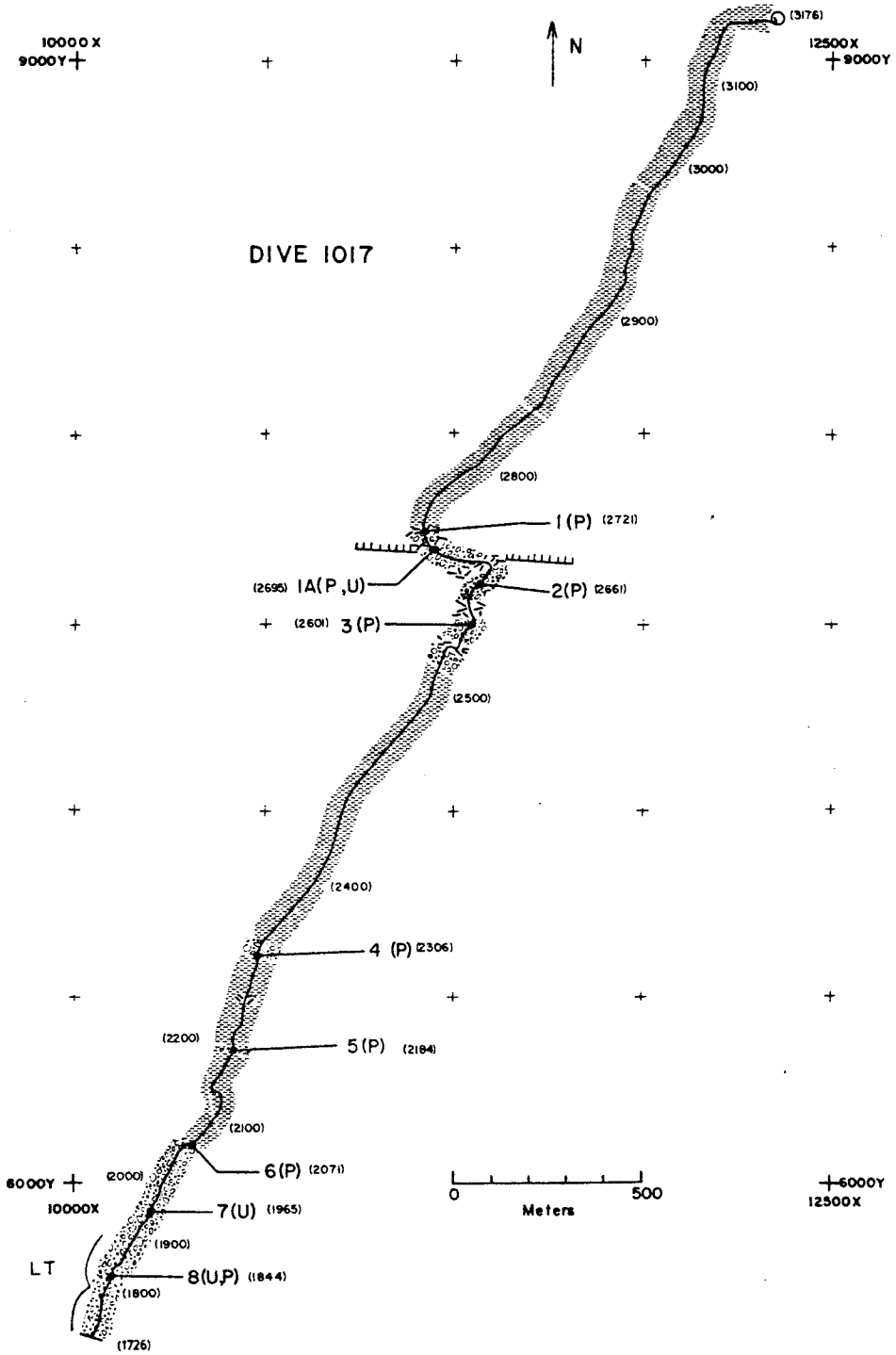
10000 X
9000Y
N
12500X
9000Y
(3176)
(3100)
(3000)
DIVE 1017
(2900)
(2800)
1 (P) (2721)
(2695) 1A(P,U)
2(P) (2661)
(2601) 3(P)
(2500)
(2400)
4 (P) (2306)
(2200)
5(P) (2184)
(2100)
6(P) (2071)
6000Y
(2000)
10000X
7(U) (1965)
(1900)
LT
8(U,P) (1844)
(1800)
(1726)
0
500
Meters
6000Y
12500X

Figure 2-6: Geology along track, depth versus distance, ALVIN 1017. Symbology and track are shown in Figure 2-4. Lower line equals depth along track from pressure sensor readout from ALVIN. Upper line is a translation of the lower line up and to the left to produce a swath of seafloor. Approximate course headings are shown. Sample locations are shown. Dashed lines are possible faults.

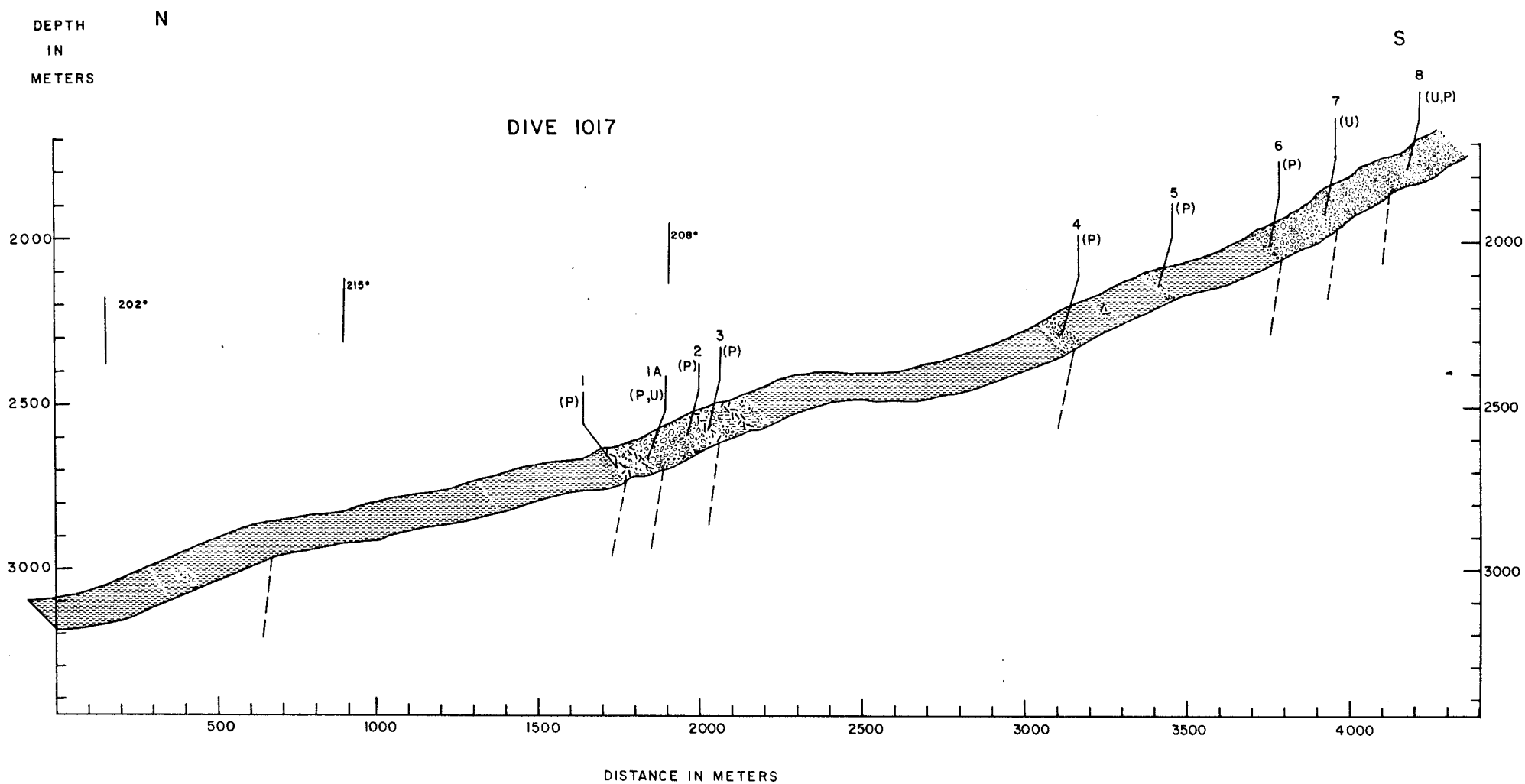
DEPTH
IN
METERS
N
S
DIVE 1017
202°
215°
208°
(P)
1A
(P,U)
2
(P)
3
(P)
4
(P)
5
(P)
6
(P)
7
(U)
8
(U,P)
2000
2500
3000
500
1000
1500
2000
2500
3000
3500
4000
DISTANCE IN METERS

Figure 2-7: Geology along track, X-Y, ALVIN 1018. Symbols and track location are shown in Figure 2-4.

DIVE 1018

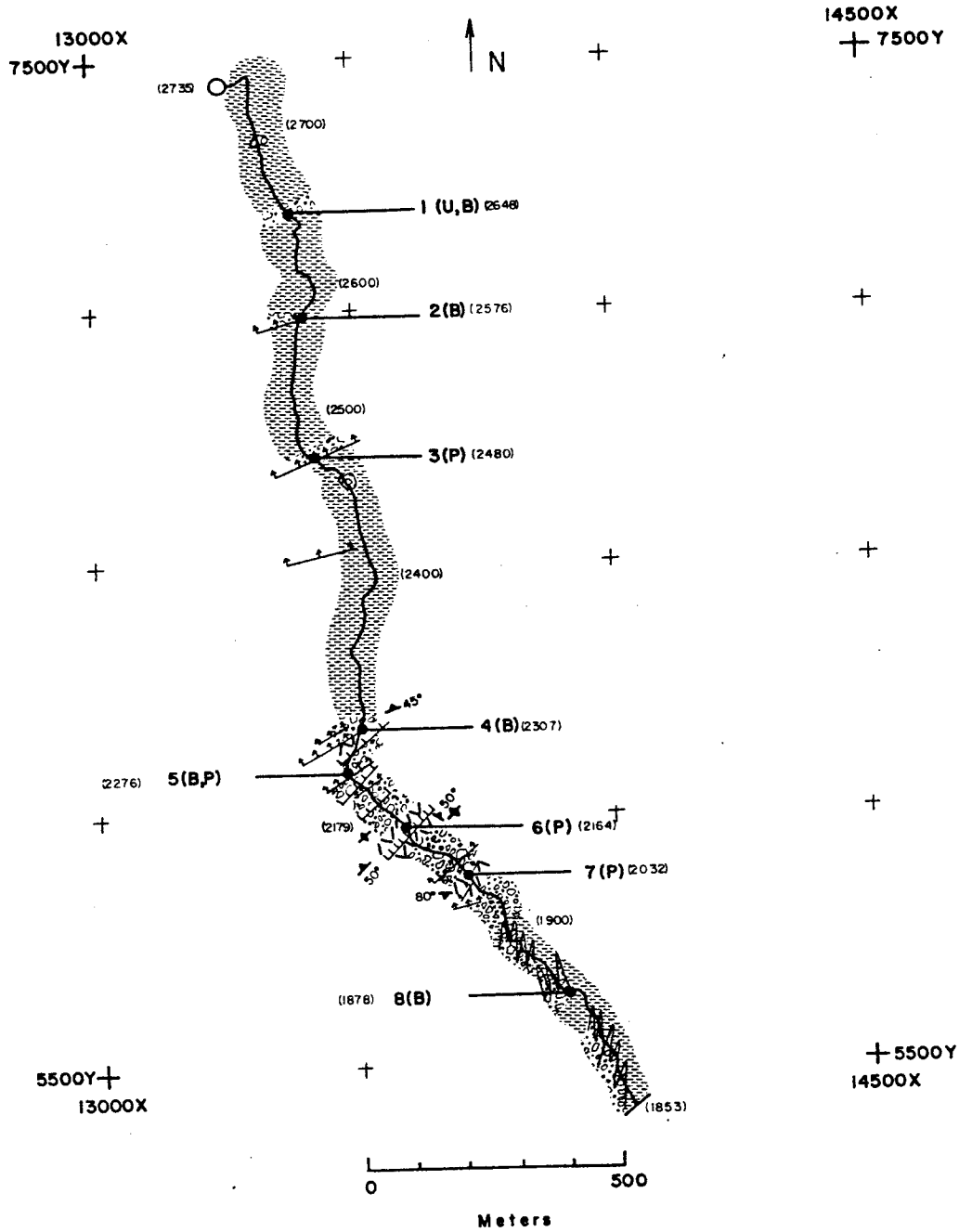
13000X
7500Y
14500X
7500Y
N
(2735)
(2700)
1 (U,B) (2648)
(2600)
2(B) (2576)
(2500)
3(P) (2480)
(2400)
4(B) (2307)
(2276)
5(B,P)
(2179)
6(P) (2164)
7(P) (2032)
(1900)
(1878)
8(B)
(1853)
5500Y
13000X
5500Y
14500X
0
500
Meters

Figure 2-8: Geology along track, depth versus distance, ALVIN 1018. For explanation of figure construction see Figure 2-6; see Figure 2-4 for map key and location of track.

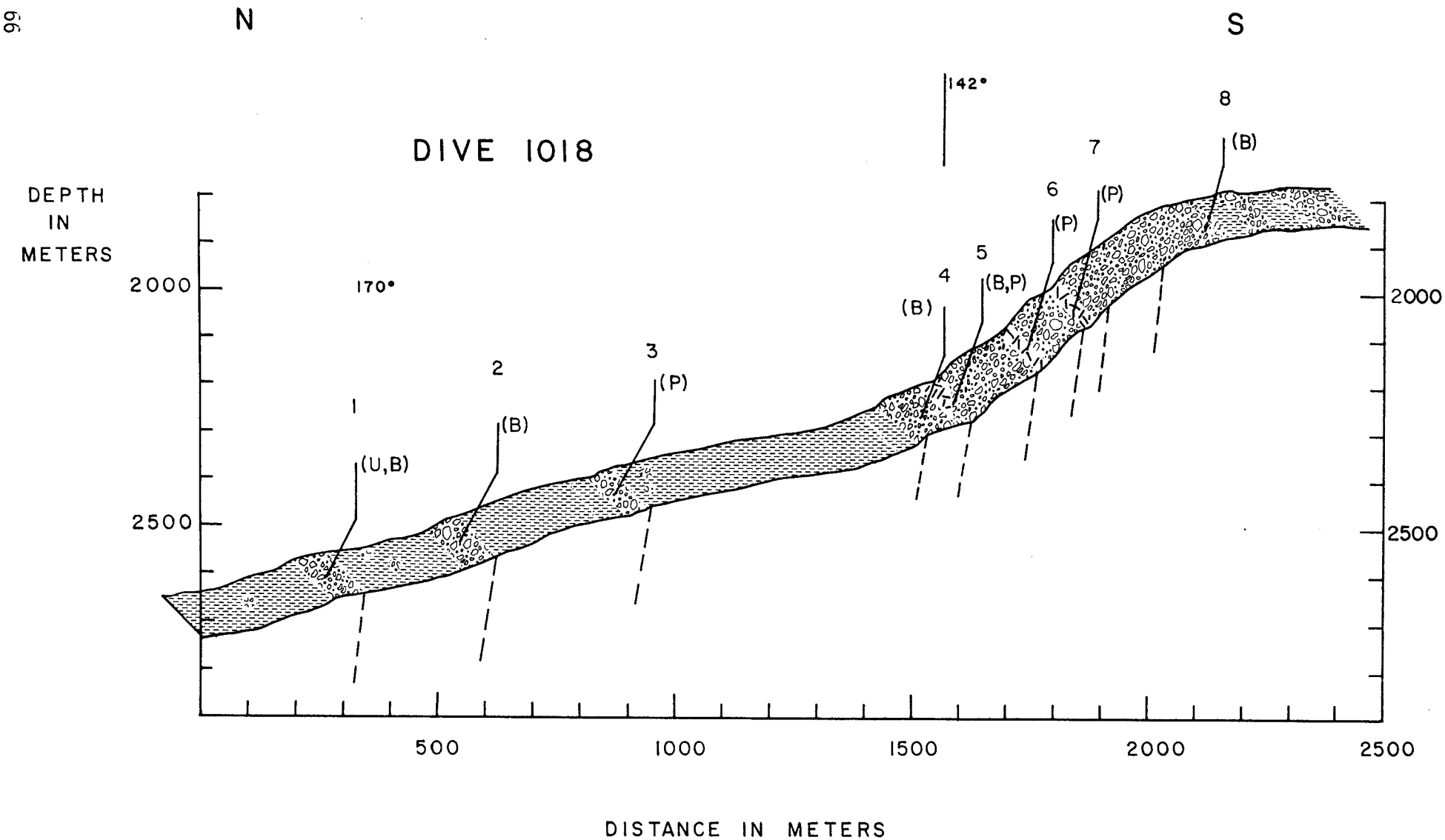
N
S
DIVE 1018
142°
170°
8
(B)
7
(P)
6
(P)
5
(B,P)
4
(B)
3
(P)
2
(B)
1
(U,B)
DEPTH IN METERS
2000
2500
2000
2500
500
1000
1500
2000
2500
DISTANCE IN METERS

Figure 2-9: Geology along track, X-Y, ALVIN 1019. Map key and location of track are shown in Figure 2-4.

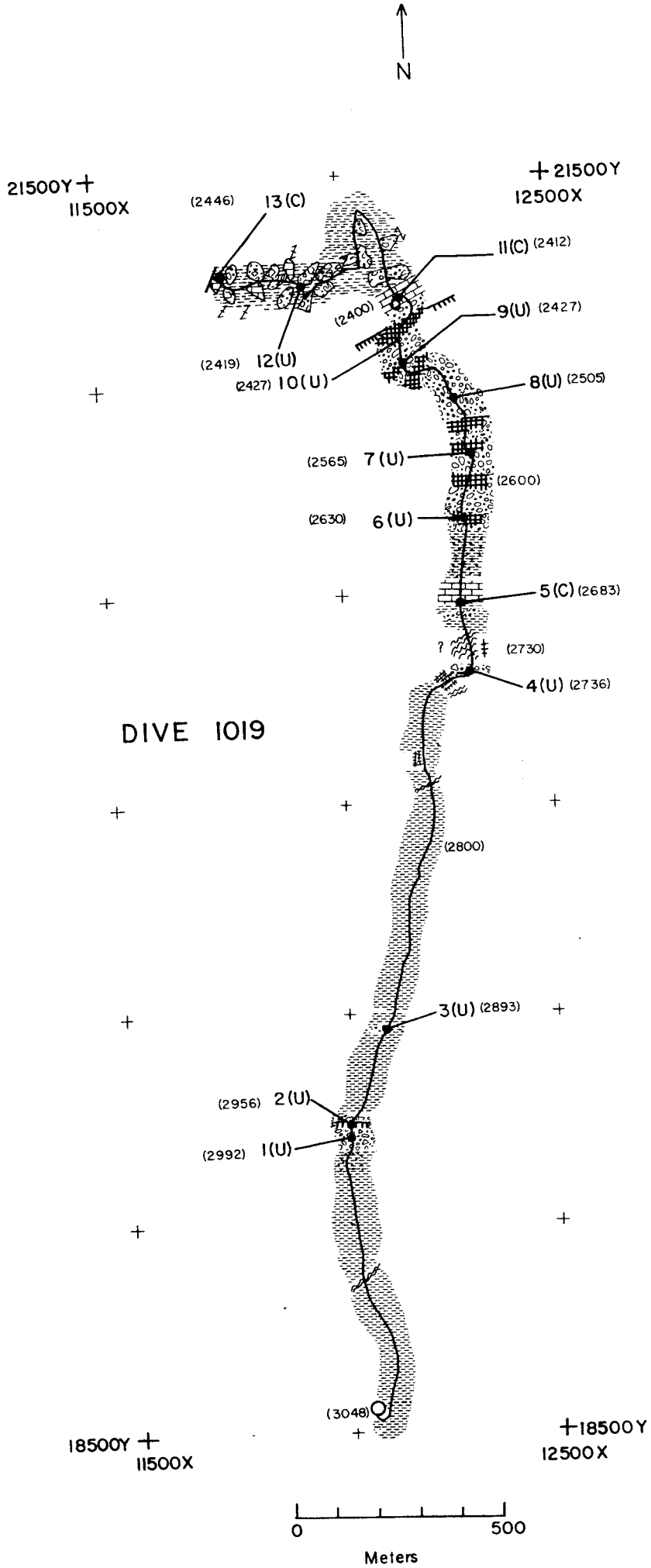
N
21500Y
11500X
21500Y
12500X
(2446) 13(C)
11(C) (2412)
(2400)
9(U) (2427)
(2419) 12(U)
(2427) 10(U)
8(U) (2505)
(2565) 7(U)
(2600)
(2630) 6(U)
5(C) (2683)
?
(2730)
4(U) (2736)
DIVE 1019
(2800)
3(U) (2893)
(2956) 2(U)
(2992) 1(U)
(3048)
18500Y
11500X
18500Y
12500X
0
500
Meters

Figure 2-10: Geology along track, depth versus distance, ALVIN 1019. For explanation of figure construction see Figure 2-6; see Figure 2-4 for map key and location of track.

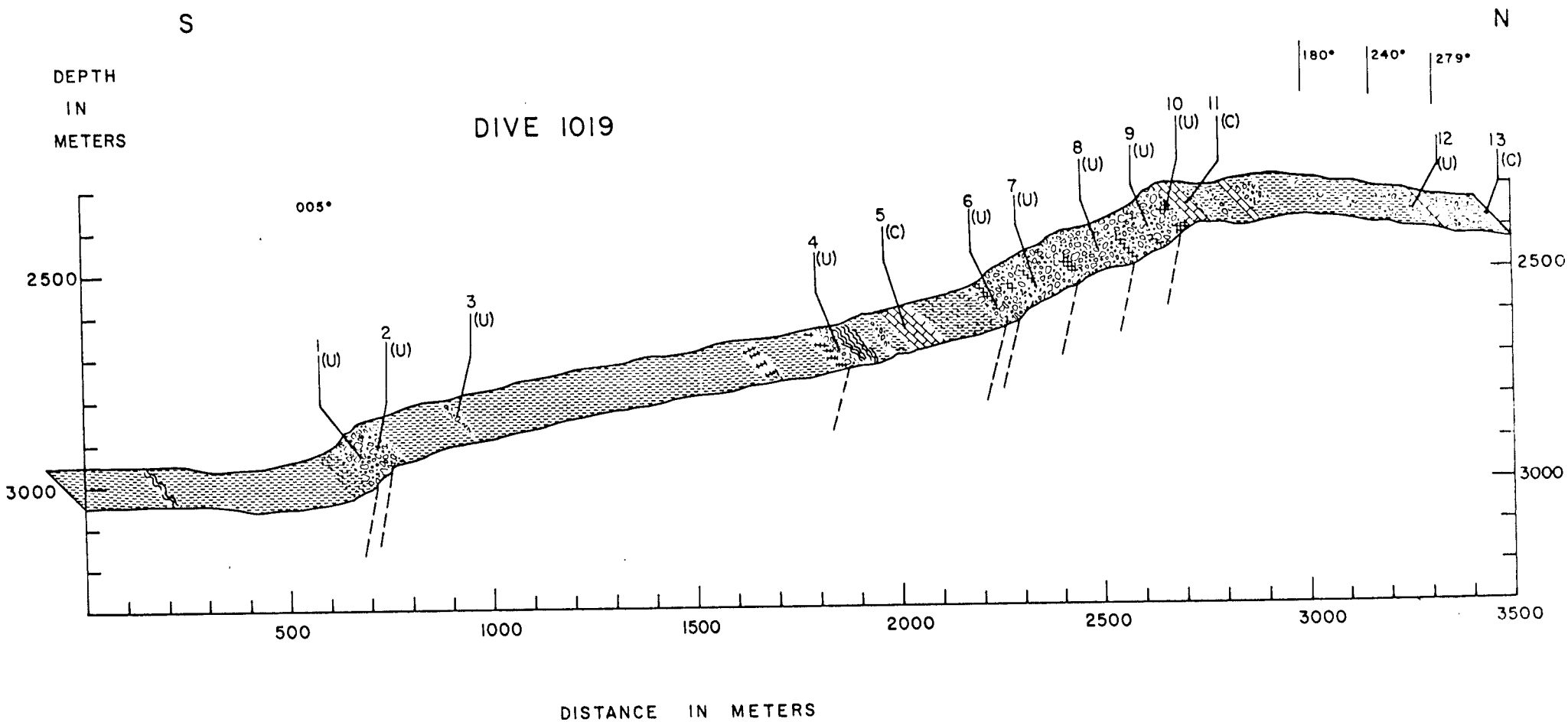
S
N
DEPTH
IN
METERS
DIVE 1019
005°
180°
240°
279°
1 (U)
2 (U)
3 (U)
4 (U)
5 (C)
6 (U)
7 (U)
8 (U)
9 (U)
10 (U)
11 (C)
12 (U)
13 (C)
2500
3000
2500
3000
500
1000
1500
2000
2500
3000
3500
DISTANCE IN METERS

Figure 2-11 Geology along track, X-Y, ANGUS 122. Map key and location of track are shown in Figure 2-4

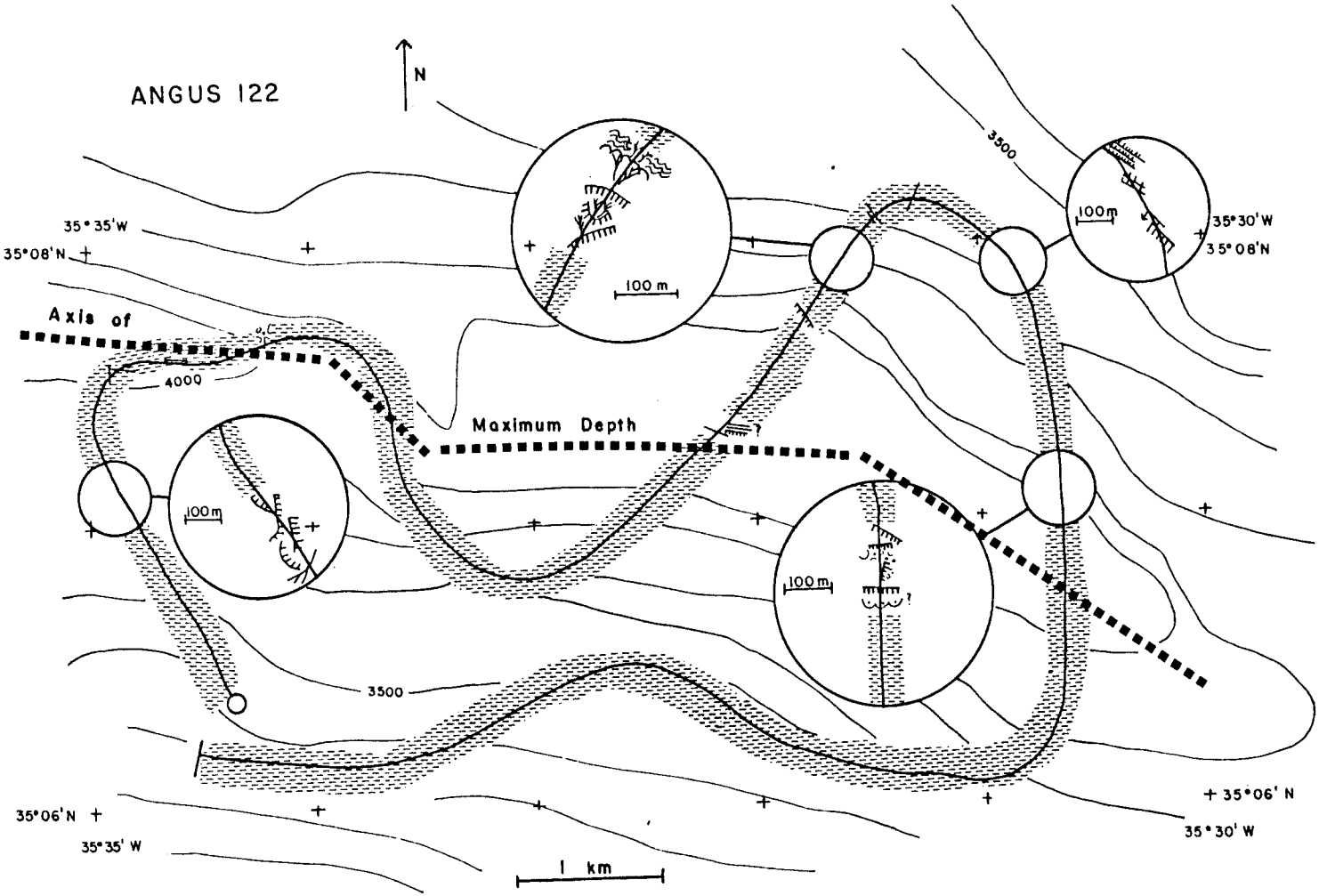
ANGUS 122
N
35°35'W
35°08'N
Axis of
4000
Maximum Depth
100 m
3500
35°30'W
35°08'N
35°06'N
35°35' W
35°06' N
35°30' W
1 km

Figure 2-12 Geology along track, X-Y ANGUS 124. Map key and location of track are shown in Figure 2-4

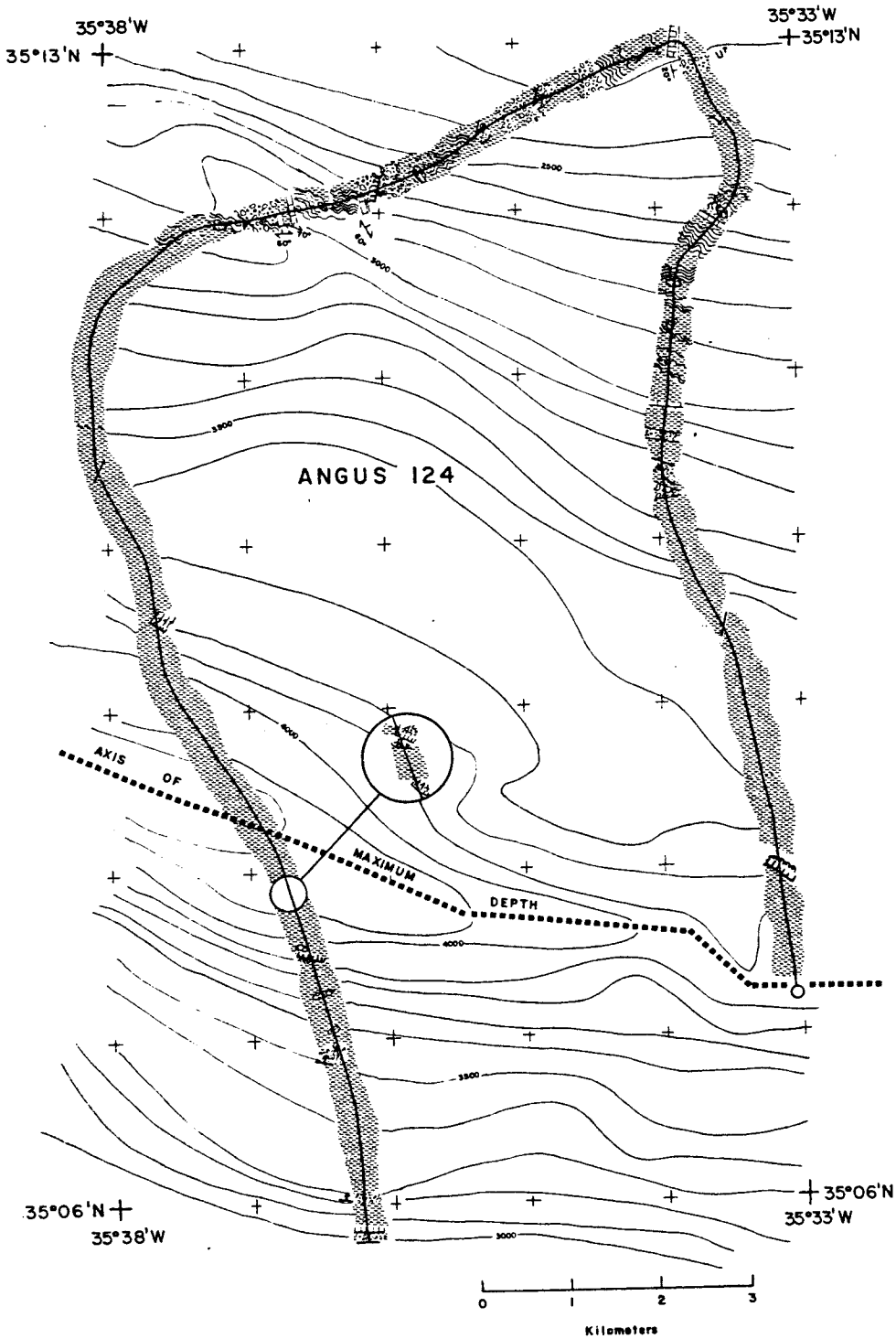
35°38'W
35°13'N
35°33'W
35°13'N
ANGUS 124
AXIS OF MAXIMUM DEPTH
35°06'N
35°38'W
35°06'N
35°33'W
0
1
2
3
Kilometers

Figure 2-13 Geology along track, X-Y, ANGUS 125. Map key and location of track are shown in Figure 2-4

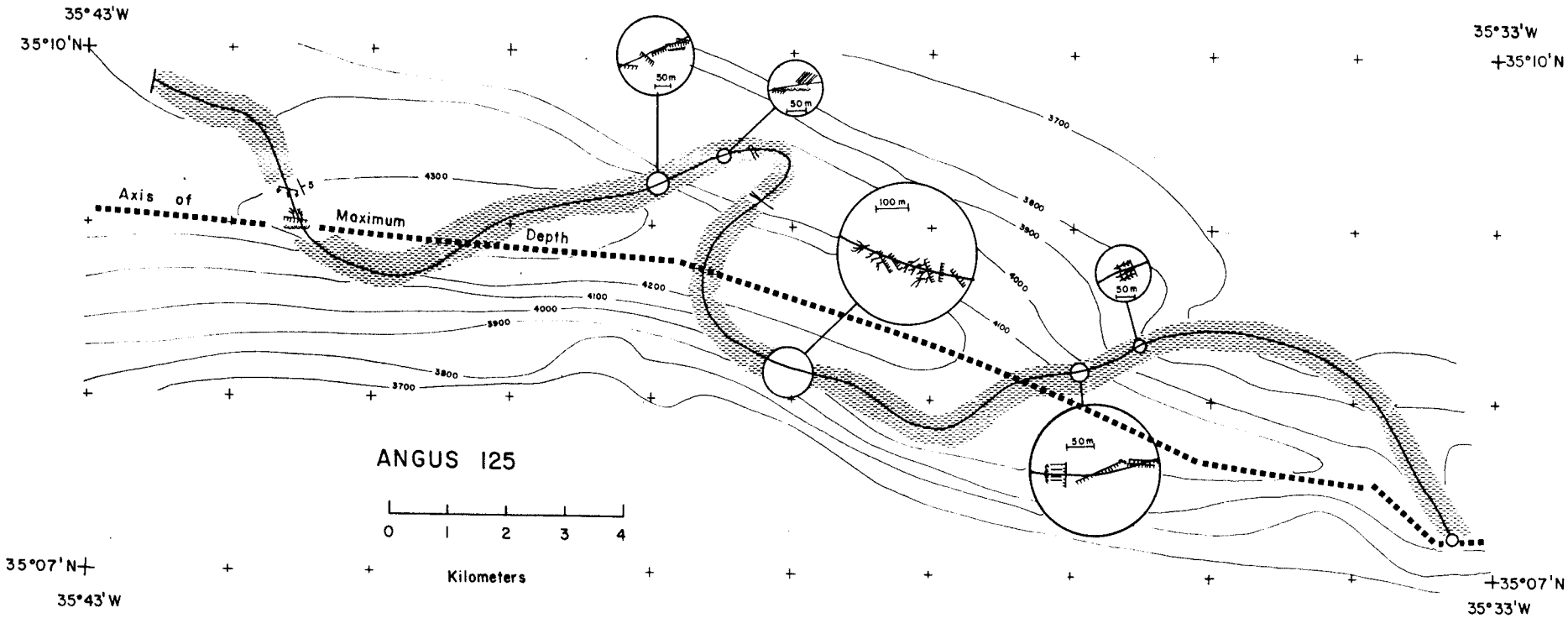
35°43'W
35°10'N
35°33'W
35°10'N
Axis of
Maximum
Depth
4300
4200
4100
4000
3900
3800
3700
3700
3800
3900
4000
4100
50m
50m
100 m
50m
ANGUS 125
0 1 2 3 4
Kilometers
35°07'N
35°43'W
35°07'N
35°33'W

Figure 2-14 Geology along track, X-Y, ANGUS 126. Location of track shown in Figure 2-2.

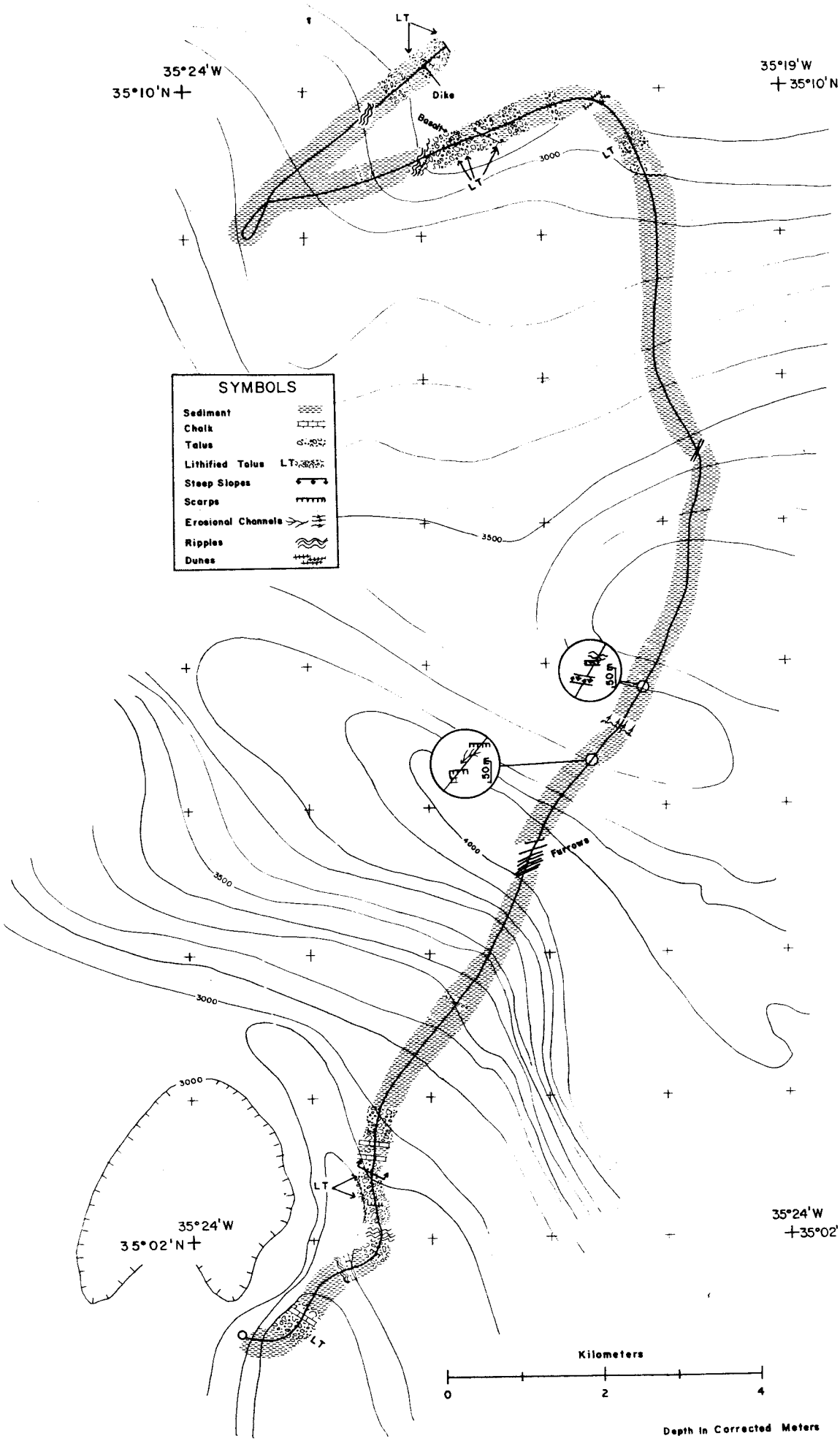
35°24'W
35°10'N
35°19'W
35°10'N
LT
Dike
Basalt
3000
3500
4000
SYMBOLS
Sediment
Chalk
Talus
Lithified Talus
Steep Slopes
Scarps
Erosional Channels
Ripples
Dunes
Furrows
35°24'W
35°02'N
35°24'W
35°02'N
Kilometers
0
2
4
Depth in Corrected Meters

Figure 2-15 Cross-section of the Oceanographer transform interpreted from the bathymetric, ANGUS, and ALVIN data

CROSS SECTION OCEANOGRAPHER TRANSFORM

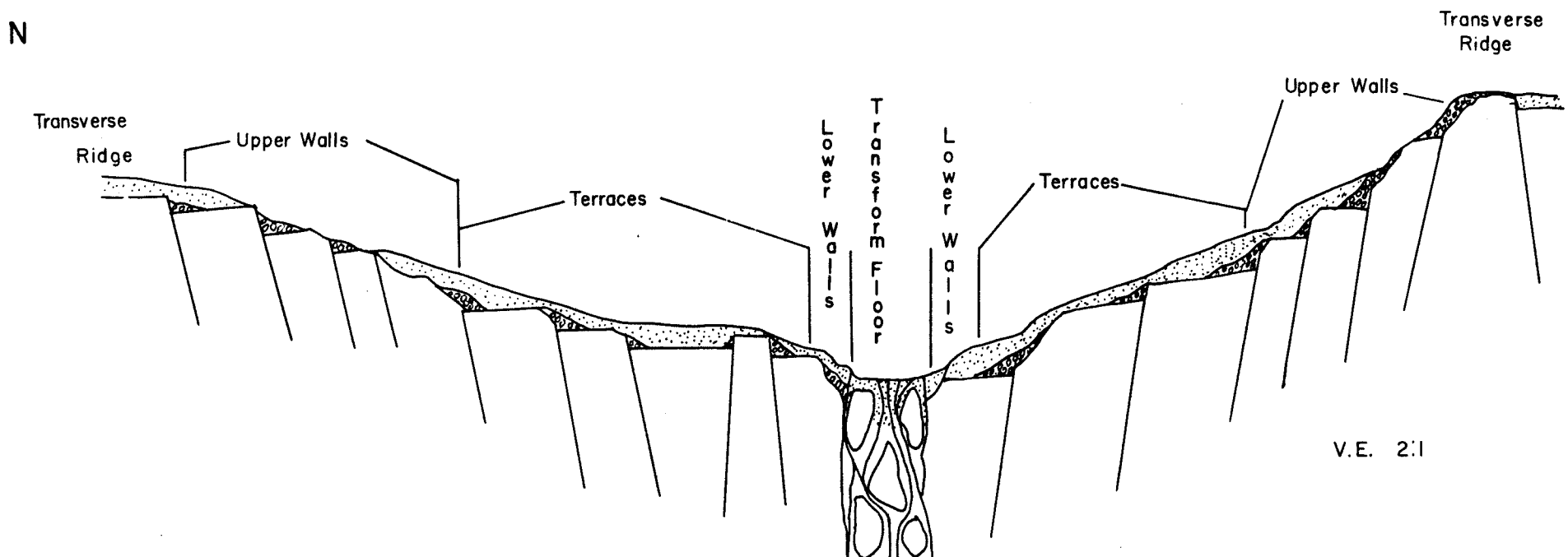

Figure 2-16

ANGUS 124, 35º08'N, 35º33'W. Field of view 5 x 7 meters. Probable fault scarp in carbonate mud with debris flow at base. Debris flow shows extensive signs of reworking by bottom grazers.

Figure 2-17

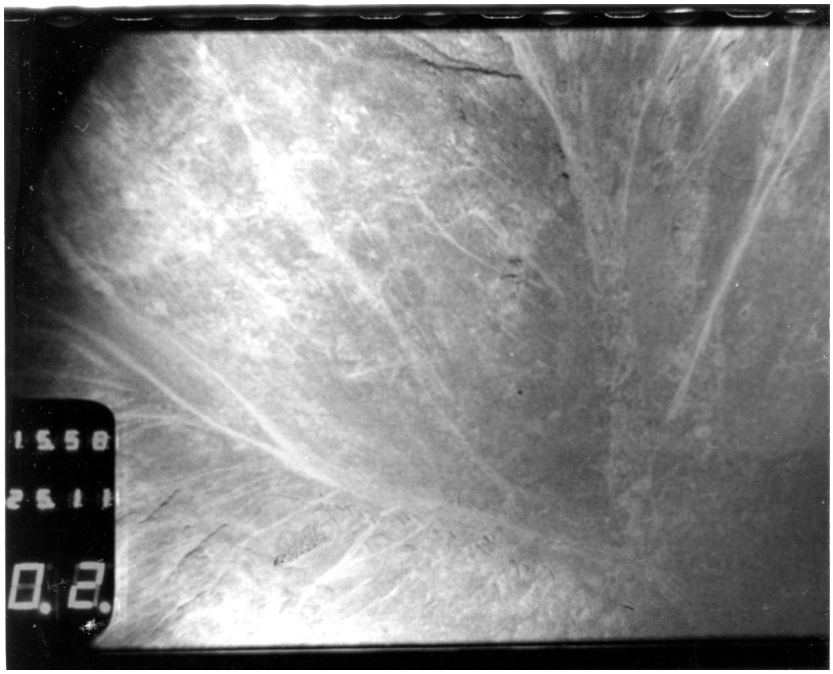

ANGUS 122, 35º08'N, 35º07'W. Field of view 4 x 6 meters. Fault scarp in poorly consolidated carbonate showing extensive evidence of gullying and degradation. Lighter streaks are exhumed (?) sediment flowing downhill.

Figure 2-18

ANGUS 126, 35º02.6'N, 35º22.5'W. Field of view 5 x 7 meters. Lithified carbonate encrusted with manganese that is interpreted to show substantial erosion of original sediment probably by winnowing.

Figure 2-19

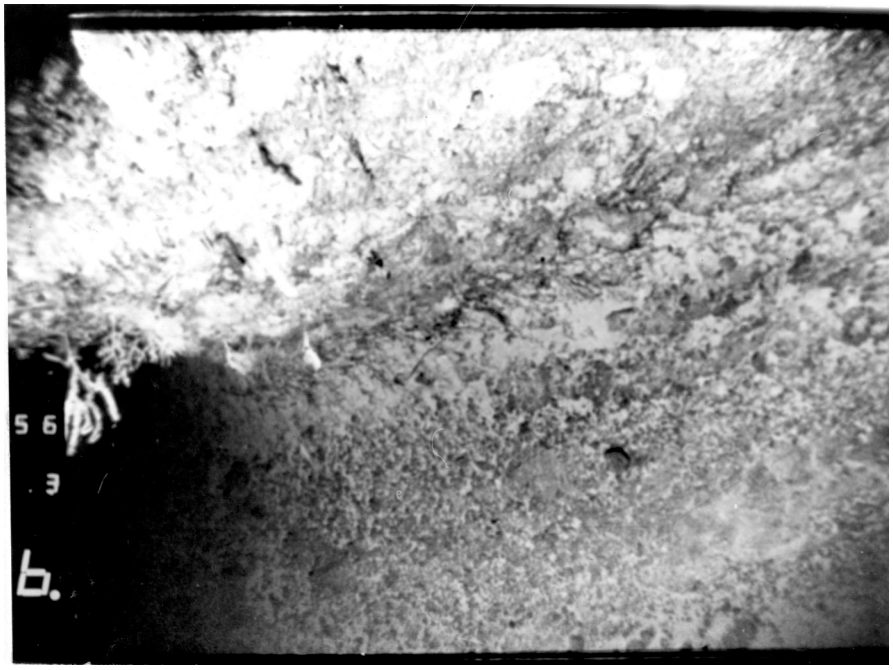

ANGUS 126, 35º02.2'N, 35º22.5'W. Field of view (4-6) x (4-10) meters. Steep wall of lithified breccia. Minor amounts of sessile faunas.

Figure 2-20: Rose diagram of fault orientations in sediment from ANGUS lowerings 122, 124, and 125

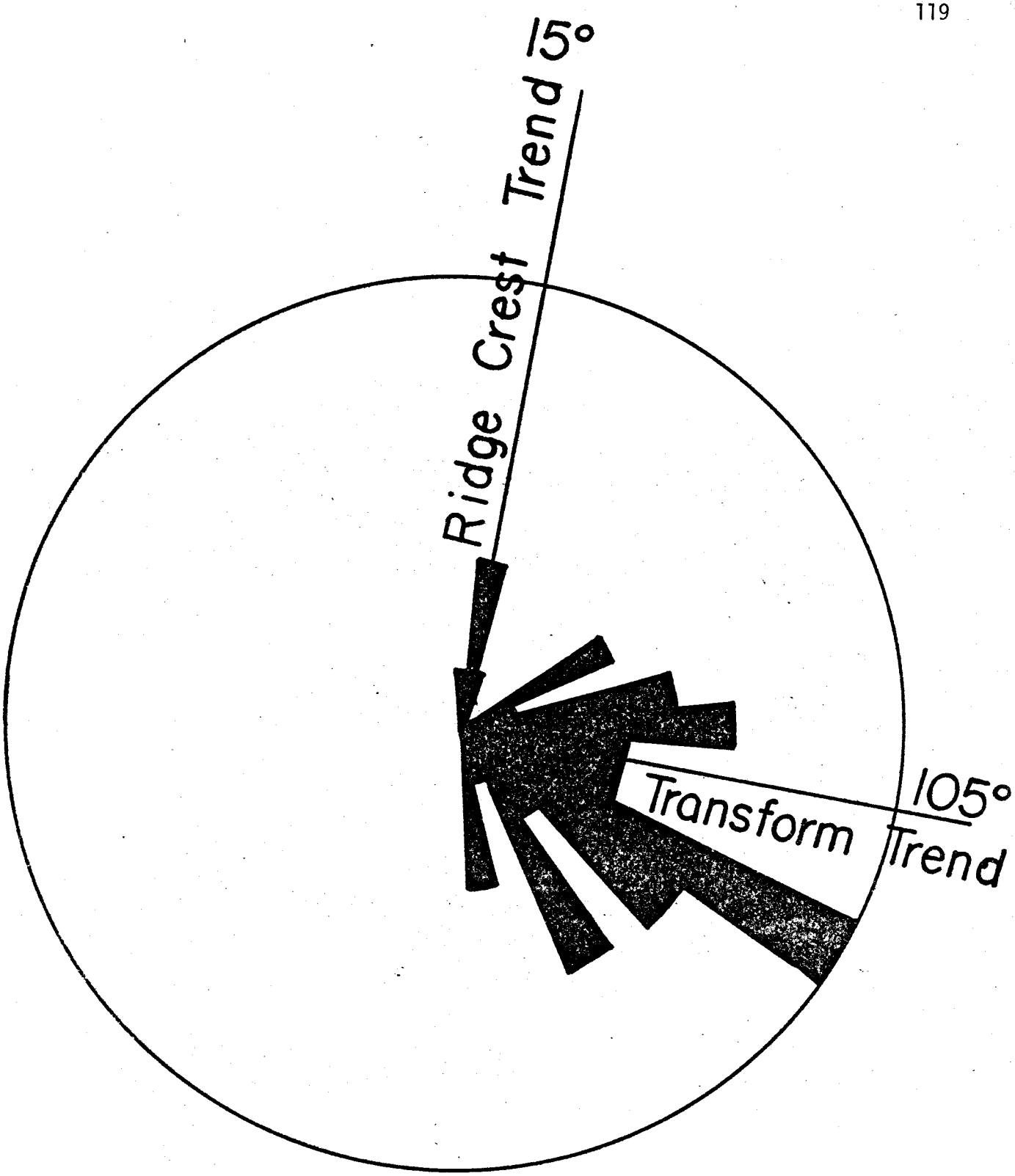
15°
Ridge Crest Trend
105°
Transform Trend

Figure 2-21

ANGUS 124, 35º12'N, 35º33.6'W. Field of view 5 x 7 meters.
Low amplitude possible wave ripples in carbonate mud.

Figure 2-22

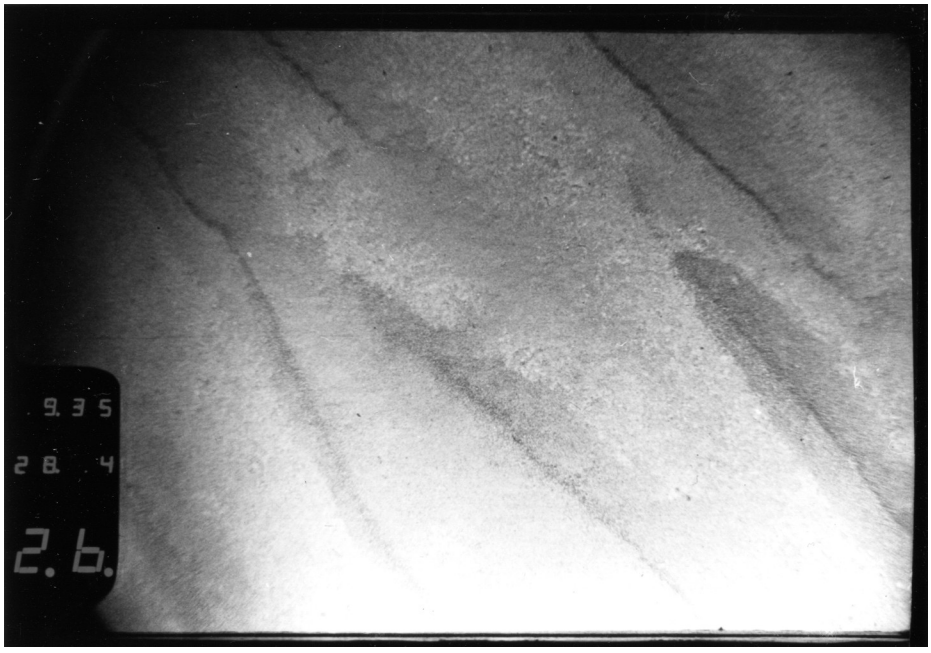

ANGUS 126, 35º10'N, 35º20'W. Field of view 5 x 7 meters. Longditudinal triangular ripples in unconsolidated pteropod shells. These form parallel to the direction of the current flow.

Figure 2-23

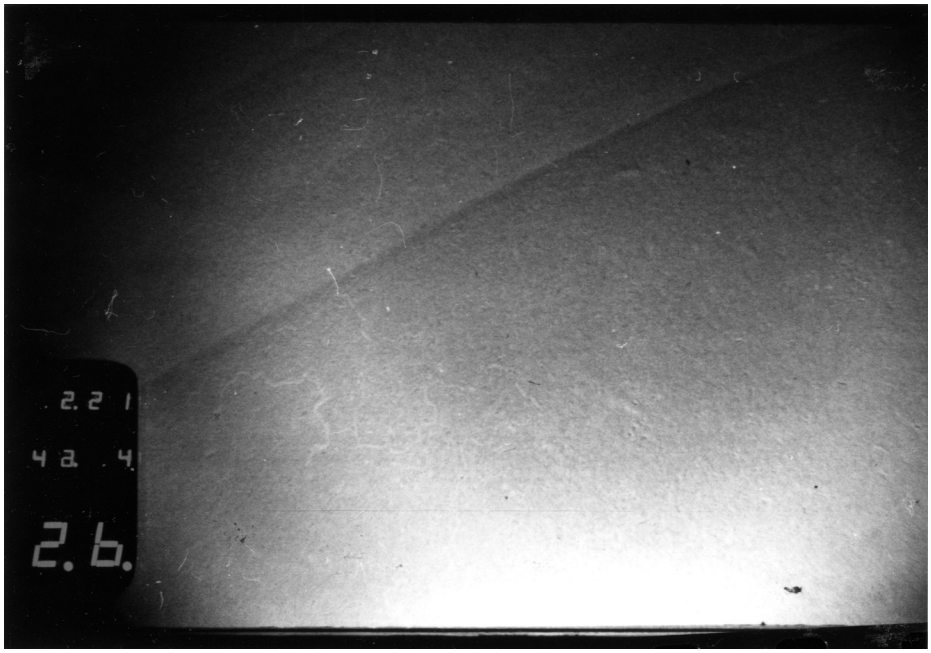

ANGUS 126, 35º04.6'N, 35º26.2'W. Field of view 5 x (5-8) meters. Parallel grooves (abyssal furrows) in carbonate ooze. These are believed to form parallel to the direction of the prevailing current.

Figure 2-24

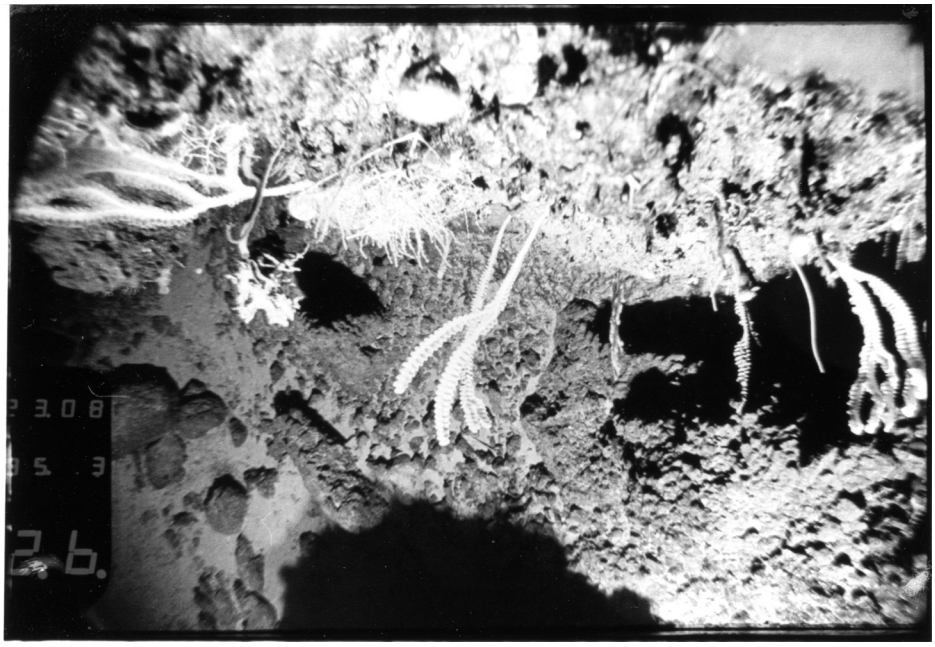

ANGUS 126, 35º02.2'N, 35º22.5'W. Field of view 4 x (3-8) meters. Steep breccia wall with luxuriant growth of sessile faunas.

Figure 2-25

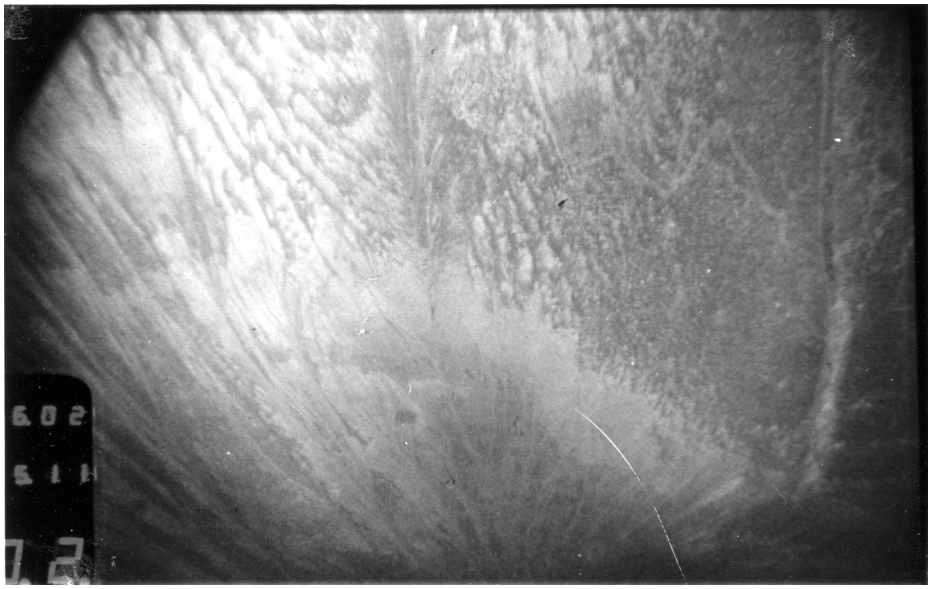

ANGUS 122, 35º08'N, 35º31.7'W. Field of view 5 x 7 meters. Shoestring rills forming in unconsolidated sediments at the head of a scarp.

Figure 26: ALVIN 1018, $35^{o}03.8'N$, $35^{o}31.4'W$. Field of view 3 X 4 meters. Heavily jointed and foliated gabbros.

CHAPTER III

SPECULATIONS ON THE ORIGIN OF TRANSFORM TOPOGRAPHY

Systematic efforts to map transform topography have met with decided success, yet few investigators have attempted to formulate models which accomodate most of the topographic data, at least insofar as the origin of transform topography is concerned. Instead, most research efforts have been designed to tackle specific problems (Johnson, 1967; Fox et al., 1969; Bird and Phillips, 1975; Schroeder, 1977; Davis and Lister, 1977; Lonsdale, 1978; Lonsdale and Shor, 1979; Searle, 1979; Searle, 1981; Fox et al., in prep., and many others). With the exception of Menard and Atwater, 1969, few investigators have suggested models of the origin of transform topography. I offer here a simple conceptual model which addresses the issue of the origin of transform topography. The model depends upon the work of Gallo and Fox (1979); therefore I will present those aspects of their model that are indispensable to this paper.

In its simplest form what Gallo and Fox (1979) have argued is that ridge-transform transform faults juxtapose lithospheric blocks of different thermal structure across a narrow boundary. This causes heat to be transferred across the transform fault from the hotter block to the colder block; the resulting change in thermal structure of both blocks alters their mechanical properties so that part of the older and colder block becomes asthenosphere and asthenosphere near the younger, hotter block becomes more viscous or solidifies as mantle (Gallo and Fox, 1979). Another of their conclusions is that the transform fault is listric or curved at depth towards the younger, thinner plate near an offset ridge axis (Figure 1). Gallo and Fox (1979) suggest that the transform fault near the ridge axis must be listric because a listric boundary minimizes the thickness of lithosphere under-

going shear (Figure 1). Any other configuration would increase the amount of work necessary to accomodate plate motion. This model does not depend on the plate boundary being listric. All that is required is the plate boundary not be vertical near the intersection and that it intersect with the asthenosphere beneath the younger plate.

The second concept that merits attention is a description of what the lithosphere supply conduit looks like in three dimensions near the transform. The conduit as described by Lachenbruch (1973) is a vertically walled cleft along which material freezes or accretes to at the same rate as the cleft diverges. Sleep and Biehler (970) reasoned that near transforms a third boundary was present (the older plate) and that asthenosphere tended to freeze or become more viscous along this additional boundary. Neither Lachenbruch (1973) nor Sleep and Biehler (1970) have attempted to depict the conduit near the transform, which is the purpose of this paper (Figure 3-2a, 2b,3a,3b).

The most significant aspect of this model is that as soon as the plate boundary becomes listric towards the younger plate a gap forms between the two plates beneath the inside corner of the ridge-transform intersection (Figures 3-2b,3a); thus the conduit becomes elongated parallel to the transform (Figure 3-2b). The degree of elongation is proportional to how far the transform boundary is displaced at depth towards the younger plate. One way to visualize the conduit is as follows: Take a sheet of paper held lengthwise; imagine that the vertical plane so formed is the plane of the transform. Now imagine that the ridge crest intersects the transform at your right hand. If the ridge crest terminates on the side of the paper facing you, then fold the lower right-hand

corner of the paper into a gentle curve towards you. That is the shape of one side of the conduit. Now visualize an array of particles moving parallel to the initial plane. This array of particles moves parallel to each other as well as away from the surface of the conduit; it does not matter what the starting configuration is (Figure 3-2a), the particle motion will be unaffected and the volume of new lithosphere generated will be constant. Another feature this exercise demonstrates is that the part of the transform that undergoes partial extension varies with how much the paper is folded.

From this rather modest concept implications arise that are not obviously related to the conduit. The first of these implications is why large-offset transforms tend to have great relief and great width. The relief and the width of most large-offset transforms may be due to the conduit being elongated beneath the transform axis and the younger plate (Figure 3-2b). The curvature of the conduit at depth subjects lithosphere there to stretching. It is this partly divergent motion not the strike-slip motion of the particles which causes mass to be removed on a steady-state basis from beneath the intersection deep and the transform axis (Figure 3-4). In effect the transform axis behaves like a rift valley. Mass is continually removed from beneath the axis of the transform by plate motion (Figure 4); this mass deficit is partially made up by flow of asthenosphere into the extended region. The remaining mass that cannot flow into the extended because of viscous drag uplifts the walls of the conduit. Thus dynamic compensation is effected between the axis of the transform and the bordering walls of the transform in a manner that is analogous to

the compensation between the rift valley and the crestal mountains.

In another possible parallel to rift valley formation recent mapping in the Oceanographer transfrom (see chapter 2) revealed that the gradients are not uniform into the transform axis from the transform walls. Instead the much steeper upper wall province gives way to the much gentler terraces as the axis is approached. I believe that the terraces may be the site of conjugate normal faulting where extension may be accomodated and that the great relief of the upper wall province may be due to asymmetric normal faulting which accomodates little or no extension in a manner that is analogous to the rift valley (Figure 3-1). An alternate possibility is that the steep, upper wall province has not suffered the same degree of mass wasting as the lower walls.

Another implication of the steady-state removal of mass from beneath the axis of the transform is that as the transform offset becomes less along a common plate boundary both the width of the transform and relief should go to zero (Figure 3-5). What Figure 3-5 also shows is that as the listric boundary lessens so does the topographic effects associated with it. Stated differently large-offset transforms should have greater relief and width for dynamic reasons than short-offset transforms along the sameboundary.

Several other parameters should vary with distance from the intersection deep. As the conduit becomes progressively more curved at depth near the transform, eventually strike-slip particle motion ceases to exist and the transform gives way to oblique spreading. It is this oblique spreading at depth that helps to keep the axis of the transform at a depressed elevation.

The conduit is strongly asymmetric (Figure 3-2b) which carries

with it substantial secondary implications. Most important probably is that the recovery effects of the seafloor are not likely to be symmetric about the intersection deep (Figure 3-5). Instead gradients into the intersection deep should be steeper from the fracture zone side going into the intersection deep rather than going from the transform side into the intersection deep. This is due to the fact that extension at depth continues to occur into and along the transform axis farther than it does towards the fracture zone continuation (Figure 3-2b). Therefore recovery effects will be completed sooner on the fracture zone side of the deep than from the transform side of the deep (Figure 3-6). In the Oceanographer transform (Schroeder, 1977 and Fox et al., in prep.) and the Tamayo transform (Tamayo Scientific Team, 1980a,c) gradients are significantly steeper from the fracture zone side towards the intersection deep than from the transform side towards the intersection deep. This is shown schematically in Figure 3-6.

Another characteristic of the curved conduit is that parcels of lithosphere do not rise to a level of isostatic equilibrium on the same side of the ridge at different locations at the same time. At the midpoint of the ridge between two transforms viscous drag effects are least and judging from the response of the seafloor complete recovery effects are fastest there (Schroeder, 1977 and Fox et al., in prep.). Near the transform viscous drag effects are greatest (Sleep and Biehler, 1970) and recovery effects will take longer there primarily because extension beneath the axis of the transform and the inner wall will continue long after it has ceased at other locations along the ridge (Figure 3-2b). What should

happen frequently is that some blocks of lithosphere near the transform will still be rising whereas other adjoining blocks may have started to subside as they age. This sets up vertical gradients (strain) within the plate which must be accomodated by either flexure or faulting (Figure 7). This idea is potentially testable since the transverse ridges of transforms should be either horsts or monoclines. One test of this idea would be to look for signs of faulting on the side of the transverse ridge facing away from the transform, but the very low strain rates and high rates of mass-wasting involved may render recognition of the faults unresolvable with conventional surface ship equipment.

One consequence of the viscous drag varying with distance from the intersection region (parallel to the ridge, Sleep and Biehler, 1970) is that short ridge segments between two offsetting transforms will tend to be hourglass shaped, that is, wide and deep at both ends and narrow and shallow in the middle (Figure 1). This shape is observed of transforms and the rift valleys in the FAMOUS area (Choukroune et al., 1978) and the Oceanographer transform and associated rift valleys (Schroeder, 1977 and Fox et al., in prep.). Since the viscous drag component is maximum near the ridge-transform intersection and decreases along the ridge and along the transform, both ridges and transforms of slow-spreading centers should be hourglass shaped for dynamic reasons.

If this model of the conduit shape is correct, then periodically the inside corner should become "leaky" and the site volcanism. Most of the time this volcanism is expected to be relatively insignificant, but occasionally conditions may be

favorable for more voluminous eruptions.

One of the concepts that has gained considerable acceptance in the scientific community is that the principal transform displacement zone is extremely narrow (<2km) (Choukroune et al., 1978; Lonsdale, 1978; CYAMEX and Pastouret, 1981; Tamayo Scientific Team, 1980a, b, c; OTTER, 1980). This may well be the case for the surface trace of the fault in the center of the transform, but I believe that the transform is probably very wide (> 5km) at depth near each ridge-transform intersection (Figure 3-2b). The implications for transforms preserved as ophiolites should be clear. Material rising within the conduit will be subjected to simultaneous emplacement, shear, and extension. The total width of the high strain zone which may develop may exceed 10 km.

The last concept to be addressed in terms of the origin of transform topography is why there are Pacific type transforms which may lack transverse ridges and why there are Atlantic type transforms which tend to possess them. Much but not all of the difference can be attributed to the fact that Atlantic transforms juxtapose a much greater age contrast per unit length of offset (Figure 3-8). A major unknown in this discussion is whether or not the rheology of the lithosphere and the asthenosphere remain constant at different spreading rates where the age constrast across the transform is the same. One possibility is that the rheology of the lithosphere and/or the asthenosphere does not remain fixed and that strain softening of the lithosphere or strain hardening of the asthenosphere occurs preferentially in in fast spreading centers. Either effect will reduce the listric

nature of the plate boundary and all the properties of the listric boundary. I propose that just as the minimum work configuration for the intersection of slow spreading centers is a listric boundary, at fast spreading centers the listric nature of the plate boundary is less for a given age contrast that it is for slow spreading centers (Figure 3-9). This reduces the relief of some of the Pacific transforms.

Any model should be consistent with all or most of the applicable data. It is my belief that the model presented here is consistent with most of the topographic data set from transform faults. I have deliberately avoided discussions of what happens during changes in the pole of relative motion (Menard and Atwater, 1968; Dewey, 1975) because that introduces complexities not readily predictable within the framework of this model. If changes in fracture zone topography are as predictable during pole changes as Menard and Atwater (1968) suggest, then this model should perhaps be viewed as complimentary to their model.

Figure 3-1 Map view of transform showing maximum deviation of the plate boundary from a vertical plane (darkened region); cross-section of ridge-transform boundary system.

GENERALIZED RIDGE / TRANSFORM MORPHOLOGY

(Slow Spreading Center)

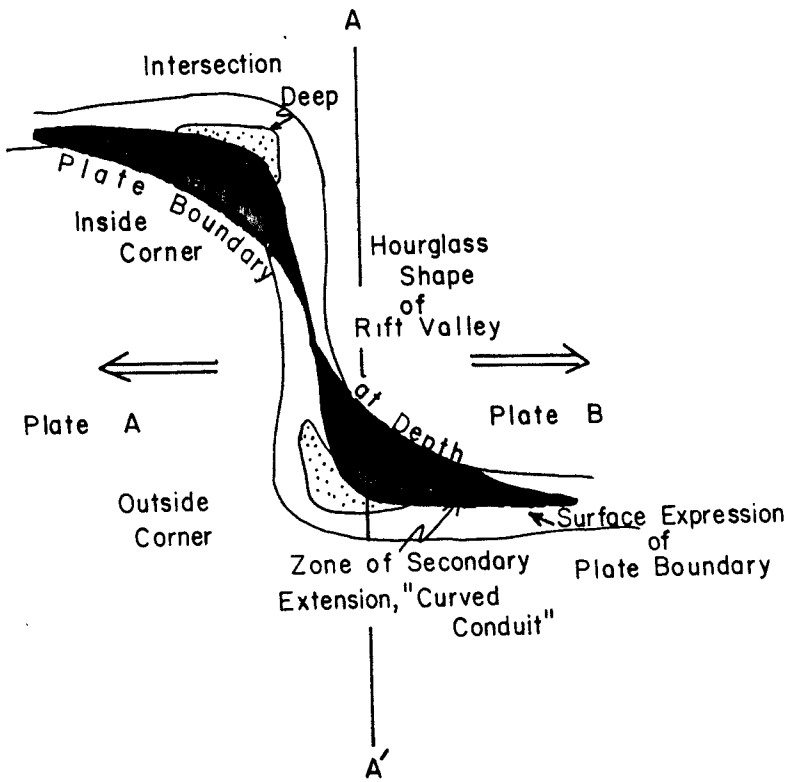

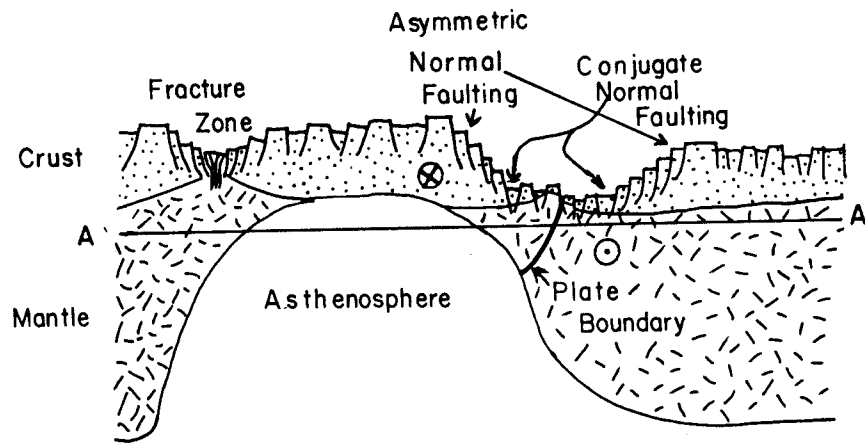

Figure 3-2a Different ridge geometries still create the same volume of lithosphere per unit time.

Figure 3-2b Map view of the conduit showing relationship of particle motion to conduit walls.

Ridge Crest Between Plates A and B; 3 Geometries Which all have $d\alpha/dt = C$

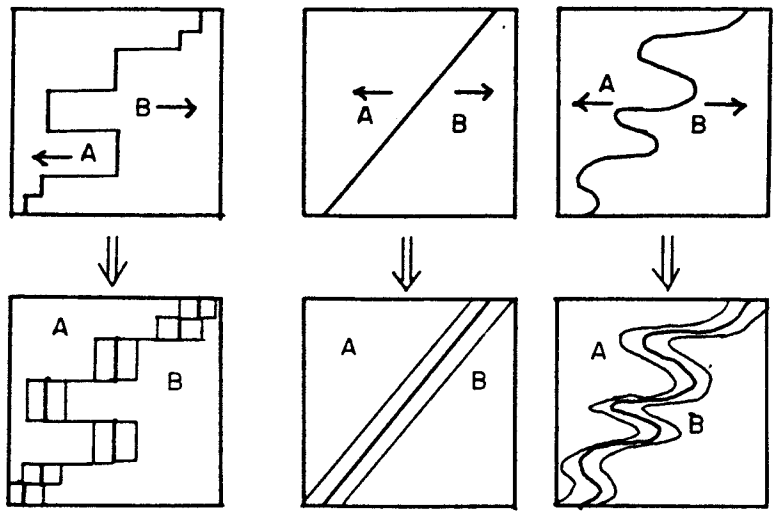

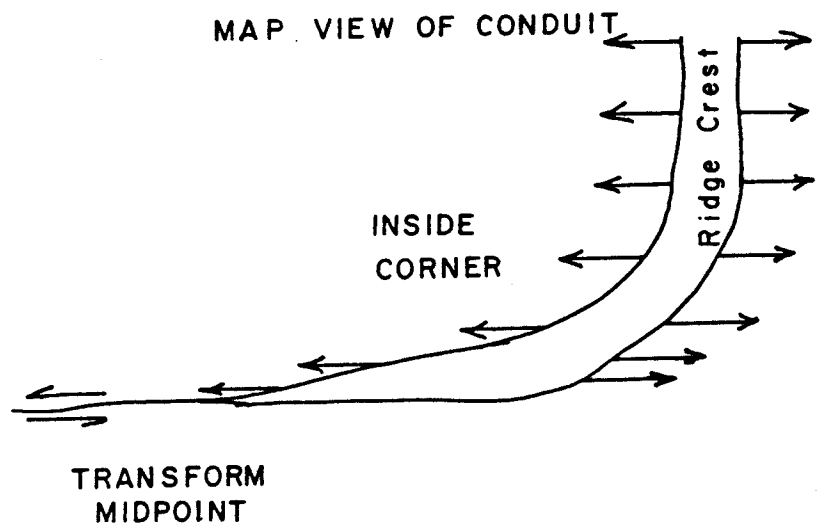

Figure 3-3a Block diagram showing the surface of decoupling between the plates.

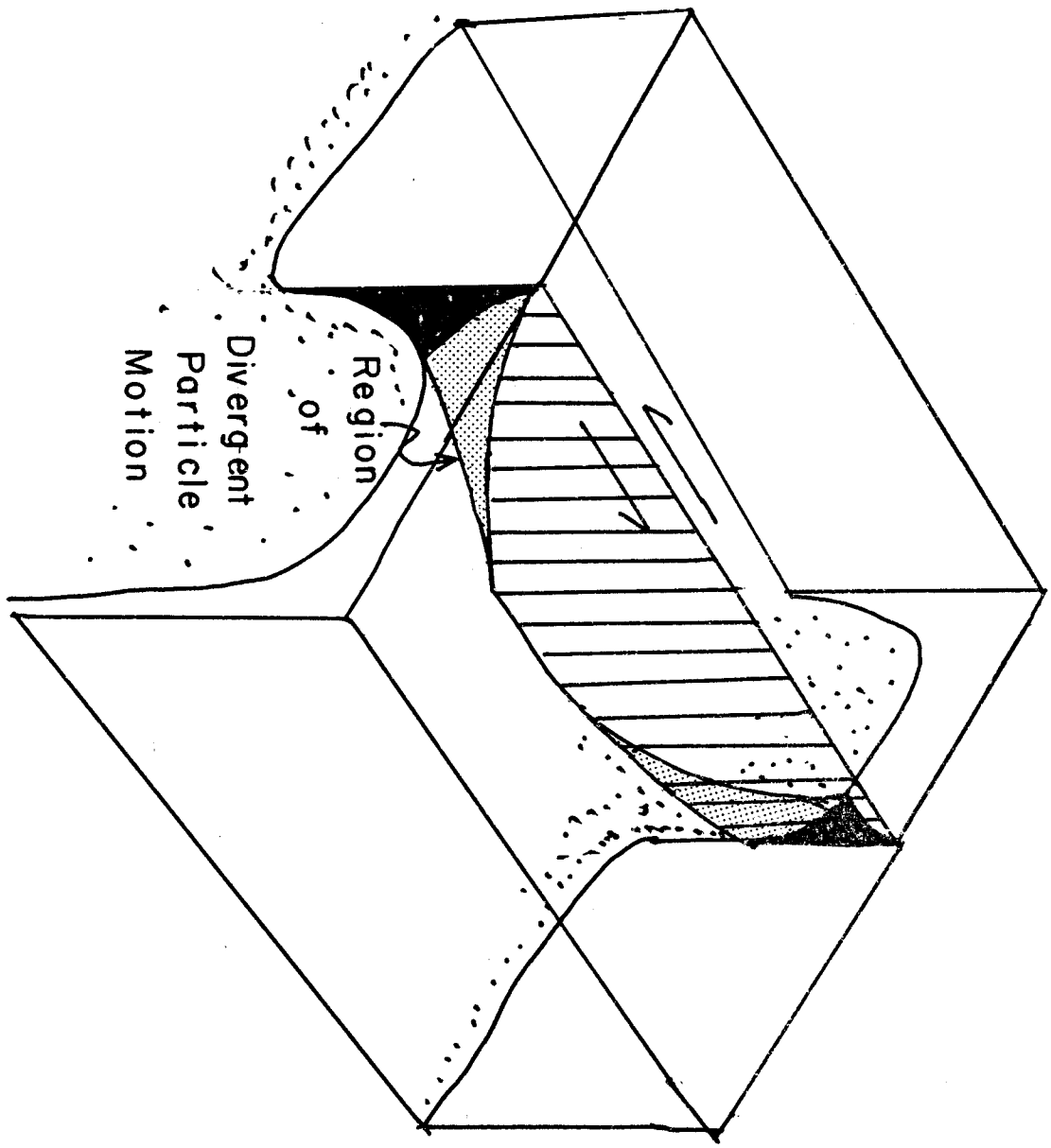
Region
of
Divergent
Particle
Motion

Figure 3-3b Block diagram showing the change in the listric nature of the plate boundary towards the transform midpoint.

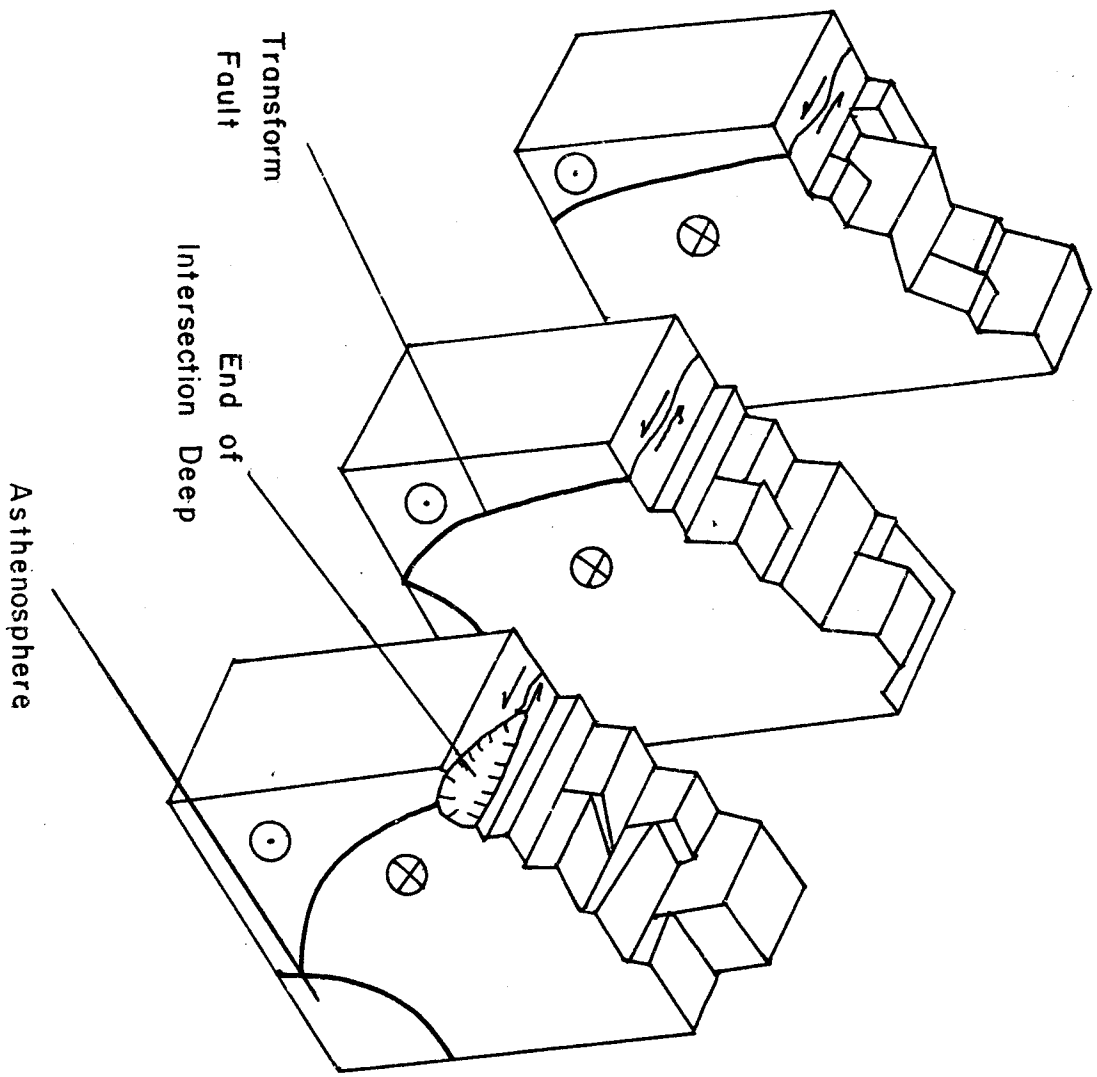
Transform Fault
End of Intersection Deep
Asthenosphere

Figure 3-4 Map views of the conduit at different depths.

Offset = 50 Km

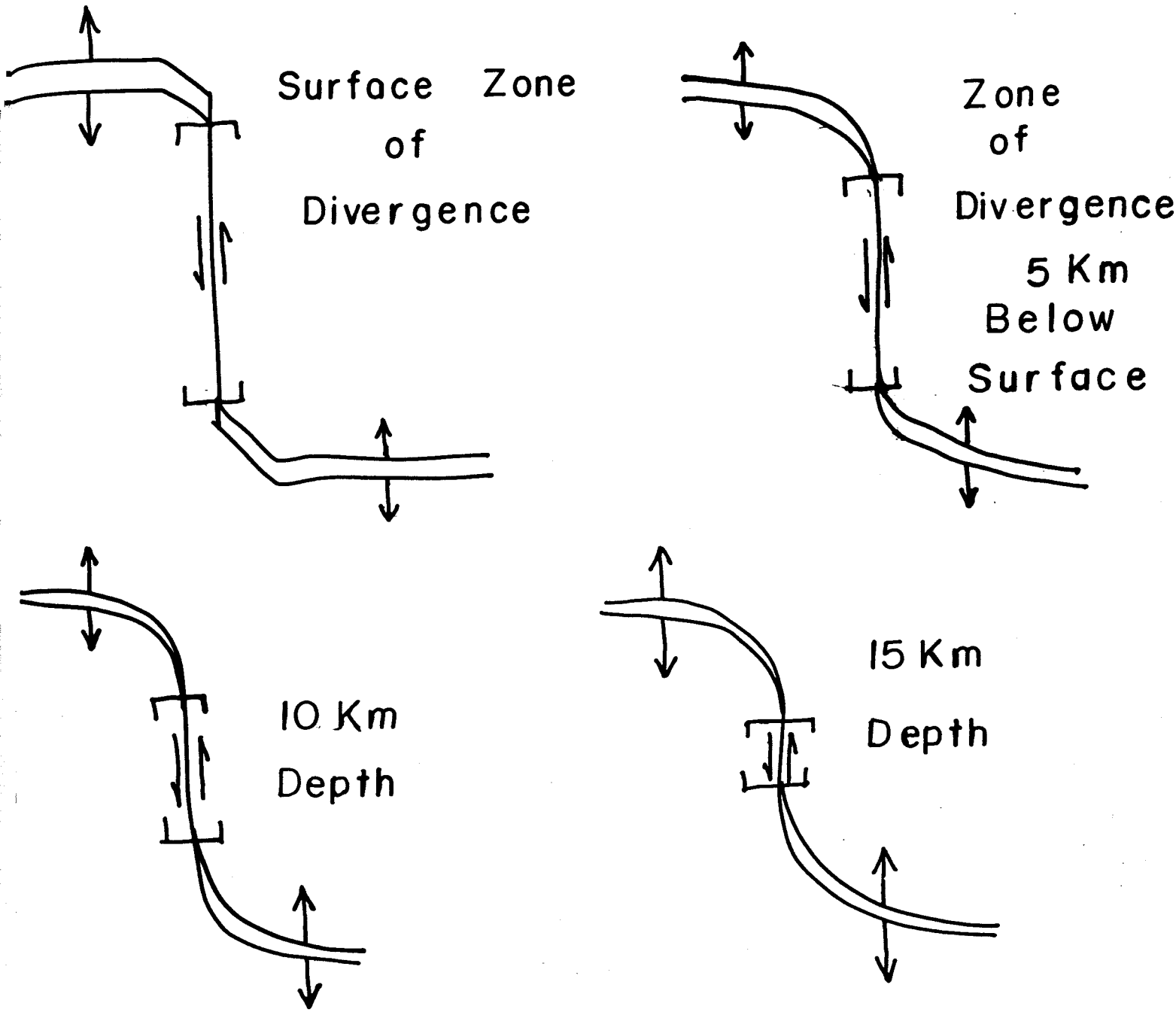

Bracketed Regions = Strike-Slip Motion

Figure 3-5 Different age contrast across the transform with second much less that the first.

Slow Spreading Center Large Offset

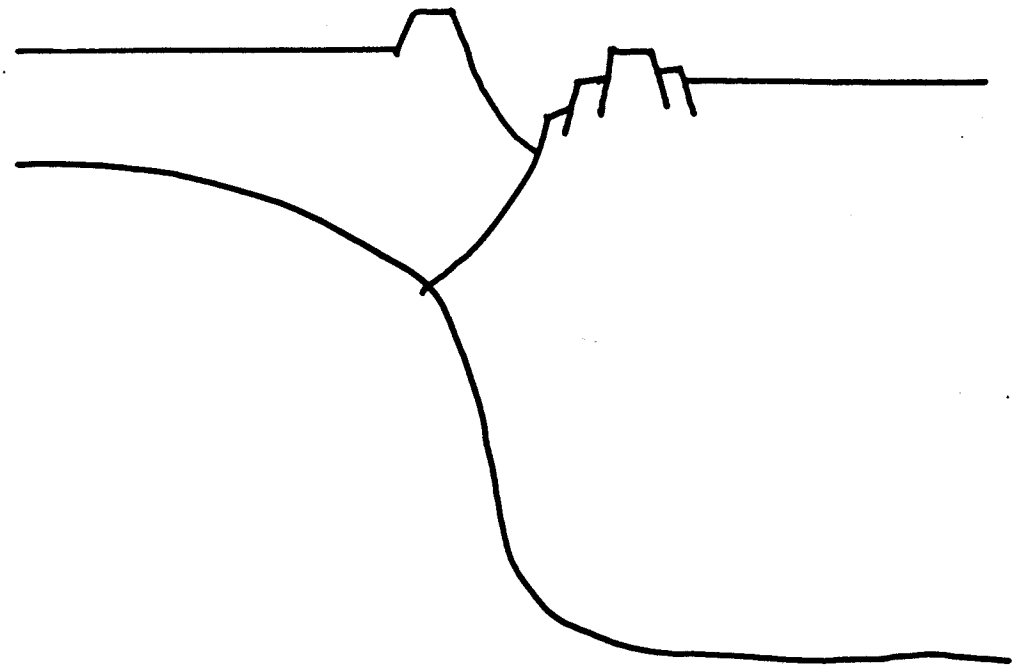

Slow Spreading Center Small Offset

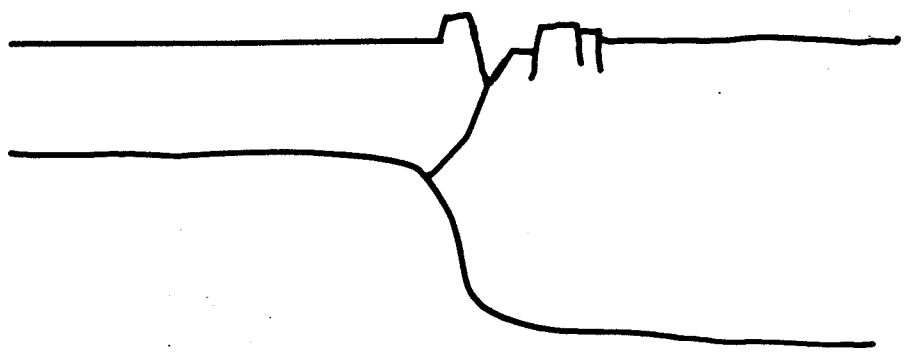

Figure 3-6a Recovery effects away from the intersection deep.

Recovery Effects of Seafloor Away From Intersection Deep

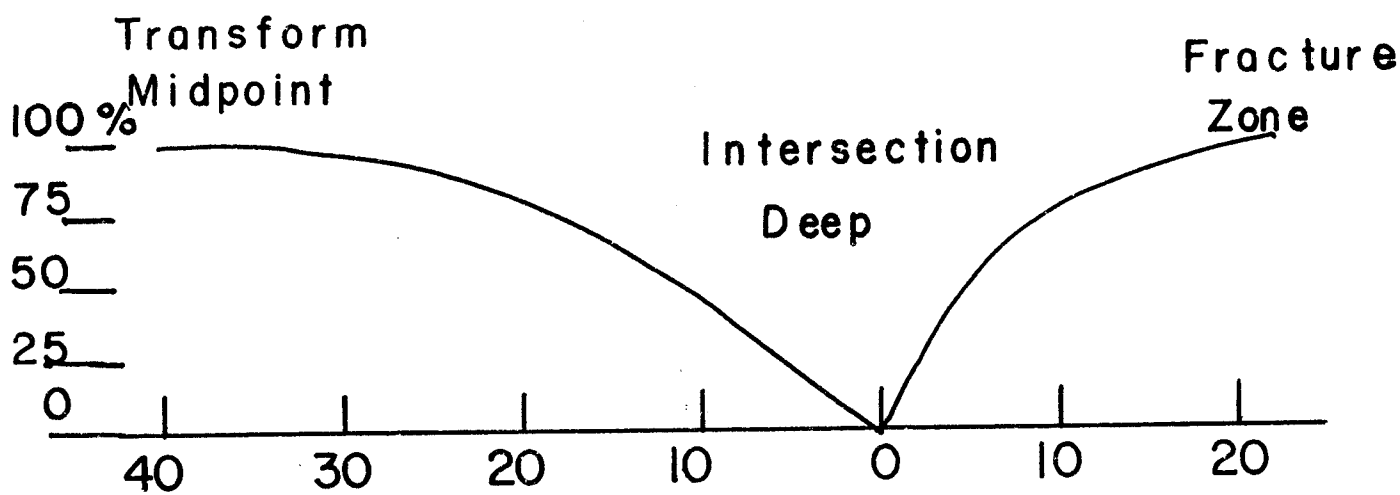

Figure 3-6b Six successive cross-sections which show the midpoint of the ridge (A-A'), the bordering transverse ridge (E-E'), and the axis of the transform (G-G'). Recovery to a level of isostatic equilibrium is quickest at the midpoint of the ridge and slowest at the transform.

IDEALIZED CROSS SECTIONS PERPENDICULAR TO SLOW SPREADING CENTER

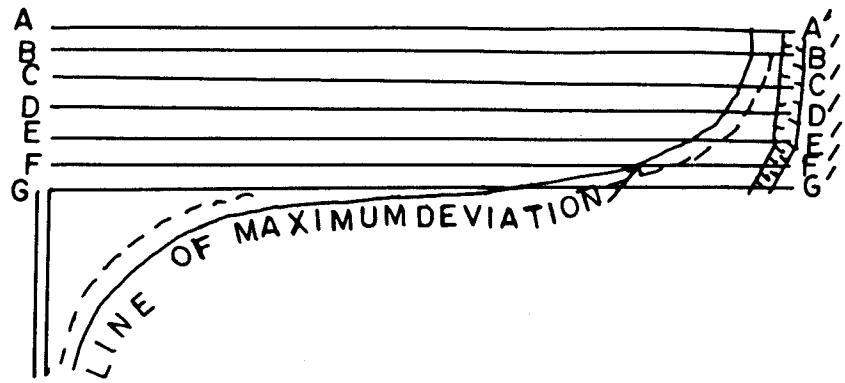

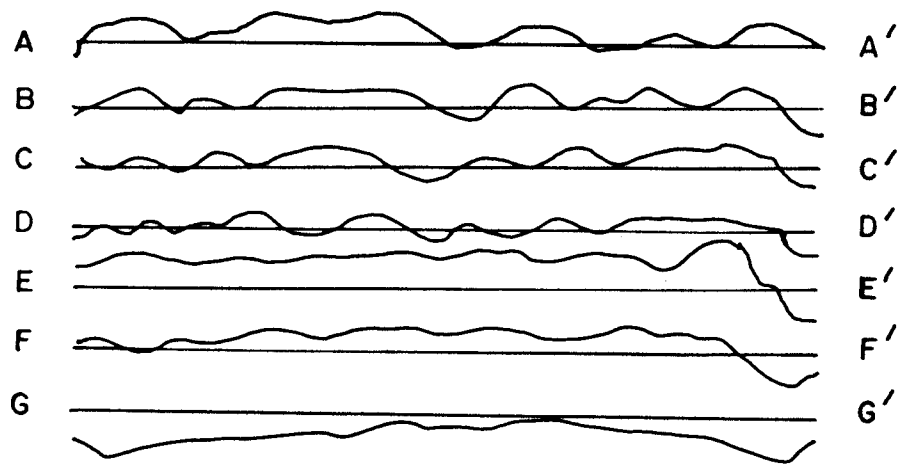

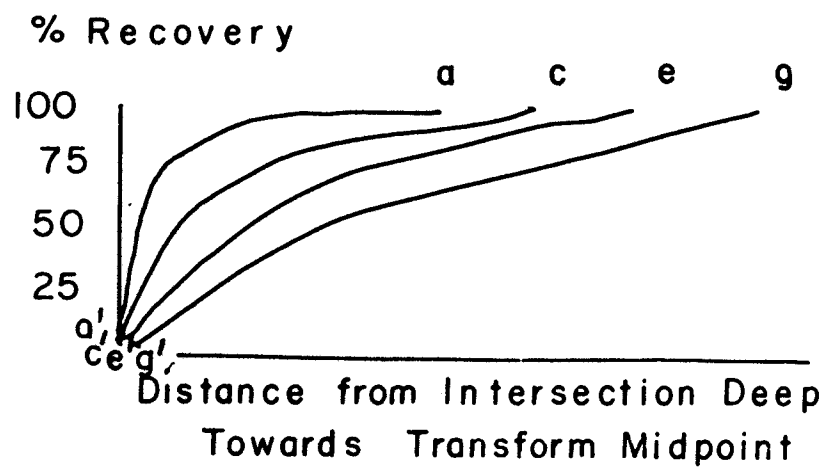

Figure 3-7 Origin of transverse ridges as horsts or monoclines.

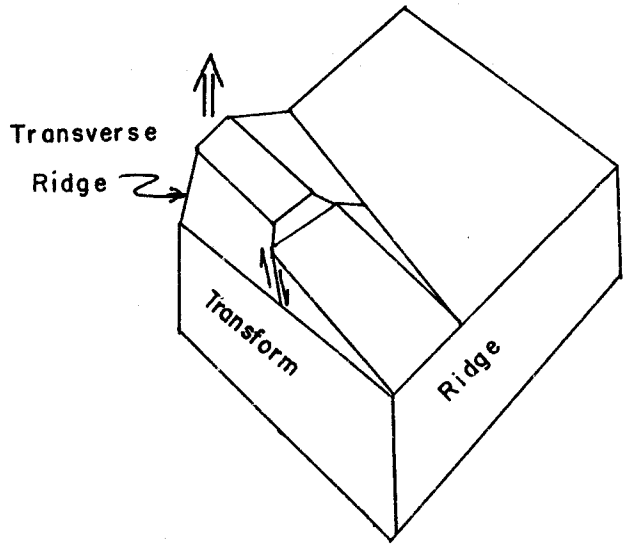

Faulting Accomodated Strain

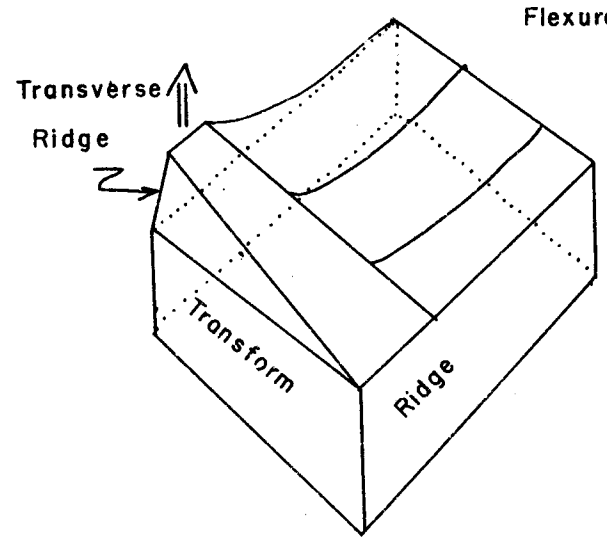

Flexure Accomodated Strain

Figure 3-8 Similar transform offset, different spreading rates.

Slow Spreading Center
100 Km Offset

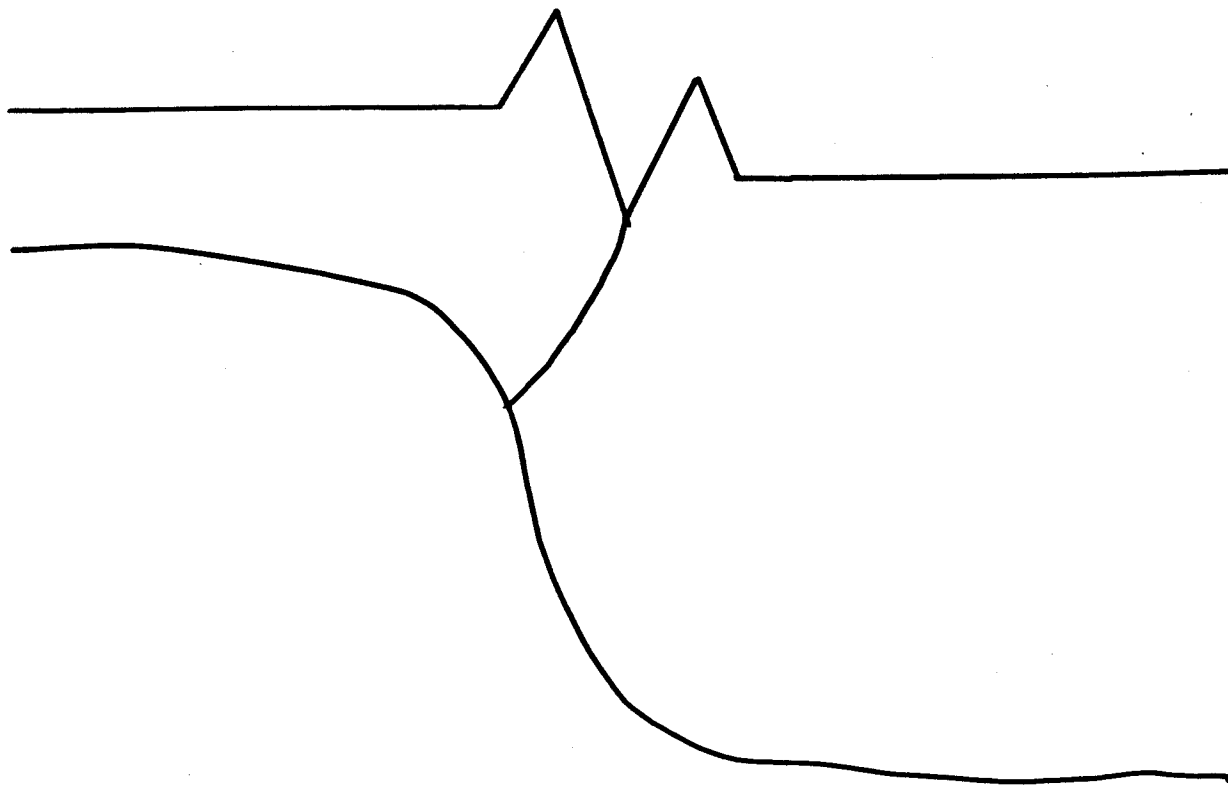

Fast Spreading Center 100 Km Offset

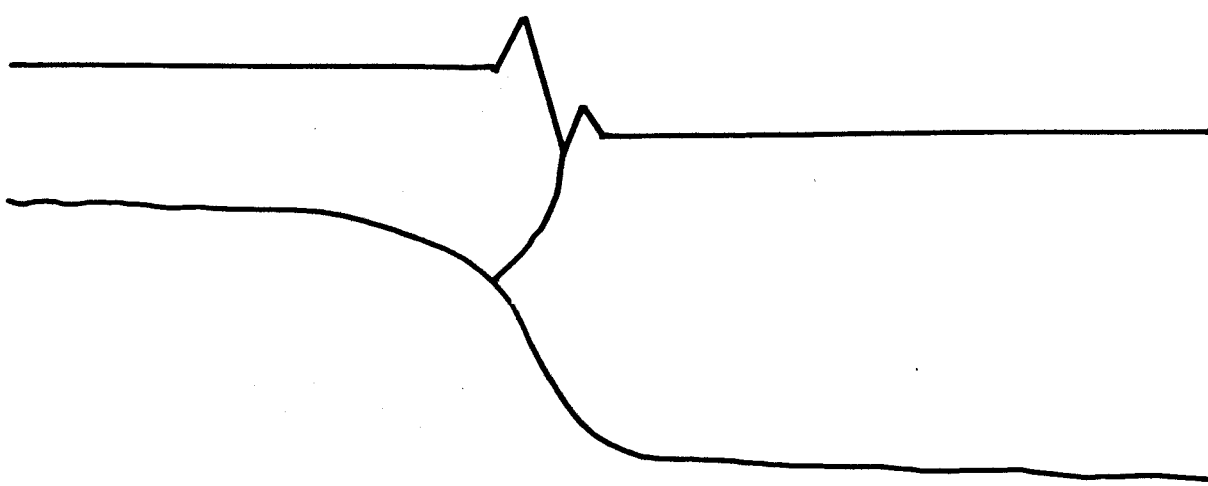

Figure 3-9 Possible difference in plate boundary geometries between Atlantic and Pacific transforms.

TYPE 1 "ATLANTIC" TRANSFORM
SLOW SPREADING RATE

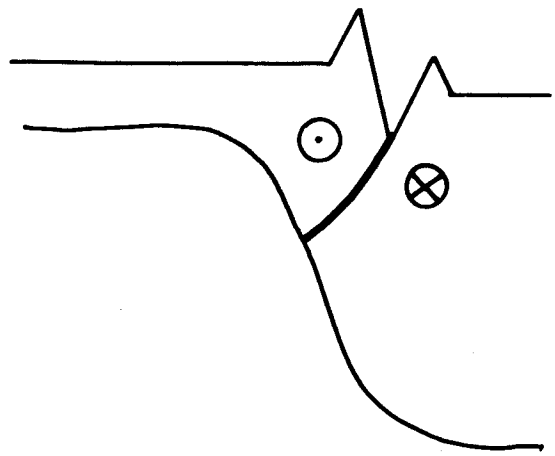

TYPE 2 "PACIFIC" TRANSFORM
INTERMEDIATE SPREADING RATE

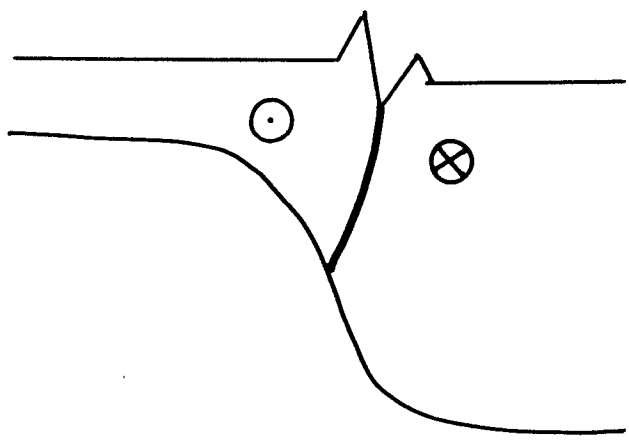

TYPE 3 "PACIFIC" TRANSFORM
FAST SPREADING RATE

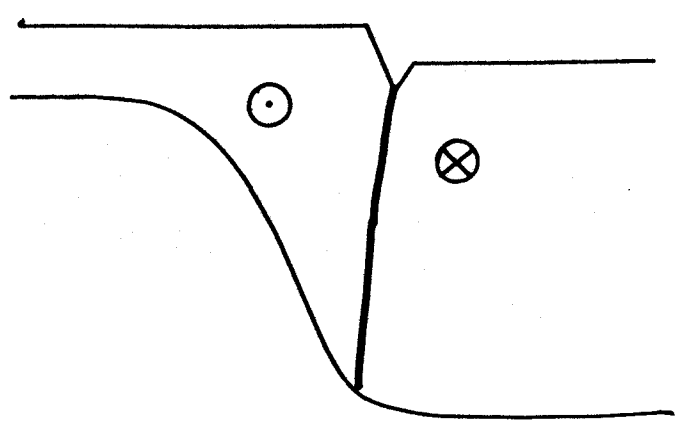

BIBLIOGRAPHY

ARCYANA (1975) Transform fault and rift valley from bathyscape and diving saucer, Science, v. 190, p.108-116.

Bagnold, R. A. (1941) The physics of blown sand and desert dunes, Methuen and Co., Publ., Lond., 265p.

Bird, P. and J.D. Phillips (1975) Oblique spreading near the Oceanographer fracture, Jour. Geophys. Res., v. 80 #29, p. 4021-4027.

Bonatti, E. and J. Honnorez (1976) Sections of the earth's crust in the Equatorial Atlantic, Jour. Geophys. Res., v. 81 , p. 4104-4116.

Choukroune,P., J. Francheteau, and X. Le Pichon (1978) In situ along transform fault A in the FAMOUS area, Mid-Atlantic, Geol. Soc. Amer. Bull., v.89, p. 1013-1029.

Cochran, J. R. (1973) Gravity and magnetic investigations in the Guiana Basin, western Equatorial Atlantic, Geol. Soc. Amer. Bull., v. 84, p. 3249-3268.

Collette, B.J., H. Shouten, K. and A.P. Slootweg (1974) Structure of the Mid-Atlantic Ridge Province between 12° and 18°N, Mar. Geophys. Res., v. 2, p.143-179.

Courtillot, V., P. Tapponnier and J. Varet (1974) Surface features associated with transform faults: a comparison between observed examples and an experimental model, Tectonophysics, #24, p. 317-329.

Crane, K. (1976) The intersection of the Siquieros transform fault and the East Pacific Rise, Mar. Geol. v. 21, p. 25-46.

Crowell, J.C. (1974a) Origin of late Cenozoic Basins in southern California, In: Modern and Ancient Geosynclinal Sedimentation, R.H. Dott, Jr. and Robert H. Shaver, Eds., Soc. Econ. Min. Spec. Publ., #19, p. 190-204.

Crowell, J.C. (1974b) Sedimentation along the San Andreas Fault, California, In: Modern and Ancient Geosynclinal Sedimentation, R. H. Dott, Jr and R. H. Shaver, Eds., Soc. Econ. Paleon. and Min. Spec. Publ., #19, p.292-303.

CYAMEX Scientific Team and L. Pastouret (1981) Submersible structural study of the Tamayo transform fault, East Pacific Rise at 23°N. Project Rita, Mar. Geophys. Res. v. 9, p. 53-86.

Davis, E.E. and C.R.B. Lister (1977) Tectonic structures on the Juan de Fuca Ridge, Geol. Soc. Amer. Bull. v. 88, p. 346-363.

Detrick, R.S., J.D. Mudie, B.P. Luyendyk and K.C. Macdonald (1973) Near bottom observations of an active transform fault (Mid-Atlantic Ridge at 37°N), Nature Physical Science, #246, p.59-61.

Detrick, R.S. and G.M. Purdy (1980) The crustal structure of the Kane fracture zone from seismic refraction studies, Jour. Geophys. Res., v. 85, B7, p.3759-3778.

Dewey, J.F. (1975) Finite plate motions: some implications for the evolution of rock masses at plate margins, Amer. Jour. of Sci. 275-A, p. 260-284.

Ewing, M. and F. Mouzo (1968) Ocean bottom photographs in the area of the outcrops, North Atlantic Ocean, Proc. Nat. Sci. v. 61, #3, p. 787-793.

Flood, R. (1981) Longitudinal triangular ripples in the Blake-Bahama Basin, Marine Geology, v. 39, p.13-20.

Folk, R.L. (1976) Rollers and ripples in sand streams and sky, Sedimentology, #23, p. 649-669.

Fox, P.J. (1978) The effect of transform faults on the character of the oceanic crust, Geol. Soc. Amer. Abs. with Prog. v. 10, #7, p. 403.

Fox, P.J., R.S. Detrick and G.M. Purdy (1980) Evidence for crustal thinning near fracture zones: implications for ophiolites; In: Ophiolites: Proceedings of the International Ophiolite Symposium., A. Pangyiotou, Ed., Geol. Survey of Cyprus, p. 161-168.

Fox, P.J., A. Lowrie and B.C. Heezen (1969) Oceanographer fracture zone, Deep-Sea Research, v. 16, p.59-66.

Fox, P.J., E. Schreiber, H. Rowlett and K. McCamy (1976) The geology of the Oceanographer fracture zone-A model for fracture zones, Jour. Geophys. Res. v. 81, p. 4117-4128.

Fox, P.J., F. Schroeder, R. Moody, and W. Pitman (in press) The Oceanographer fracture zone: morphology and evolution of structures at a slowly accreting plate boundary.

Francheteau, J. (1973) Plate tectonic model of opening of the Atlantic Ocean south of the Azores, In: Implications of continental drift to the earth sciences, D.H. Tarling and S.K. Runcorn, Eds. Academic Press, #1, p. 197-202.

Francheteau, P., P.Choukroune, R. Hekinian, X. Le Pichon and H.D. Needham (1976) Oceanic do not provide sections deep sections in the crust, Can. Jour. E. Sci., v. 13, #9, p.1223-1235.

Gallo, D.G. and P.J. Fox (1979) The influence of transform faults on the generation of oceanic lithosphere, Trans. AGU. #60, p. 376.

Gallo, D.G., E.R. Rosencrantz and D.B. Rowley (1980) Oblique structures at ridge-transform intersections: implications for ridge dynamics and pole determinations, EOS, Trans. AGU, v. 61, #17, p. 358.

Harms, J.C. (1969) Hydraulic significance of some sand ripples, Geol. Soc. Amer. Bull., v. 80, p. 363-396.

Heezen, B.C. and C.D. Hollister (1969) Deep-sea current evidence from abyssal sediments, Marine Geology, #1, p. 141-174

Heezen, B.C. and C.D. Hollister (1971) The face of the deep, Oxford Univ. Press 695p.

Hollister, C.D., R.A. Flood, D.A. Johnson, P. Lonsdale, and J.B. Southard (1974) Abyssal furrows and hyperbolic echo traces on the Bahama Outer Ridge, Geology, v. 2, #8, p. 395-400.

Hollister, C.D., J.B. Southard, R.D. Flood and P.F. Lonsdale (1976) Flow phenomenon in the benthic boundary layer and bedforms beneath deep-current systems, In: The benthic boundary layer, I.V. McCave Ed., New York, p. 183-204.

Hoose, P.J., B.E. Tucholke, R.W. Embley and P.F. Lonsdale (1979) Abyssal furrows on sediment swells on the western Bermuda Rise, Trans. AGU, #60, p. 855.

Horton, R.E. (1945) Erosional development of streams and their drainage basins, hydrophysical approach to quantitative morphology, Geol. Soc. Amer., #56, p. 275-370.

Johnson, G.L. (1967) North Atlantic fracture zone near 53^{o}N, Earth and Plan. Sci. Letts., #2, p. 445-448.

Karson, J. and J.F. Dewey (1978) Coastal Complex, western Newfoundland: an early Ordovician oceanic fracture zone, Geol. Soc. Amer. Bull. v. 89, p. 1037-1049.

Kent, D.K., N.D. Opdyke, B.M. Honorez and P.J. Fox (1977) Magnetic properties of dredged oceanic gabbro and the source of marine magnetic anomalies, Geol. Soc. Amer. Abstracts with programs, v. 8, #7, p. 1048.

Lachenbruch, A.H. (1973) A simple mechanical model for oceanic spreading centers, Jour. Geophys. Res.v. 78, #17, p. 400-418.

Laughton, A.S. (1963) Microtopography, In: M.N. Hill, Ed. v. 3, The Seas, New York, p.437-472.

Le Pichon, X. (1968) Seafloor spreading and continental drift, Jour. Geophys. Res. v. 73, p. 3661-3697.

Le Pichon, X. J. Francheteau and J. Bonnin (1973) Plate Tectonics, Elsevier Scientific Publishing Co., 300p.

Lonsdale, P. (1978) Near-bottom reconnaissance of a fast-slipping transform fault zone at the Pacific-Nazca plate boundary, Jour. Geol., #4, p. 451-472.

Lonsdale, P. and A. Shor (1979) The oblique intersection of the Mid-Atlantic Ridge with Charlie-Gibbs transform fault, Tectonophysics, #54, p. 195-209.

Lonsdale, P. and F.N. Spiess (1977) Abyssal bedforms explored with a deeply towed instrument package, Marine Geology, v. 23, p. 57-75.

Macdonald, K.C., K. Kastens, F.M. Spiess, and S.P. Miller (1979) Deep-tow studies of the Tamayo transform fault, Mar. Geophys. Res. #4, p. 37-70.

Merzer, A.M. and R. Freund (1975) Buckling of strike-slip faults in a model and in nature: Geophys. Jour. of the Royal Society, #43, p. 517-530.

Menard, H.W. and T. Atwater (1968) Changes in the direction of sea floor spreading, Nature, v. 219, p. 463-467.

Menard, H.W. and T. Atwater (1969) Origin of fracture zone topography, Nature 222, p. 1037-1040.

Moody, R.H., D.G. Gallo and P.J. Fox, The origin of transform topography (In prep).

Morgan, W.J. (1968) Rises, trenches, great faults and crustal blocks, Jour. Geophys. Res. v. 73, p. 1959-1982.

Needham, H.D. and J. Francheteau (1974) Some characteristics of the rift valley in the Atlantic Ocean near 36°48'North, Earth and Plan. Sci. Letts., v.22, p. 29-43.

Osmaston, M.F. (1971) Genesis of ocean ridge median valleys and continental rift valleys, Tectonophysics, #11, p. 387-405.

OTTER Scientific (1980) Oceanographer Transform Field Experiment 24 June to 18 July, 1980. Off. Nav. Res. Spec. Rep., 10p.

OTTER Scientific and P.J. Fox (1980) The geology of the Oceanographer transform: Submersible and deep-towed camera investigation, EOS Trans. AGU, v. 61, p. 1105.

Phillips, J.D., H.S. Fleming, R.H. Feden, W.E. King, and R. K. Perry (1975) Aeromagnetic study of the Mid-Atlantic Ridge near the Oceanographer fracture zone, Geol. Soc. Amer. Bull., #383, p. 619-646.

Phillips, J.D. and H.S. Fleming,(1978) Multi-beam sonar study of the Mid-Atlantic Ridge rift valley, Geol. Soc. Amer. Map and Chart Series, MC-19.

Rabinowitz, P.D. and G.M. Purdy (1976) The Kane fracture zone in the western central Atlantic Ocean, Earth and Plan. Sci. Letts. v. 33, p. 21-26.

Ramberg, I. and Tj. H. van Andel (1977) Morphology and tectonic evolution of the rift valley at lat. 36°30'N, Mid-Atlantic Ridge, Geol. Soc. Amer. Bull., v. 88, p. 577-586.

Robb, J.M. and M.F. Keen (1975) Structure of the Vema fracture zone from gravity and magnetic intensity profiles, Jour. Geophys. #80, p. 4441-4445.

Schroeder, F.W. (1977) A geophysical investigation of the Oceanographer fracture zone and the Mid-Atlantic Ridge in the vicinity of 35°N, Unpub. Ph.D thesis, Columbia University, 458p.

Searle, R.C. (1979) Side-scan sonar studies of North Atlantic fracture zones, Jour. Geol. Soc. Lond. v. 136, p.283-292.

Searle, R.C. (1981) The active part of Charlie-Gibbs fracture zone: a study using sonar and other geophysical techniques, Jour. Geophys. Res. v. 86, #B1, 243-262.

Shibata, T., S.E. DeLong, and R. Walker (1979) Abyssal tholeiites from the OFZ, I. Petrology and fractionation, Contr. Min. Petrol., #70, p. 89-102.

Sleep, N.H. (1969) Sensitivity of heat flow and gravity to the mechanism of seafloor spreading, Jour. Geophys. Res. v. 74 p. 542-549.

Sleep, N.H. and S. Biehler (1970) Topography and tectonics at the intersection of fracture zones with central rifts, Jour. Geophys. Res. v. 75, p. 2748-2752.

Sleep, N.H. and B. Rosendahl (1979) Topography and tectonics of mid-ocean ridge axes, Jour. Geophys. Res. v. 84, p. 6831-6839.

Stroup, J.B. and P.J. Fox, P.J. (1981) Geological investigations in the Cayman Trough: Evidence for thin oceanic crust along the Cayman Trough, Jour. Geol. v. 57, p. 351-366.

Sykes, L.R. (1967) Mechanism of earthquakes and nature of faulting on the mid-ocean ridge, Jour. Geophys. Res. v. 72, p. 2131-2153.

Tamayo Scientific Team (1980a) Tectonics of a ridge-transform intersection zone: Tamayo-East Pacific Rise, Gulf of California, Trans. Amer. Geophys. Union, v. 61, #17.

Tamayo Scientific Team (1980b) Submarine landsliding at the eastern end of the Tamayo transform fault, Gulf of California, Trans. Amer. Geophys. Union, v. 61, #17.

Tamayo Scientific Team, (1980c) East Pacific Rise-Tamayo transform intersection, Geol. Soc. Amer. Abstracts with programs, Fall 1980.

Tchalenko, J.S. (1970) Similarities between shear zones of different magnitudes, Geol. Soc. Amer. Bull., #81, p. 1625-1640.

Tucholke, B.E. (1979) Furrows and focussed echoes on the Blake Outer Ridge, Marine Geology, #31, p. 13-20.

Udias, A., A. Lopez Arroyo and J. Mezcua (1976) Seismotectonics of the Azores-Alboran region, Tectonophysics, #31, p. 259-289.

Walker, D., T. Shibata and S.E. DeLong (1979) Abyssal tholeiites from the Oceanographer transform, II. Phase equlibria and mixing, Contr. Min. Petrol., #70, p. 111-125.

Wallace, R. (1978) Geometry and rates of change of fault-generated range fronts, North-Central Nevada, Jour. Res. U.S. Geol. Surv., v. 6 #5, p. 637-650.

Wilcox, R.E., T.P. Harding and D.R. Seely (1973) Basic wrench tectonics, Amer. Assoc. Petrol. Geol. v. 57, p. 74-96.

Woodside, J.M. (1972) The Mid-Atlantic Ridge near 45°N. XX. The gravity field, Can. Jour. Ear. Sci. v. 9 p. 942-959.

Young, A. (1972) Slopes, K.M. Clayton, Ed. Edinburg, Oliver and Boyd, 288p.